Microfluidic Interfacing for Primary Endocrine Tissue: Developing Bioanalytical Methodologies and Novel Fabrication Methods for Cell Culture and Analysis

by

Jessica Elizabeth Crumbley Brooks

A dissertation submitted to the Graduate Faculty of
Auburn University
in partial fulfillment of the
requirements for the Degree of
Doctor of Philosophy

Auburn, Alabama
December 10, 2016

Keywords: Microfluidics, 3D-Printing, Diabetes and Metabolic Diseases, Pancreatic Islets, Adipocytes, Immunoassays

Approved by

Christopher J. Easley, Chair, Knowles Associate Professor of Chemistry and Biochemistry
Curtis Shannon, Hunt Professor and Chairman of Chemistry and Biochemistry
Holly Ellis, Professor of Chemistry and Biochemistry
Robert L. Judd, Boshell Professor of Pharmacology

Abstract

In order to bridge the gap between microfluidic designs and real world applications, microanalysis systems were developed using minimalistic design attributes which could be readily paired with compatible bioanalytical assays. Chapter 2 discusses monolithic fabrication methods which have been developed for incorporation of macroscale structures within microfluidic devices in order to accommodate on-chip cell culture and secretion sampling of primary, murine endocrine tissues. Rigid, polymer templates were hand constructed and served as molds in PDMS to generate millimeter scale fluidic reservoirs which could directly interface with microchannels. Initial hand fabricated templates were utilized for pancreatic islet and isolated adipocyte secretion sampling over 1 hour time periods where insulin and adiponectin concentrations were analyzed via ELISA. While these hand fabricated templates were proven adequate for cell culturing purposes, there were minor disadvantages associated with the templates. To improve upon the template fabrication process, designs were digitized for 3D printing purposes. 3D printing of templates provided not only more rapid and robust production of templates, but also allowed for easily designing templates with increased structural complexity. Microfluidic devices fabricated in this manner were used for temporally resolved sampling and quantization of insulin and glycerol secreted from pancreatic islets and adipose tissue explants. 3D templating methods were further utilized in Chapter 3 for real-time analysis of fatty acid uptake within adipose tissue explants. Real-time analysis was performed on-chip through a novel, fluorescence based assay designed in-house. This assay exploits the natural binding of fatty acids to the protein albumin and allows for homogenous monitoring of fatty acid uptake through fluorescently labeled fatty acid analogues and bovine serum albumin which was modified with covalently attached quencher molecules. Proximity immunoassays were developed and discussed in Chapter 4 for analysis of small

volume samples such that microfluidic secretion samples could be analyzed without the need for expensive, high volume assays such as ELISA. Real-time quantitative PCR and square wave voltammetry were used as readout methods for proximity assays to quantitate insulin and leptin in cell secretion samples as well as serum. Chapter 5 represents a collaborative effort which branches out from the focus of endocrine tissue on-chip, while maintaining the theme of simplistic, low volume microanalysis systems. A droplet generating device was utilized for actinide metal-ligand binding analysis through UV-Vis specrtal shifts. Finally, Chapter 6 summarizes this work in its entirety and provides an outlook into future projects stemming from these topics.

Acknowledgments

I would like to thank my research advisor Dr. Easley for mentoring me during my time here at Auburn. You have taught me not only about research and science, but also how to be a confident leader. Thank you to my committee members: Dr. Shannon, Dr. Ellis, and Dr. Judd. Through classes, projects, and insightful discussions; you have all encouraged me and pushed me further as a person and a scientist. Dr. Kim, thank you for always taking the time to answer my questions and teaching me the best ways to plan and execute experiments. Without your guidance and pipetting skills I would not have accomplished this work. Leah and Kennon, you guys have no idea how much your friendship and encouragement boosted me through the years. You both somehow managed to be strong leaders for me as well as some of my best friends. Seeing how you handled graduate school and maintained your eagerness for science was an inspiration to all of us. Mani, I will always regret that we put you in 380 and did not get to really know you that first year. You are hilarious and a constant source of enthusiasm, thank you for always brightening up the lab. Li, you are one of the smartest, hardest working people I know. Thank you for challenging me to push myself. Mark, I will be forever jealous of all the eclectic skills you have. Thank you for always geeking out with me and putting up with my crazy antics. Dylan, you are going to have such a successful career in whatever path you decide to take. Being able to teach you was a wonderful and humbling experience. Thank you for restoring some faith in the future generations of scientists. Cheryl, Jiaming, Jean, Adriana, Kat, Juan, Gebriel, and Niamat thank you for your friendship and knowledge throughout our time together. I have learned from all of you and I am very thankful for everyone's continual support.

These past few years have been challenging, and I would not have succeeded without all of the amazing people I have had the privilege to call my friends. Charmaine, from day

one I knew you and I were going to tackle this beast together. Through smiles, tears, and everything in between; you always told me to look for the good in things. Thank you for being a bright light in a sometimes dark world. Nick, I don't think you realize how smart and important you really are. You may not always say much, but your considerate actions speak for you. Thank you for showing me how meaningful it can be to worry less and always remain patient.

Thank you to everyone at Auburn. Whether we saw each other everyday or only a few times a semester, you have all been like a second family to me. I am going to miss you all so much. Everyone has touched my life in one way or another and I will be forever grateful.

Finally, I would like to thank my family for their unwavering support and encouragement. None of this would have been possible without you. Your faith and love has shown me that no matter what I will always have a steadfast support system. I love you all!

Table of Contents

List of Figures

List of Tables

List of Abbreviations

Re	Reynold number
Ab	Antibody
AC	Adenylyl Cyclase
Ag	Antigen
ARs	Adrenergenic Receptors
BHB	β-hydroxybutyrate
BHQ	Black Hole Quencher
BSA	Bovine Serum Albumin
BSA-Q	BSA with Quencher
C(t)	Cycle Threshold Value
DMEM	Dulbeccos Modified Eagle Medium
ELISA	Enzyme Linked Immunosorbent Assay
ESI-MS	Electrospray Ionization Mass Spectroscopy
eWAT	Epididymal White Adipose Tissue
FAF BSA	Fatty Acid Free BSA
FBS	Fetal Bovine Serum
FFA	Free Fatty Acid

FFA* Fluorescently Labeled Fatty Acid Analogues

GPCR G-protein Coupled Receptors

HEPES $4-2-$hydroxyethyl$-1-$piperazineethanesulfonicacid

HGHI High Glucose/High Insulin Buffer

HMW High Molecular Weight

HRP Horseradish Peroxidase

IPA Isopropyl Alcohol

IR Insulin Receptors

K_d Dissociation Constant

LGLI Low Glucose/Low Insulin Buffer

LMW Low Molecular Weight

LOD Limit of Detection

MB Methylene Blue

MEM Minimal Essential Media

MS Micro Stereo Lithography

MUX Multiplexer

NEFA Non-esterified Fatty Acid

Oligo Oligonucleotide

PCR Polymerase Chain Reaction

PDMS Poly(dimethylsiloxane)

PKA Protein Kinase A

PLA Proximity Ligation Assay

PLAF Polylactic Acid Filament

PNA Peptide nucleic acid

qPCR Real time quantitative PCR

RPM Rotations Per Minute

T_m Melting Temperature

T1D Type 1 Diabetes

T2D Type 2 Diabetes

TCEP Tris(2-Carboxyethyl) Phosphine Hydrochloride

TG Triglycerides

TG Triglycerides

THF Tetrahydrofuran

TMCS Trimethylchlorosilane

UV Ultra-Violet

WAT White Adipose Tissue

Chapter 1

Introduction to Metabolic Disorders and Microfluidics

1.1 Diabetes and Metabolic Disorders

The prevalence of obesity, diabetes, and other metabolic syndromes has been rapidly increasing over the past decade [1, 2]. In the CDC's 2014 National Diabetes Statistics Report, 29.1 million people in the U.S. have diabetes (roughly 9.3 % of the total population). Disruption in the signaling and release of insulin is a defining characteristic of these disorders [2]. Until recently, pancreatic islets were thought to be the main endocrine regulator associated with these disease states; however, it is now known that adipose tissue also has strong ties to metabolic disorders [3, 4]. The first portion of the introduction will focus on endocrine tissue associated with diabetes and metabolic diseases in order to assert the importance of studying these tissues.

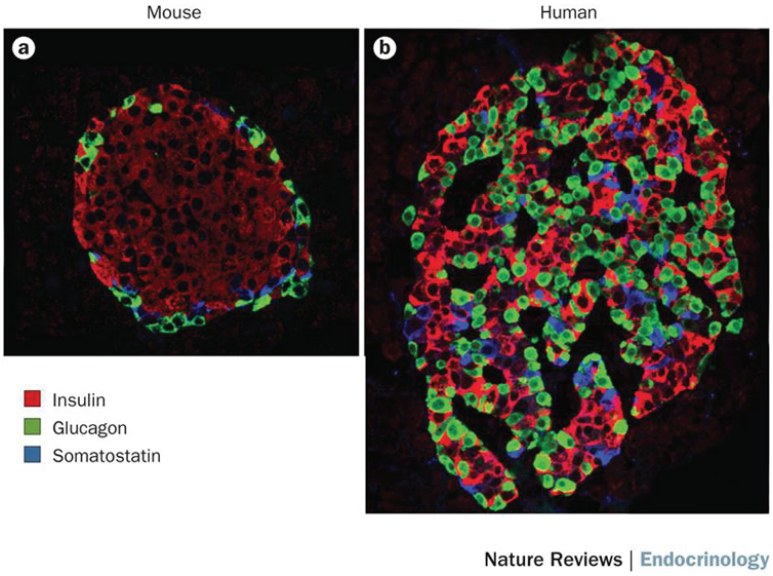

Figure 1.1: **Immunohistochemical staining of Pancreatic Islets.** Insulin (red), glucagon (green), and somatostatin (blue) are produced in the β, α, and δ-cells respectively. Reprinted by permission from Macmillan Publishers Ltd: *Nature Reviews Endocrinology* [5], copyright 2015.

1.1.1 Islets of Langerhans

The pancreas is composed of cell clusters known as islets of Langerhans. Endocrine cells within islets are responsible for glucagon (α-cells), insulin (β-cells), and somatostatin secretion (δ-cells) (Figure 1.1). In type I diabetes (T1D) the body develops an autoimmune response to β-cells, reducing their overall cell count within the pancreas. Diminished β-cells numbers result in insufficient insulin production thereby causing elevated blood glucose levels in those with T1D [1]. The more predominant form of diabetes, type II (T2D), stems from impaired insulin response from the β-cells [6]. T2D is associated with elevated glucose and insulin due to the β-cells resistance to insulin.

Healthy islets respond to increased blood glucose levels via biphasic insulin secretion. An initial rapid burst of insulin correlates to the first phase; followed by prolonged, lowered insulin secretions in phase two (Figure 1.2B) [6]. As glucose is taken into the β-cells, K_{ATP} channels close, causing the cells to become depolarized. After depolarization, $[Ca^{2+}]_i$ increases as well as cellular exocytosis rates [7]. During phase one, exocytosis of immediately available granules is the predominant source of insulin, whereas phase two is hypothesized to release reserve pools of granules (Figure 1.2A) [8]. While changes in $[Ca^{2+}]$ stimulate insulin release, the mechanism behind this interaction differs in the two phases of release. It is clear, therefore, that insulin secretion dynamics play a pivitol role in endocrine function.

1.2 White Adipose Tissue

Until relatively recently, white adipose tissue (WAT) has been considered solely as a source of insulation and energy storage; however, WAT is now established as endocrine tissue capable of secreting hormones that are tied with obesity and other metabolic disorders [3, 4, 10]. Adipose tissue is comprised of fat cells, known as adipocytes, which secrete metabolically active adipokines. The primary functions of these cells include lipid metabolism for storage and release of triglycerides (TG), glycerol, and free fatty acids (FFAs) as well as adipokine secretion for metabolic signaling [4, 10, 11, 12].

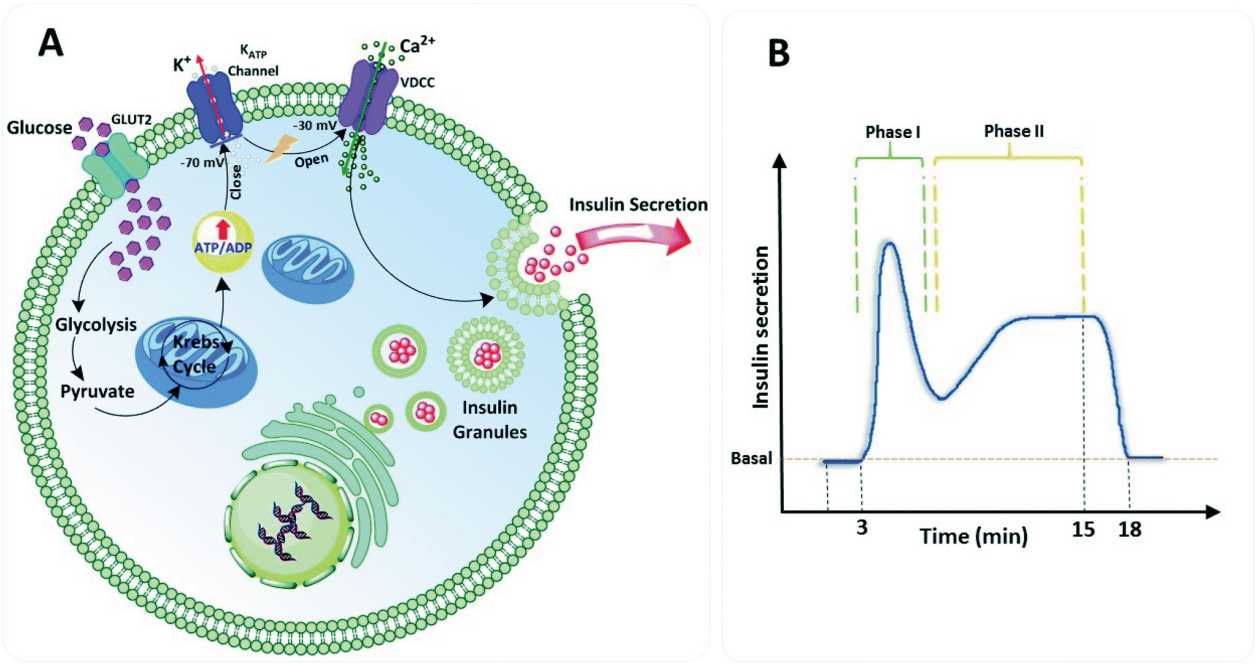

Figure 1.2: **Glucose stimulated insulin secretion pathway.** A) Insulin secretion from pancreatic β-cells. B) Profile of biphasic insulin release. Phase one represents rapid burst of insulin in the first five minutes following glucose stimulation. Phase two represents prolonged insulin secretion at lower concentrations than phase one. Reproduced in part from [9] with permission of The Royal Society of Chemistry.

1.2.1 Adiponectin

Produced solely by adipocytes, adiponectin consists of a C-terminal globular domain, a collagenous tail domain, a variable region, and an N-terminal signal sequence Multiple forms of adiponectin are found within the body − trimers, low molecular weight complexes (LMW), and high molecular weight complexes (HWM) [13, 14]. The relative abundance of each form of adiponectin varies between genders and is also indicative of metabolic disorders. HMW adiponectin is understood to be the most biologically relevant form of the protein and has been shown to be significantly reduced in healthy males in comparison to healthy females as well as in obese individuals in comparison to lean individuals [14]. Insulin sensitivity is increased when adiponectin is properly regulated within the body; and, as hypoadiponectinemia begins, insulin resistance as well as T2D can develop [3]. Since commercial assay kits

are used with relatively large sample volumes (10-100 μL), little is known about adiponectin secretion dynamics, but some evidence exists to highlight its importance [15].

1.2.2 Leptin

Often referred to as the "hunger hormone", leptin is responsible for regulating food intake as well as stimulation of energy expenditure. When leptin reaches receptors in the hypothalamus, the brain signals to reduce food intake and increase energy expenditure [12]. This signaling pathway can be disrupted through leptin resistance from the hypothalamic receptors or through production of mutated leptin leading to leptin deficiency [16]. In leptin resistance, despite the body synthesizing leptin properly, leptin receptors do not recognize the protein [17]. Without the leptin-hypothalamus feedback system, the body does not reduce food intake, leading to issues such as obesity and diabetes. Production of abnormal leptin correlates to abnormally low non-mutated leptin levels within the body which also results in obesity [18]. Administration of exogenous leptin has been shown to help reverse metabolic side effects in the case of mutated leptin; however, it is not observed to have the same outcome with leptin resistant individuals [16, 17]. While exact mechanisms of leptin regulation and production are not completely understood; insulin, FFAs, glucocorticoids, cytokines, and β antagonists have been shown to mediate these processes [3, 18]. Akin to adiponectin, leptin secretion requires further studies to fully understand the dynamics behind the protein.

1.2.3 Triglycerides and Free Fatty Acids

In adipocytes, excess energy is stored as triacylglycerol and can be broken down into glycerol and FFAs via lipolysis when needed (Figure 1.3). FFAs can be secreted into the blood only through adipocytes, and deficiencies in the secretory process have been linked to T2D and obesity [19, 20]. Epinephrine, isoproterenol, niacin, and β-hydroxybutyrate (BHB) have been shown to either stimulate or suppress lipolysis through binding with adrenergic

receptors (ARs), β-ARs and α_2-ARs, on the surface of the adipocyte [15, 21]. Both the α and β receptors are categorized as G-protein coupled receptors (GPCR), where α_2-ARs are associated with the inhibitory G-protein (G_i) and β-ARs are associated with the stimulatory G-protein (G_s).

Niacin and BHB activate G_i, inhibiting G-protein interaction with adenylyl cyclase (AC); whereas isoproterenol and epinephrine activate G_s and AC [15, 19]. Increased AC activity yields increased conversion of ATP to cAMP, which in turn activates protein kinase A (PKA). Lipases within the adipocyte are phosphorylated by PKA, stimulating the breakdown of TG to glycerol and FFAs [21, 22]. Additionally, when insulin binds to insulin receptors (IR) in the adipocyte, IR auto-phosphorylation occurs followed by several subsequent kinase activations resulting in amplified degradation of cAMP to 5-AMP. PKA is then inactivated and lipolysis becomes suppressed [21, 22]. While there are quantitative methods for determining TG, glycerol, and FFAs concentrations; there are limited processes for monitoring real-time fluctuations on live cells.

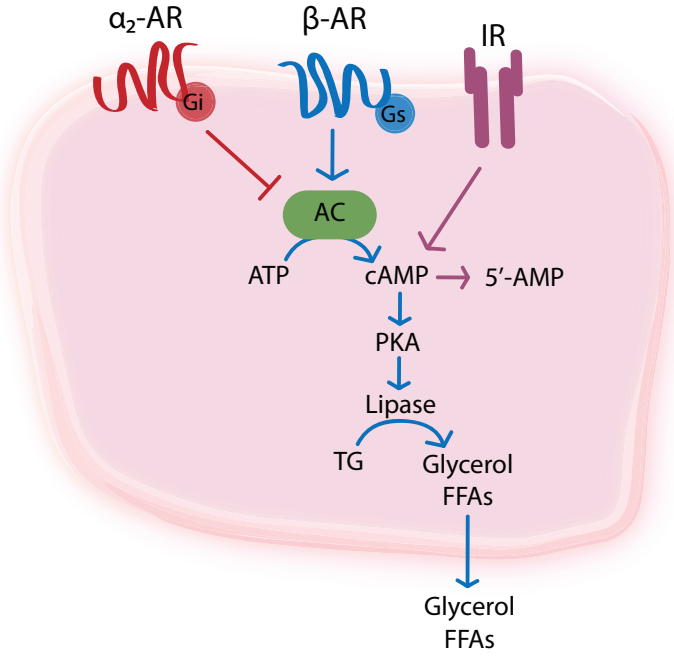

Figure 1.3: **Lipolysis scheme.**. Receptors on the surface of adipocytes such as α_2-ARs (red), β-ARs (blue), and IR (purple) play a role in lipolysis. Niacin and BHB interact with α_2-ARs to activate G_i and inhibit lypolysis. Isoproternol and epinepherine bind to β-ARs to activate G_s and promote the breakdown of triglycerides to FFAs. When insulin binds to IR cAMP breakdown is increased resulting in 5'-AMP, glycerol, and FFAs.

1.3 Microfluidics

To address some of the analytical deficiencies noted above, miniaturized analysis is capable of limiting dilution of components secreted by cells and increasing dynamic information. In fact, miniaturization is a long standing goal driving the development of todays technology. Stemming from this driving force, microfluidic devices were first reported in the 1970s when Stanford produced a microfluidic gas chromatography chip [23]. From this point forward, essentially all types of analytical methodologies were attempted to be scaled down to the microfluidic scale. Microdevices can be used simply as a means to physically separate sample components for storage or off-chip analysis [24, 25, 26], but detection methods have also been developed for on-chip sensing [27, 28]. Absorbance [29, 30], fluorescence [31], chemiluminescence [32, 33], and refractive index measurements [34] have all been incorporated to be measured directly from the chip [35]. The ultimate goal for many of these devices is to incorporate sample processing, separations, detection, and readout into a single microfluidic device. Combinatorial devices are often refereed to as "lab-on a-chip" and "organ- on a-chip" platforms, and they are one of the most rapidly growing subsections of microfluidics. However, before specific microdevice applications for endocrine tissue are described, some of the foundational concepts and characteristics of microfluidic devices will be highlighted.

1.3.1 Microfluidic Device Fabrication

Originally, the main fabrication techniques for microfluidic devices included glass and silicon etching; however, these methods involve harsh chemical reagents and time consuming clean room based fabrication [36, 37]. In order to circumvent using specialized tools for the fabrication process, soft lithography techniques began to emerge as an alternative fabrication process. Not only does soft lithography almost eliminate the need for clean room equipment and dangerous chemicals, it is also a much faster a cheaper prototyping technique [23, 36, 38].

In order to fabricate a microfluidic chip using soft lithography, a silicon wafer with raised channel templates must first be created as a master mold. Channels are designed digitally and

then printed as high resolution photomasks. Depending on the application, photomasks are either mostly opaque except for the design region, or they are transparent in all regions except for the designs. There are two main forms of photoresist associated with photolithography; positive and negative. In negative resists, when ultra-violet (UV) light passes through the mask, only the regions exposed to light will polymerize and become more resistant to solvent washes. When positive photoresists are exposed to UV light, they become more susceptible to the developer solvent allowing exposed regions to be washed away [39] Most devices shown in this dissertation were fabricated using a negative photoresist, specifically SU-8, due to its robustness and rigidity for multiple templating cycles.

Once the silicon master wafer has been fabricated, it can be used as the template for soft lithography devices repeatedly until it is physically damaged or a new design is desired. One of the most predominantly used polymers for microfluidic device substrates in soft lithography is poly(dimethylsiloxane) (PDMS). PDMS is an ideal candidate for rapid prototyping of microfluidic designs because it is cheap, easy to use, optically transparent at wavelengths down to 280 nm, biocompatible, air-permeable, and has surface groups which can altered with a variety of surface treatments [36, 38]. Monomeric PDMS is mixed with a crosslinking catalyst and poured onto a photoresist patterned silicon wafer to form polymeric PDMS in the form of the wafer design. Once the PDMS has fully cured, it can be peeled off the wafer and prepared for use (Figure 1.4).

Native, cured PDMS is inherently hydrophobic; however, plasma oxidation air plasma treatment can be used to form silano groups on the surface, rendering the channels temporarily hydrophilic. The surface of the PDMS can revert back to its original state through the migration of unreacted PDMS monomers [40, 41]. By applying additional hydrophilic surface treatments, a more permanent surface can be achieved. Additionally, untreated PDMS has been proven to swell in organic solvents and absorb small molecules, dyes, and proteins [40]. Surface treatments can be performed to produce optimal channel conditions for sample type and device application [25, 41, 42]. In reference to on-chip cell culture, there are a variety

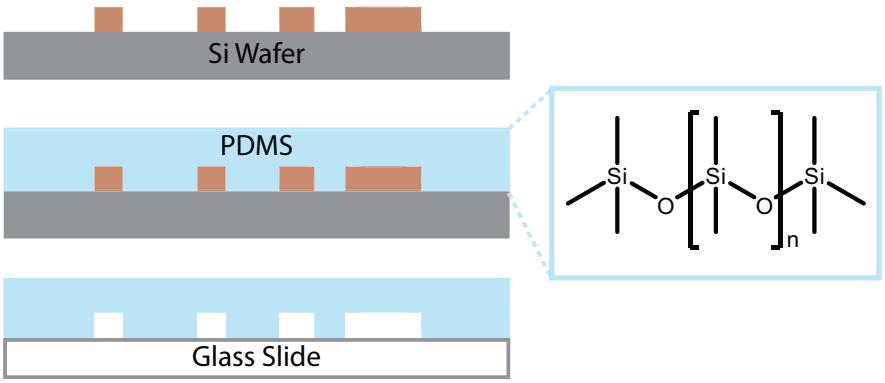

Figure 1.4: **Soft lithography fabrication of microfluidic devices.** Uncured PDMS is poured over a clean silicon master wafer. After PDMS has cured, the solidified polymer can be removed from the master wafer. Channel design impressions are left in the PDMS. Glass slide and PDMS can be plasma oxidized and bonded together to form the final microdevice.

of modifications that improve qualities such as cell adhesion, protein absorption, and overall flow of the device [43]. In the following chapters, all devices are fabricated via PDMS and are bonded through air plasma oxidation and surface treated with BSA (aqueous platforms) or Aquapel (organic platforms).

1.3.2 Properties of Microscale Environments

Microfluidic devices typically maintain channel dimensions between 10-100 μm, with volumes in the micro down to femto liter. At such small dimensions, physical and chemical properties of the micro environment do not mirror those at the macro scale. Flow profiles, diffusion, mixing, and surface properties are some of the most impacted characteristics in microdevices. Because of this, bench-top methods cannot simply be scaled down to the microscale and expected to function properly. Devices must be designed with the unique properties of the microscale environment in mind, in order to produce microdevices which can accurately mimic their macro scale counterparts.

1.3.2.1 Flow and Mixing in Microchannels

Liquid flow in macroscale environments such as plumbing inside a house can be classified as chaotic or turbulent. When liquid flow is confined into microchannels, turbulent flow is lost and laminar flow profiles dominate. Flow velocity (υ), channel length (l), and kinetic viscosity (μ) are all determining factors in flow classification. Typically, the Reynolds number (Re) is calculated to determine flow profiles (Equation 1.1). Channels with Re <2000 maintain laminar flow, while channels Re >2000 exhibit turbulent flow. Microfluidic systems typically exhibit Re <10, meaning that laminar flow dominates and streams in the microchannels flow side by side. The interfaces between laminar solutions allow for liquid mixing only by diffusion across the liquid-liquid interface [44, 45]. While this property can be advantageous, customized fluid mixing is often required for on chip reactions and sample homogeneity. Microstructures such as grooves in channel walls or curved, serpentine channels can passively mix fluids on the microdevice [46]. Active mixing can be accomplished through circular peristaltic pumping, electrowetting, and acoustic actuation [46, 37, 47]. Incorporation of mixing mechanisms is imperative for many biological assays done on-chip. While active mixers can be very accurately controlled and actuated rapidly (milliseconds), they require complex structures and external pumps and electronics for actuation [38, 46].

$$Re = \frac{vl}{\mu}$$

Reynolds number equation. Flow velocity (υ), channel length (l), and kinetic viscosity (μ). (1.1)

Flow through microfluidic devices can be broken down into two categories: active and passive. Much like mixing, active flow control requires internal microstructures and external vacuum control through syringe pumps, solenoids, and vacuum pumps. Pumps and solenoids can be used to control flow rate through the microdevice. Simple, straight channel devices

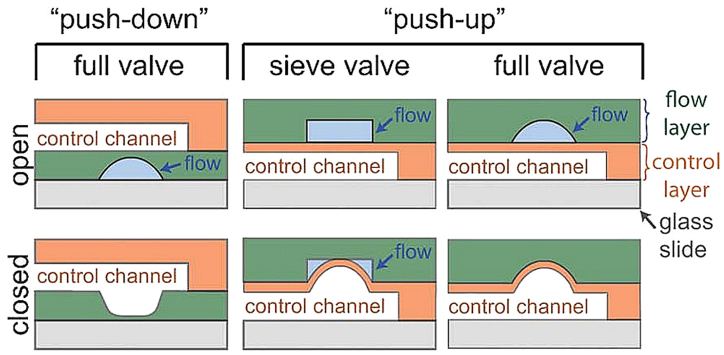

Figure 1.5: **Microfluidic valve designs.** Side view of two-layer push-down and push-up devices. Pressurization of control channel deflects membrane separating the layers, closing valve (compare top and bottom). Valves with square flow channel profiles leave pockets of fluid flow (blue), creating a sieve (push-up configuration, left column). Valves with rounded flow channel profiles seal completely (push-up configuration, right column) Reproduced from [50] with permission of The Royal Society of Chemistry.

can only be moderately controlled and are not generally conducive for multiplexing and on-chip assays. Elastomeric valves and pumps can be built into devices for precise fluid control. Not only can these structures aid in flow rate control, but they can also function to start/stop and divert flow [37, 48].

Incorporation of valves into microdevices requires multilayer chip designs with thin, elastomeric membranes between channel layers. Two most common valve types are push-up and push-down valves (Figure 1.5). A thin membrane separates a fluid channel layer and a control channel layer, and the valve is actuated by applied pressure in order to close the fluid channel [49]. In push-up valves, the fluid layer is on the top, and the control layer is on the bottom; whereas in push-down valves, the opposite is true. Rounded fluid channel, geometry produces a better seal when closed as compared to square flow channels which exhibit flow leakage in the channel corners. Push-up valves require lower pressure for membrane actuation and are therefore more commonly incorporated into devices [49, 47, 50].

1.3.3 High Throughput Devices

Valved devices can be readily scaled from single throughput to high throughput because of their ability to redirect flow. Inlet and outlet ports can be shared by many channels without cross contamination. Valve actuation can be digitally controlled through pressurized solenoids directly connected to logic gate based computer programs. Digital control paired with the high performance of the microvalves allows precise liquid handling in the nanoliter scale, which is nearly impossible by hand. Sample solution of even a few μL can be pumped from a single inlet well into 10's-100's of assay channels for parallel analysis. Peristaltic micropumps in line with assay channels can rapidly mix sample and assay solution for high throughput, multiplexed devices. The trade off with this concept is that the higher number of valves and pumps in a device, the more difficult it is to fabricate, program, and use these chips [51, 48].

1.4 Microfluidic Cell Culture

In vitro cell culture methods were first established in 1912; interestingly, they have not significantly evolved since then. These low throughput, high volume methods have served well for maintaining and growing cell lines but are not adequate methods for dynamic interrogation of cells [52]. Because microdevices are capable of meticulous handling of small volumes, cell treatments can be applied with great accuracy to thousands or single cells in a highly controlled fashion that would be impossible in a Petri dish or culture flask. In conventional culture systems, cells remain in stagnant media which accumulates secretions and waste over time. In flowing microfluidic systems, media is constantly being replaced and washed over cells, much like how fresh blood bathes cells in the body.

In 2007, Stephen Quake's group published a fully automated microfluidic cell culture system involving 96 separate culture chambers on a single device (Figure 1.6) [53]. Cell chambers were 60 nL in volume, and media was supplied to each chamber from a 16-input mixer and multiplexer, allowing individually formulated media solutions for each chamber

that could be distributed individually or by groups. In this report, human primary mesenchymal stem cells were cultured and monitored in parallel with customized wash times, volumes, and media composition. The incredible flexibility of this fully automated device provides a high throughput platform that can be customized to fit a wide variety of cell types and treatments. Additionally, because of the small cell chamber volumes, reagent and media use is nominal (<30 μL per reagent) compared to that of traditional systems. A study of this magnitude could not be performed at the macroscale with the same precision and control over cell maintenance, proliferation, and differentiation. For this reason, the high complexity of this device is overshadowed by the experimental possibilities it has to offer.

Incorporating sample preparation, separation, and analysis onto a single device is another advantageous application of actively controlled microfluidics. An example of this is from the graduate work of my adviser, Christopher Easley, where he helped develop a fully integrated microdevice capable of accepting whole blood for genetic analysis in under 30 minutes [54]. Murine blood samples containing *Bacillus anthracis* were applied directly to the chip and purified through solid phase extraction. Target sequences were then amplified through PCR and separated via microelectrophoresis. On chip valves provided means for sample flow control, active pumping, and injections (Figure 1.7). Amplified sample and DNA standards could be injected simultaneously for analysis of both amplicon presence and size. Fully integrated devices capable of accepting complex biological samples are ideal for rapid detection.

Microfabricated valves and external controls for pressure, temperature, voltage, etc have made it possible for microfluidic devices to perform complex flow profiles and mixing as well as on chip assays and sample analysis. In most cases, the actions performed on these microdevices are impossible to do on the macroscale and would be near impossible on the microscale with out active controls. However, while the advantages of microfluidic platforms have seemingly high potential to impact cellular biology, there is still a disjunction between the research focused on designing and engineering microdevices and biological research [55,

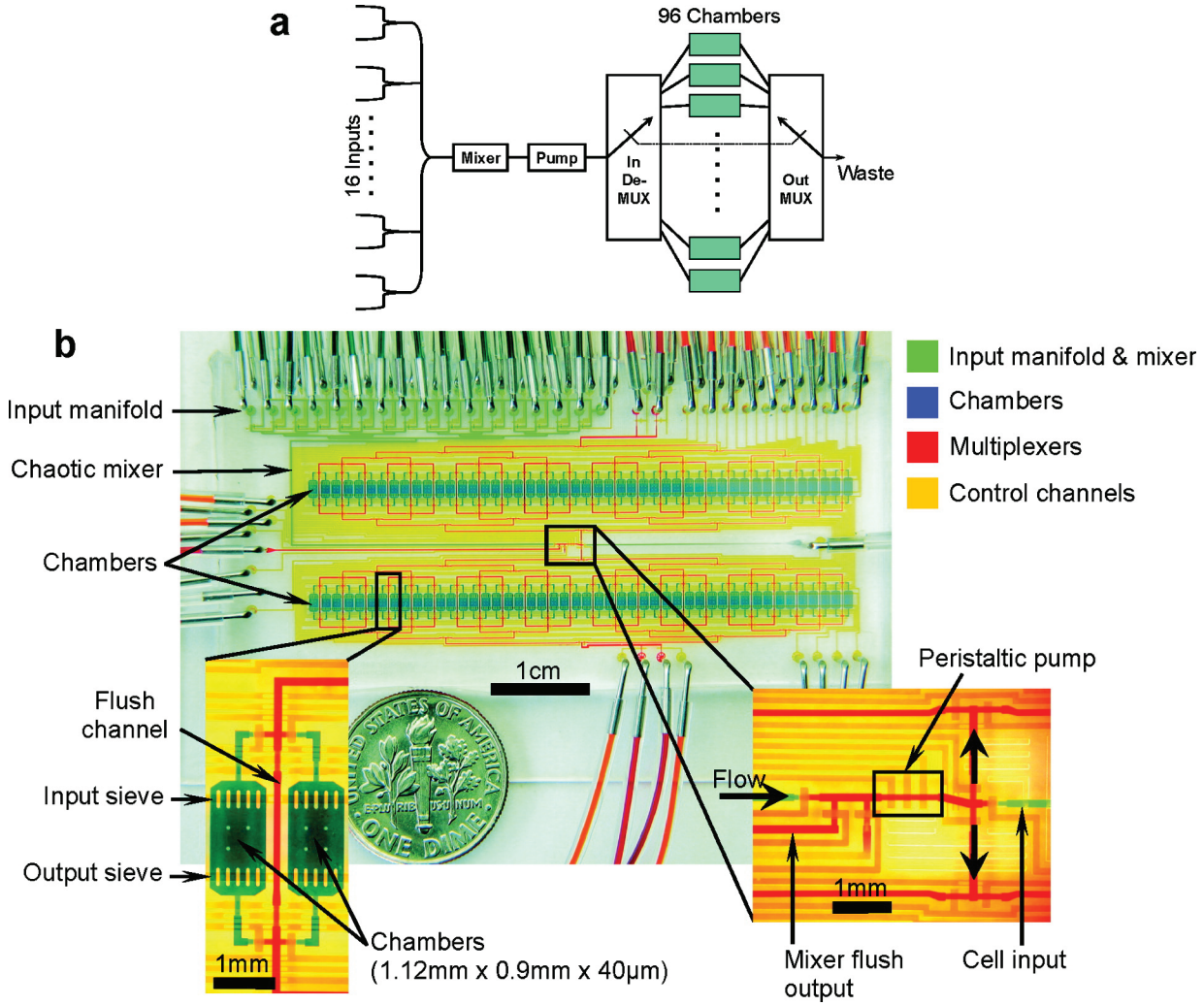

Figure 1.6: **High throughput cell culture device.** A) Simplified schematic diagram of the fluidic path in the chip (MUX, multiplexer). B) Annotated photograph of a chip with the channels filled with colored water to indicate different parts of the device. The left inset gives a closer view of two culture chambers, with the multiplexer flush channel in between them. The right inset shows the root of the input multiplexer, with the peristaltic pump, a waste output for flushing the mixer, and the cell input line. Reprinted with permission from [51]. Copyright 2007 American Chemical Society.

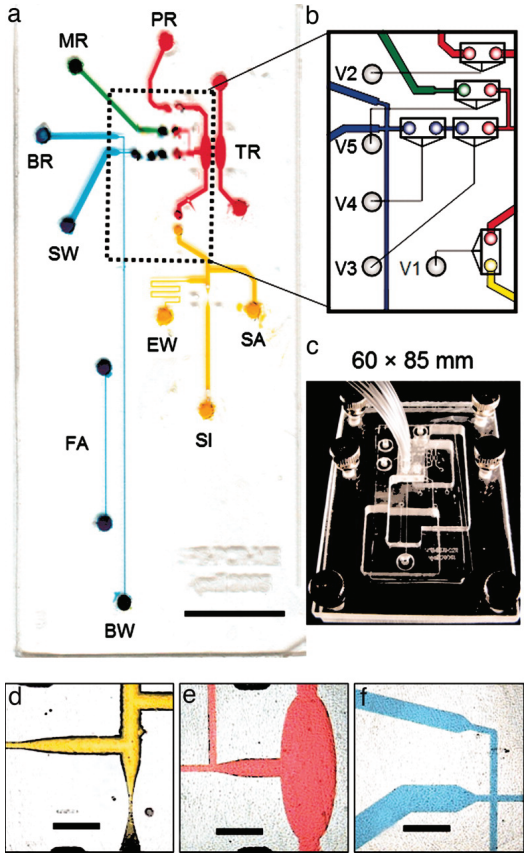

Figure 1.7: **Fully integrated microdevice for rapid genetic anaylsis.** A) Dyes are placed in the channels for visualization (Scale bar, 10 mm.). Domains for DNA extraction (yellow), PCR amplification (red), injection (green), and separation (blue) are connected through a network of channels and vias. SPE reservoirs are labeled for sample inlet (SI), sidearm (SA), and extraction waste (EW). Injection reservoirs are labeled for PCR reservoir (PR), marker reservoir (MR), and sample waste (SW). Electrophoresis reservoirs are labeled for buffer reservoir (BR) and buffer waste (BW). Additional domains patterned onto the device include the temperature reference (TR) chamber and fluorescence alignment (FA) channel. The flow control region is outlined by a dashed box. Device dimensions are 30.0 63.5 mm, with a total solution volume >10 μl. (Scale bar, 10 mm.) B) Schematic of flow control region. Valves are shown as open rectangles. V1 separates the SPE and PCR domains. V2 and V5 are inlet valves for the pumping injection, V3 is the diaphragm valve, and V4 is an outlet valve. C) Device loaded into the manifold. D) Intersection between SI and SA inlet channels, with the EW channel tapering to increase flow resistance. (Scale bar, 1 mm.) E) Image of PCR chamber with exit channel tapering before intersecting with the MR inlet channel. (Scale bar, 1 mm.) F) Image of cross-tee intersection. (Scale bar, 1 mm.) The relative sizes of the BR, SW, and BW channels create the difference in volume displacement during the pumping injection and affect how the resistance is dropped under an applied separation voltage. Reprinted with permission from [54]. Copyright 2006, National Academy of Science, USA.

56]. Microfluidic devices, especially those geared toward pushing the limits in bioanalysis and rapid detection, should not only be accessible to microfluidic "experts", but non-experts alike.

In order to fully exploit the potential that microfluidic bioanalysis devices have to offer, there needs to be a better balance between device complexity and application. The field of microfluidics is rapidly growing, but it is expanding at a much slower rate. More and more microfluidic devices and techniques are being developed by microfluidic experts, while fewer of the devices are being extended for use to non-experts. In some cases devices could be of immediate use for biological studies, but many researchers that would benefit the most are either not aware of the devices or they are not capable of using them on their own. On the other hand, while some devices are novel and applicable to biological samples, they are not standardized, making it difficult to perform biologically relevant studies with easy to interpret results. In order to bridge these gaps, microdevices need to be designed in such a manner that specialized equipment is not required to fabricate and operate these devices. The microdevice designs presented herein represent our efforts to provide easy to use, biologically relevant platforms for both microfluidic experts and non-experts.

1.5 Endocrine Tissue on Microfluidic Devices

Microfluidic platforms offer a variety of advantages for in depth interrogation of biological tissue and cell dynamics. Reduced sample requirements, precise control of small volumes, rapid prototyping, bio-compatibility, and the ability to incorporate direct detection methods allow for microscale studies to be performed on tissue which are unattainable on macroscale platforms. By focusing on simple devices which are highly applicable to current needs in bioanalysis, novel investigations can be performed in order to elucidate mechanisms of cell dynamics. The following sections provide a brief overview of current microfluidic methods in reference to endocrine tissue culture.

1.5.1 Pancreatic Islets

To date there are several microfluidic research groups which culture and sample pancreatic islets on microdevices; however the majority of these publications utilize more complex chip designs as well as electrical interfacing and fluidic valving [9, 28, 57, 58, 59, 60, 61]. The Kennedy group has published many reports for on-chip islet monitoring. In 2009 they described a radial, glass chip capable of high throughput, automated, on-line insulin monitoring from individual islets simultaneously (Figure 1.9). Up to 15 islets could be tested at once with 10 sec temporal resolution. Insulin levels were recorded through a competitive immunoassay downstream from the assay region where samples were mixed with insulin antibodies and FITC-insulin. While the islet perfusion chambers were driven by pressure, immunoassay reagents were controlled by electroosmotic flow. Once samples and reagents had mixed, capillary electrophoresis was used in order to seperate the immunoreaction products. Additionally, Ca^{2+} oscillations could be visualized on chip with Fura-2. The fabrication of this chip is more difficult than PDMS devices; however, out of the 15 channels the authors report at least 13 were operational on each chip fabricated and individual chips could be re-used up to 10 times each before any decrease in chip performance was observed. While this chip allows for simultaneous monitoring of multiple islets with high temporal resolution, high voltage connections, relays, and computer controls are needed for the capillary electrophoresis operation.

David Eddington's group has developed microfluidic devices geared toward monitoring islet viability to improve islet transplantation processes. These chips can observe multiple groupings of islets at the same time on a three layer PDMS device (Figure 1.8) [59]. Insulin secretion, mitochondrial potential, and Ca^{2+} oscillations could be detected for both murine and human islets. Calcium oscillations and mitochondrial potential were imaged on chip, while perfusate was analyzed off chip via insulin ELISA. Imaging the cells gave high temporal resolution, whereas the insulin samples had a frequency of about 1 minute. This system does

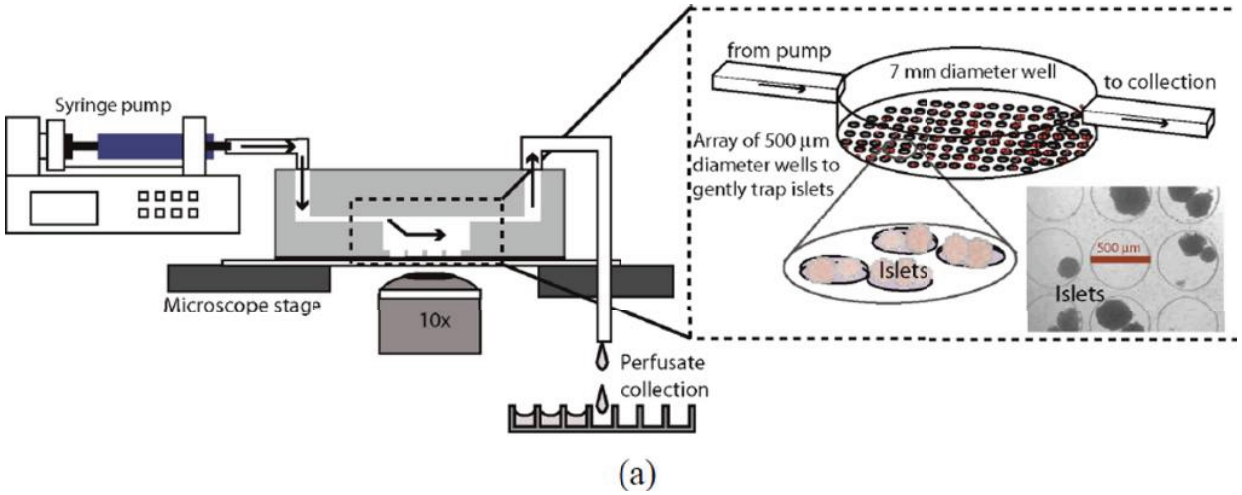

Figure 1.8: **Islet viability microdevice.** Design of the microfluidic device and image of the actual device. The schematic depicts the cross-section view and experiment setup (left part) and the isometric view of a single-chamber of PDMS microfluidic device is shown in the insert image (right part). The device contains three layers. The bottom layer consists of an array of small circular (150 μm deep, 500 μm diameter) wells that help immobilize the islets exposed to flow. The next layer is a large circular well (3 mm deep, 7 mm diameter) that encompasses the array of the tiny wells and the top-most layer is a rectangular microchannel (500 μm deep, 2 mm wide) that provides access to these wells. Reproduced in part from [59] with permission of The Royal Society of Chemistry.

require syringe pumps, but no internal valves or pumps are needed. One short coming of this device is the inability to monitor single islets.

The Easley Lab has previously designed passive, single layer chips in order to circumvent some of these issues for single islet secretion sampling (Figure 1.10) [25]. Valving and electronically controlled vacuum systems were replaced with a single hand-operated syringe and a fluidic manifold. This chip not only allowed users to easily stimulate and sample single islets, but staining and confocal imaging could also be performed on chip following sample collection.

1.5.2 Adipocytes

Primary adipose tissue can be difficult to culture on microfluidic devices, and for this reason very few studies have monitored isolated adipocytes and adipose explants on chip. In the majority of microfluidic adipocyte studies, 3T3-L1 cells are used rather than primary

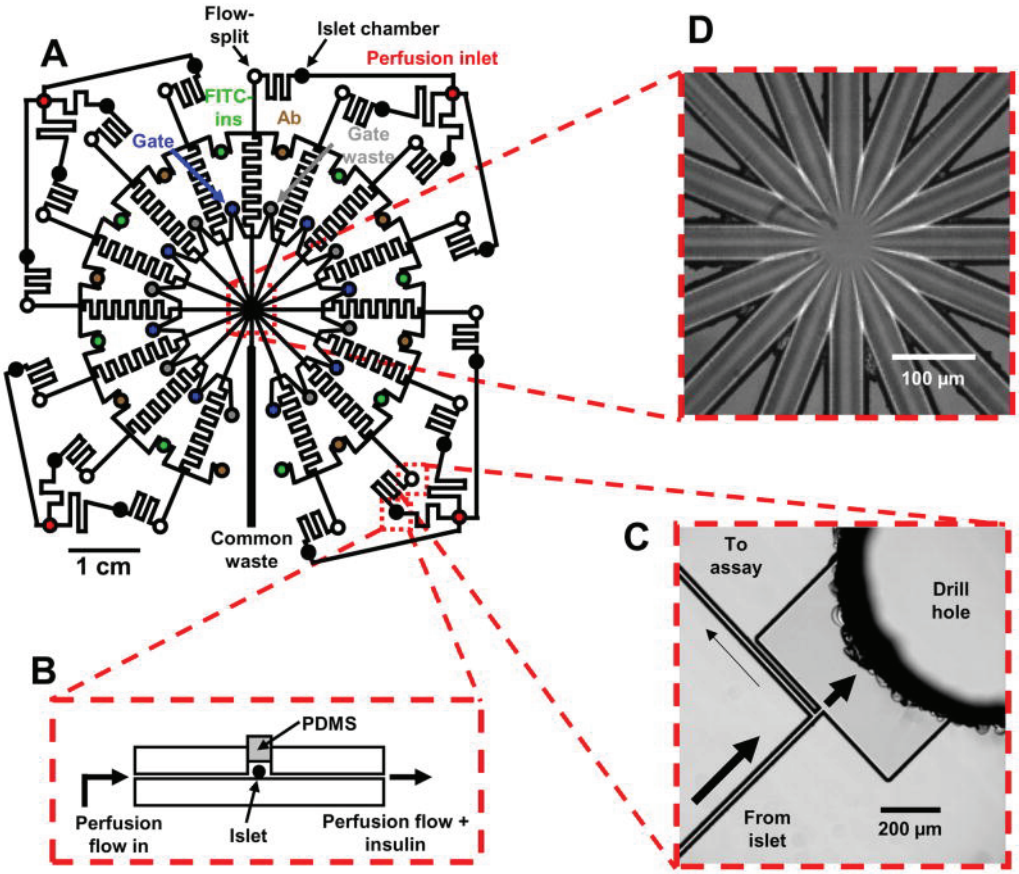

Figure 1.9: **High throughput, multiplexed device for monitoring insulin secretion.** Channel layout and images of detailed portions of a microfluidic chip for monitoring insulin secretion from 15 independent islets. A) The channel network of the entire device. Microfluidic channels are indicated by solid black lines, and circles represent fluidic reservoirs. Each type of fluidic reservoir (holding a different solution) is color-coded for clarity. B) Side-view representation (not to scale) of an islet perfusion chamber. Islets are loaded into the islet chamber with physiological buffer and then sealed with a PDMS plug under a stereomicroscope. Perfusion buffer flows over the entire islet and pushes all secreted insulin into the sampling channel. C) CCD image of an on-chip flow-split that allows the fast flowing insulin sampling stream to be compatible with the slower flow of the EOF-driven immunoassay reagents. Arrows indicate direction and estimated magnitude of flow. D) Brightfield image of the detection area taken with the CCD camera. Flow from 15 separation channels enter the center portion of the chip before flowing out through a single waste channel (bottom center in photograph). Reprinted with permission from [57]. Copyright 2009 American Chemical Society.

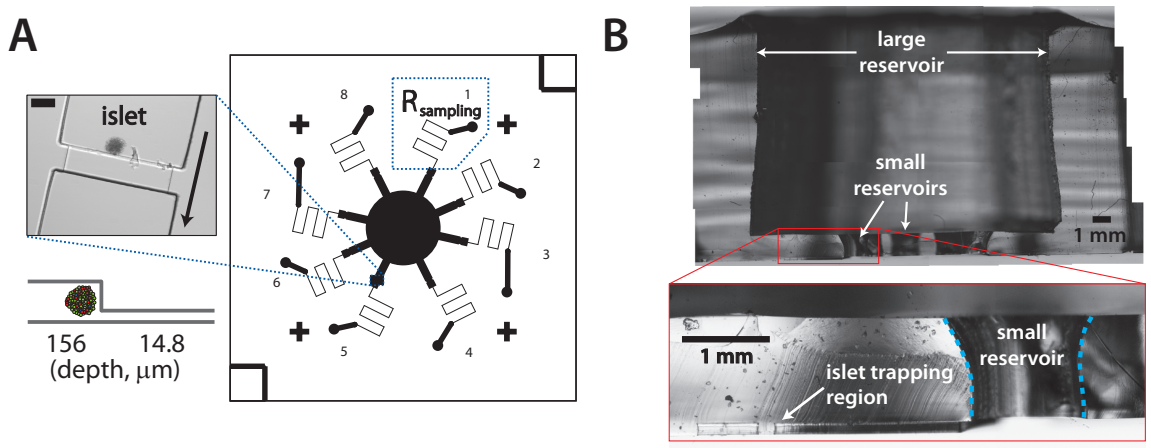

Figure 1.10: **Passive microdevice for single islet sampling.** A) Channel design for parallel sampling of 8 pancreatic islets. Multi-depth channels trapped islets at entrance of shallow (15 μm) channel. Scale bar is 100 μm. B) Cross section of typical device. Reprinted with permission from [25]. Copyright 2011 American Chemical Society.

adipose tissue [27, 62, 63, 64, 65, 66]. Of these studies, Clark et al (Kennedy group) was the first to report 3T3-L1 culture on chip as well as chemical measurements of secretions from the cells [27]. In this system, two microdevices were connected in series, first for cell culture and perfusion followed by a continuous flow assay chip. Microdevices were fabricated on glass through chemical etching and cleaning, physical milling, and incorporation of high pressure inlets. The cell culture device could be reversibly sealed so that cover slips containing 3T3-L1 cells could be placed in the chip, analyzed, and removed to make room for the next batch of cells (Figure 1.11). Secretion samples were measured on-chip using a modified commercially available absorbance based enzymatic assay for glycerol detection. Reagent and sample flow through the chip was controlled by an external syringe pump. In this system, cells could be maintained over several hours for continuous, near real-time analysis of glycerol concentrations (90 s delay between perfusion chip and assay chip).

After the investigators established the capacity for this microdevice design as an adipocyte culturing and sampling platform for glycerol, they developed a slightly modified version in order to monitor non-esterified fatty acids (NEFA) (Figure 1.12) [65]. One advantage to

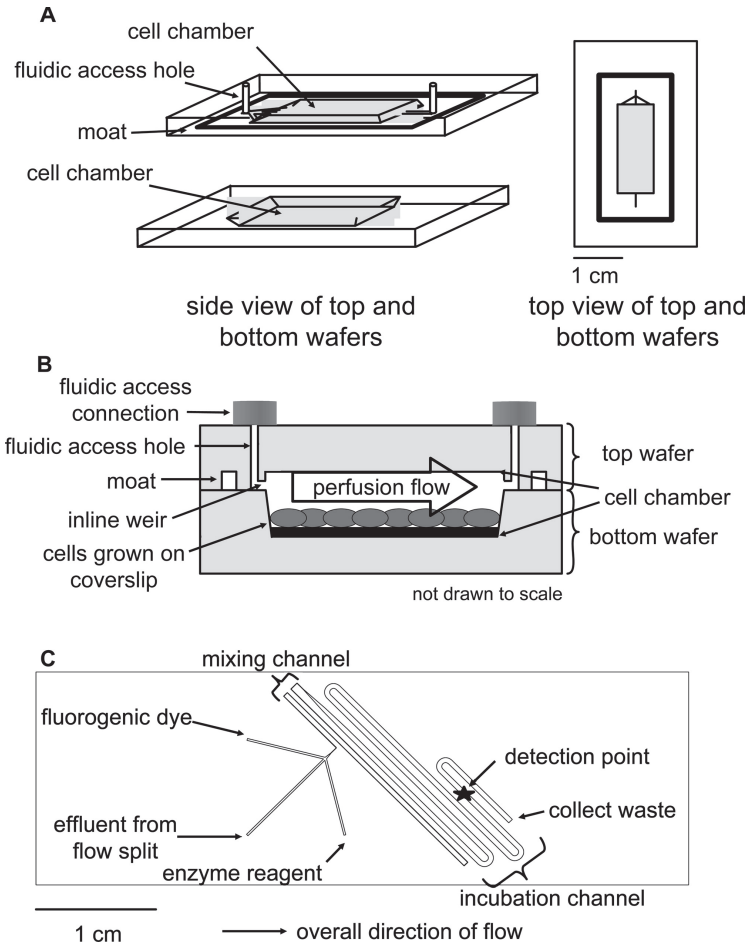

Figure 1.11: **Two-chip device for sampling of glycerol from 3T3L1 cells.** A) A diagram of the perfusion cell chip depicts the two separate wafers employed in this work. The wafers were reversibly sealed with the aid of an in-house built compression frame. B) A side view of the perfusion chip displays the cell chamber, which contained 50,000 differentiated adipocytes. Perfusion solution washed over the cells to sample secretions released from the cells. C) The enzyme assay chip was capable of performing on-line mixing of three solutions and on-line detection of the enzymatic product. The layout shows the initial mixing channel connected to the incubation channel. Reprinted with permission [27]. Copyright 2009 American Chemical Society.

the modified chip design was that instead of having two separate microdevices for cell culture and assaying, this chip combined both regions into one device, cutting the 90 s time delay down by 64%. This three layer device was also resealable for cell insertion, and had a reduced total channel volume so that 10x less reagent volume was needed in comparison to the original design. While these systems offer high temporal resolution and the capacity for coupling with alternative enzyme assays, the complexity behind the chip fabrication and operation will likely make their use impractical for non-expert users.

A few years later, the Kennedy group combined both glycerol and NEFA detection onto a multilayer PDMS device for simultaneous multiplexed measurements from 3T3-L1 cells (Figure 1.13 and 1.14) [66]. Converting to PDMS instead of glass reduces the amount of harmful chemicals used in the fabrication process; however, since it is a multilayered valved device controlled by pumps and pressure lines, there are still complicated aspects to the

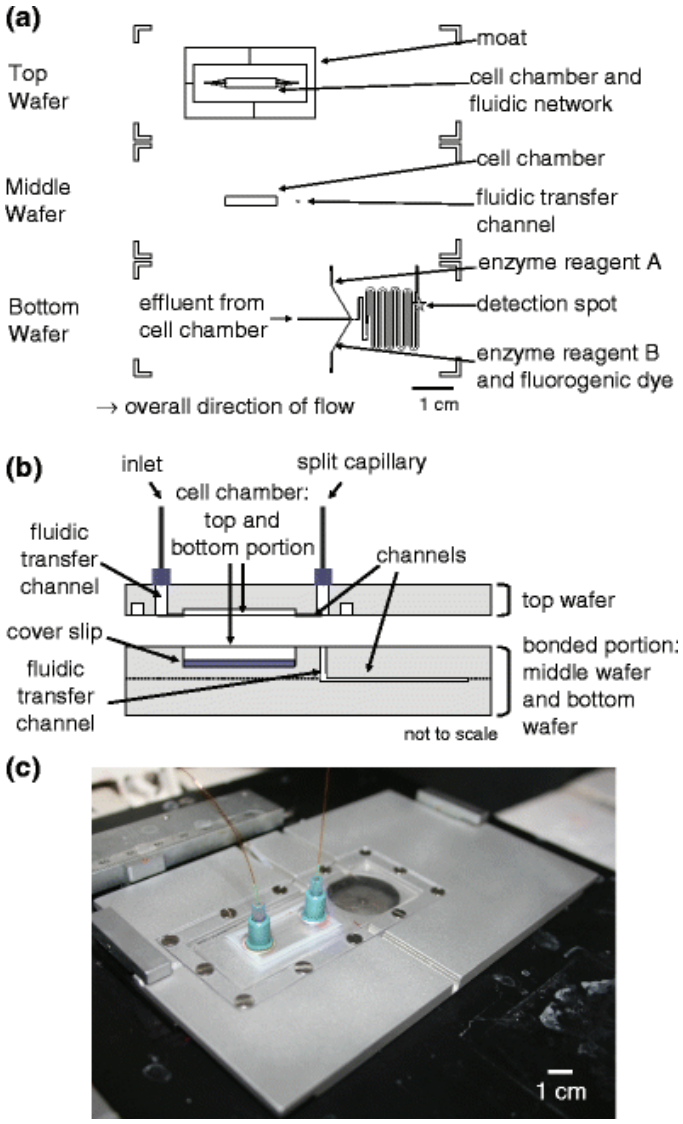

Figure 1.12: **Multilayer device for perfusion and sampling of 3T3-L1 cells.** A) The multilayer device was comprised of three separately etched glass wafers that integrated a cell perfusion chamber and fluidic channels for on-line mixing of the fluorescence-based enzyme assay. B) A side view of the cell chamber depicts the bonded and reversibly sealed portions of the device. C) An in-house-built aluminum compression frame functioned to compress the three glass wafers together enabling reversible sealing as well as to serve as a microscope stage holder. Reprinted with permission from Springer. Copyright 2010 [65], Analytical and Bioanalytical Chemistry.

device assembly and use. Additionally, to prevent hydrophobic fatty acid absorption to PDMS, channel surfaces had to be pretreated before use. Surface treatments of 20 mM SDS were applied several days after fabrication to allow the PDMS to return to its native hydrophobic state after bonding. Not only does this add an additional preparation step, but it also adds days of waiting before the devices are fully functional. For comparison, we have previously established a surface treatment for blocking absorption of fluorescent molecules, proteins, and fatty acids by treating freshly bonded PDMS chips with 0.1% BSA for 1 hour [25].

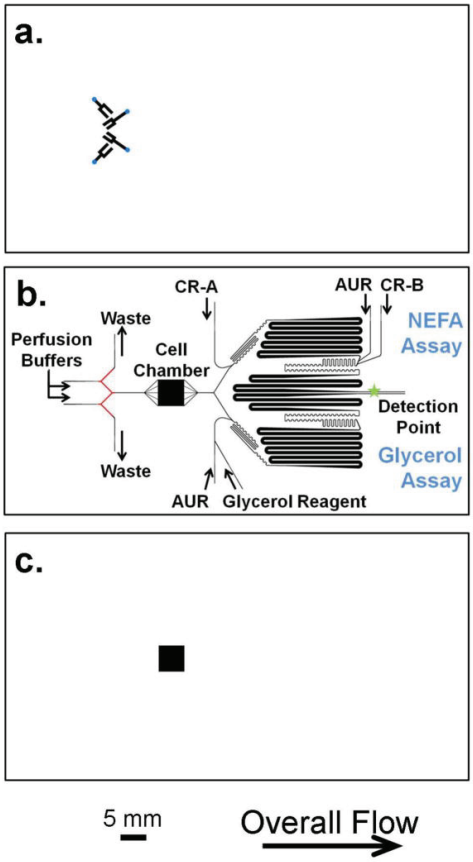

Figure 1.13: **Multilayer device design for dual analysis of glycerol and NEFA.** The control layer A), the reaction channel layer B), and the base chamber layer C) fabrication patterns are shown. The fluorogenic dye, Amplex UlraRed, is abbreviated as AUR. The blue circles in A) represent the points where access holes were punched through the PDMS, and the red line in B) indicates the portion of the design that was fabricated with AZ photoresist. Reprinted with permission from Springer. Copyright 2014 [66], Analytical and Bioanalytical Chemistry.

1.5.3 Adipose Explants

In 2015, Stephen Quake collaborated with researchers in Italy to develop a method for monitoring glucose uptake from human adipose explants on a microfluidic device (Figure 1.15) [67]. Traditionally, adipoctyes are cultured as 3T3-L1 cell lines or isolated, primary adipocytes that have been reconstituted in collagen; however, these cells do not completely represent in vivo conditions and architecture. With biopsy explants, 3D formation of the cells are retained as well as the local connections between cells. By incorporating explants onto a microdevice, this report not only gained the advantages of microfluidic systems, but the also improved biological relevance by using explants.

The explant device was three layers fabricated in PDMS with automated, solenoid control over media flow. Tissue samples could be as small as 10 mm^3 and could be maintained for several days in this device. Fresh media flow was constantly perfusing the cells, and

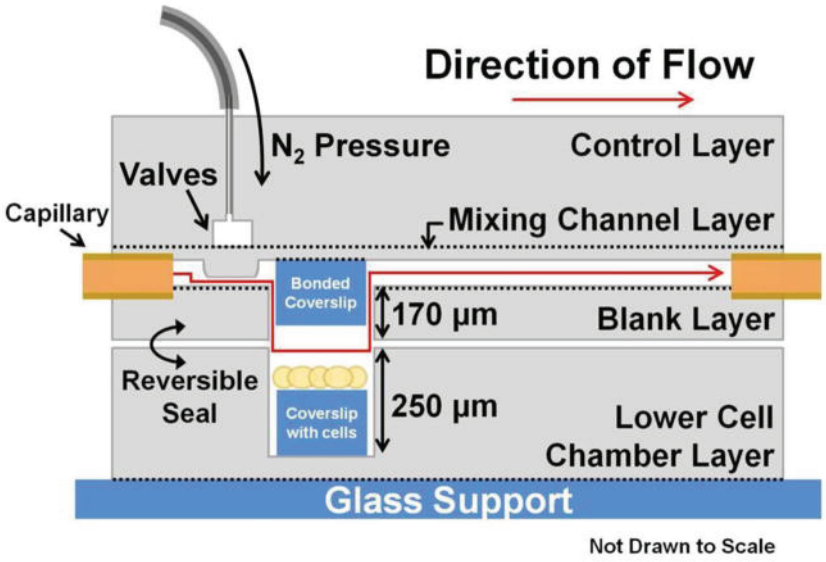

Figure 1.14: **Side view of multilayer device construction.** The dotted lines represent the interfaces between layers that were irreversibly bonded. Reprinted with permission from Springer. Copyright 2014 [66], Analytical and Bioanalytical Chemistry.

sample aliquots could be obtained by removing outlet tubes and temporarily replacing them with a dispensing needle. Outlet tubes were replaced, and the collected sample was applied to a glucometer to obtain glucose levels. While this chip represents a more physiologically relevant platform for adipose tissue, the temporal resolution of the system was constrained by the sampling process. Constant media flow is better representative of *in vivo* blood flow, but the fabrication and maintenance of the system is complicated. If on chip monitoring was incorporated onto the device, sample handling could be confined and temporal resolution could be improved.

We have previously developed a passive PDMS device capable of culturing primary adipocytes on chip (Figure 1.16) [26]. With this chip, we were able to circumvent the complications of collagen based culture on-chip and detect adiponectin fluctuations over an hour. However, there were design limitations which will be addressed more extensively in Chapter 2. For the second generation of our adipose chip, we wanted to not only improve upon the design, but also increase the temporal resolution, expand the detectable analytes, increase cell cover density on chip, and incorporate on chip detection methods.

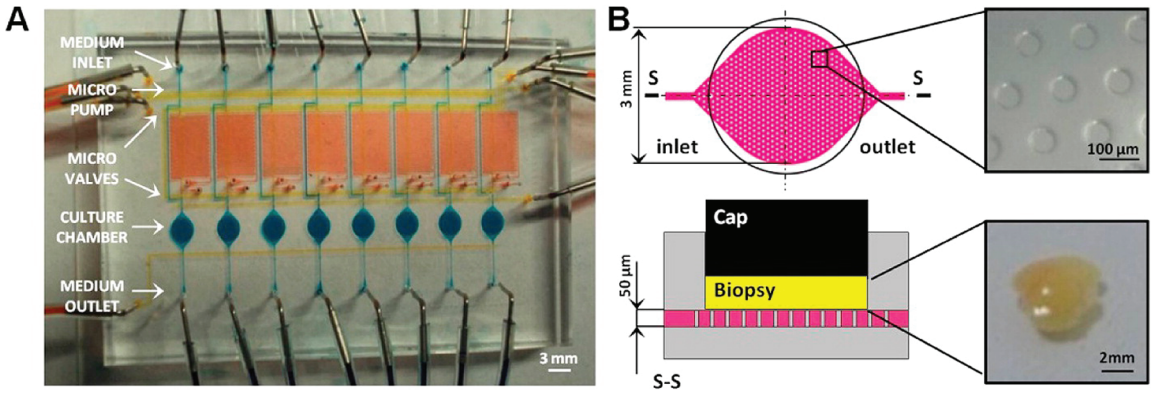

Figure 1.15: **Adipose explant device for monitoring glucose uptake.** A) Image of the multilayer microfluidic platform including 8 independent culture chambers (blue), each with its dedicated injection system (orange). Medium channels used during nonstimulatory conditions are shown in blue and control channels in yellow. B) Optimized configuration of the culture chamber (top view and section) where an array of microposts provide stable and precise placement of hAT sample. Medium distribution layer in the culture chambers is visualized with pink; yellow indicates the position of the biopsy into the culture chamber during microfluidic culture, and black indicates the polypropylene (PP) cap for sealing during culture. A representative hAT sample is also shown. Reprinted with permission [67]. Copyright 2015 American Chemical Society.

1.6 Concluding Remarks

As diabetes and metabolic disorders become more and more prevalent in society, the need for research geared toward a better understanding of endocrine tissue is also increasing. Specific cell types and proteins have been identified as major contributors to these disease states, but current culturing platforms and detection methods are insufficient with respect to monitoring cell secretion dynamics. Microfluidic platforms can be utilized in order to overcome obstacles such as stagnant cell environments and the need for high cell numbers and reagent volumes while also providing the capability to monitor cells in real-time with minimal disruption of the tissue. Current microfluidic methods for cell culture and secretion sampling allow for dynamic studies to be conducted on tissue which would be impossible to do on macroscale platforms. While there are many advantages to micro devices, adaptation of these devices to biological applications has been slowed due to complex chip designs and lack of communication between microfluidic experts and non-experts.

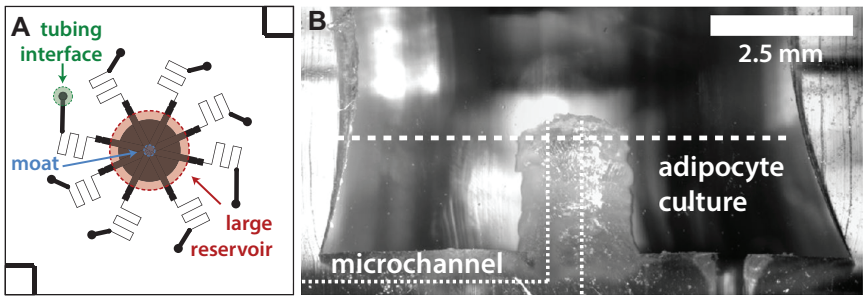

Figure 1.16: **Microfluidic design for isolated adipocytes.** A) Channel design for device. Cell culture region (red) was defined by hand fabricated inserts with central impression for moat region (blue). B) Cross section of typical device. Raised moat region allowed for fluid flow over isolated adipocytes without collagen blocking the channels.

Within this dissertation, the main goals for our work with endocrine tissue on a chip are to decrease the difficulty of device fabrication and operation, improve temporal resolution for both sample collection and on-chip sensing, and develop methods for culture of primary adipocytes on microfluidic devices with both on and off chip sample analysis which can be utilized even by research groups who do not focus on microfluidics. Chapter 2 and Chapter 3 of this work will discuss fabrication methods for interfacing millimeter scale templates with microchannels for culture, sampling, and analysis of both pancreatic islets and primary adipose tissue - with a predominant focus on adipose tissue. As we have pushed further into biological applications of cell culture in microfluidics, it became very obvious that there is a lack of assays which can easily accommodate small sample volumes, high temporal resolution, and a wide variety of target analytes. We thus have developed small volume immunoassays which targets proteins associated with endocrine disorders. In order to maximize applications, the overall design was generalizable, such that antibodies could easily be switched in the assay to target other proteins for which at least 2 antibodies are available. Details on these assays will be discussed in Chapter 4. Finally, while my work predominately focuses on the biological aspect of microfluidics, Chapter 5 represents a collaborative project which combines a previous droplet microfluidics device from our lab with metal ion sensing through inorganic ligands synthesized in the Gorden lab. Again since microfluidics offers so many advantages over traditional fluidic systems, an underlying goal in work within the Easley

laboratory is to share our expertise on microfluidics as well as expose other researchers to microfluidic tools which can further their work.

Chapter 2

Macro-to-Microfluidic Interfacing Using 3D Printed Device Templates and Fluidic Manifolds for Primary Endocrine Cell Culture and Time Resolved Sampling

2.1 Introduction

Our group's first microfluidic device was designed for passive flow control and high throughput secretion sampling from single pancreatic islets [25]. The monolithic, PDMS chip was designed such that it could be operated via a single hand held syringe and no external power sources. A rigid, polymer template was designed to mold a large fluidic reservoir suspended above microchannel inlets. This reservoir allowed for bulk media volumes between 200 - 400 μL while the cells themselves were confined to an islet trapping region in the microchannel (<1 μL in volume) [25]. Insulin secretion samples were collected over the span of an hour from individual islets and analyzed off chip with a murine insulin ELISA kit. Real time $[Ca^{2+}]_i$ measurements and volumetric confocal imaging were also conducted on-chip.

A key component to this device design was the bulk media reservoir and its interface to the channels. This structure allowed simple and rapid changing of media without disturbing the islets. A pipette could be used to quickly remove the bulk media and add fresh media and stimuli, while the cells remained in the cell trapping region. The physical switching of solution was rapid ($\sim$ 10-15 sec), and the solution change was seen by the cells in <15 sec [25]. Having the cells almost immediately exposed to the new stimulants is imperative to generate accurate secretion profiles. Much like band broadening in chromatography, if the cells are slowly exposed to stimulant instead of a crisp injection, secretions from the cells would be temporally broadened.

After in depth characterization of the islet device, we then proceeded to adapt this design for primary adipocyte secretion sampling. Isolated adipocytes are inherently buoyant and therefore float in aqueous media [26]. Collagen is often used to anchor the cells to the bottom of wells in traditional, static sampling systems; however, it cannot be added directly to microfluidic channels as it will block flow through the device. In order to accommodate for collagen plating that would not impede flow, polymer molds similar to those used in the pancreatic chip fabrication were modified to include a 1 mm central depression which casts a raised moat region in the finished microdevice [26]. Additional details are included in this chapter.

While the polymer templates provided us a method for fabrication of monolithic, "pseudo" multilayer microdevices, there were some downsides associated with their use. Fabrication of each hand made template took <1 day from start to finish, with batch to batch variability as well as major design constraints. Additionally, each template had to be individually aligned by hand. Due to the templates' light weight and small dimensions, they were prone to shift out of alignment and even completely fall over during casting. By digitizing the design and fabrication of the inserts, more robust templates could be rapidly formulated with high design precision. We thus turned to 3D computer aided design and 3D printing to improve this process, as detailed within this chapter.

Although 3D printers are widely used, high costs, resolution limitations, and printing medium properties have limited their adoption as commonplace microfluidic instruments [68, 69]. While printing of complete microfluidic devices is possible with high resolution printers, the cost of printers with resolution in the tens of micrometers still exceeds the price range for a typical research laboratory or small company [69, 70, 71, 72, 73, 74, 75]. Additionally, many of the printers capable of printing well resolved microfluidic devices utilize printing materials that are not as optimal or biocompatible as PDMS (i.e. loss of gas permeability, loss of transparency, non-biocompatible) [75, 76]. Micro stereo lithography (MS) printers are becoming more affordable (below $2500) and also maintain low printing

resolutions ($\sim$ 50μm laterally and 50 μm vertically). It has been previously established that microfluidic device templates can be printed on MS printers; however, PDMS does not cure around the printing resin. Additional steps must be taken using specialized airbrushing equipment to properly prepare the template for soft lithography [74, 75]. More affordable printers (below $2500) can now be purchased with layer resolution (z-direction) less than 50 μm and spatial resolution in the hundreds of micrometers [74, 76]. While 3D prints on this scale are inadequate for fabrication of more traditional microfluidic devices (channels with 10-50 μm widths), they should be ideal for well resolved millimetre-scale fluidic interfaces.

To simplify our reservoir design even further, we transitioned into digitized, 3D printed templates for sculpting the millimetre-scale fluidic reservoirs into the above-channel, bulk PDMS. While the consequent devices maintained passive operation and single layer soft lithography, the channel designs were altered so that time resolved secretion sampling could be easily performed on chip. Additionally, 3D printed "accessories" were designed to improve the ease of device use as well as high throughput capabilities. Devices were proven functional by temporally assaying glucose-stimulated insulin secretion from <10 pancreatic islets and glycerol secretion from 2-mm adipose tissue explants, suggesting that 3D printed interface templates could be applicable to a variety of cells and tissue types. More generally, this work validates desktop 3D printers as versatile interfacing tools in microfluidic laboratories.

2.2 Experimental

2.2.1 Reagents and Materials

Insulin, D-glucose, $4-2-$hydroxyethyl$-1-$piperazineethanesulfonicacid (HEPES), nystatin, fluorescein, tetrahydrofuran (THF), KH_2PO_4, and NaH_2PO_4 were purchased from Sigma-Aldrich (St. Louis, Missouri). Bovine serum albumin (BSA), fetal bovine serum (FBS), NaCl, $CaCl_2 \bullet 2H_2O$, disposable culture tubes, sterile 96-well plates, nalgene rapid-flow filter units and bottle top filters (PES membrane, 0.2 μm pore size, sterile), polypropylene mesh (210 μm), and blunt ended needles were purchased from VWR (West Chester,

Pennsylvania). Penicillin-streptomycin, Minimal Essential Media (MEM) non-essential amino acids solution 100X, sodium pyruvate, L-glutamine, collagenase P, collagenase type I, and Dulbecco's Modified Eagle Medium (DMEM), $MgSO_4 \bullet 7H_2O$, was purchased from ThermoFisher Scientific (Grand Island, New York). Trimethylchlorosilane (TMCS) was purchased from Alpha Aesar (Ward Hill, MA). Channel masks were designed using Adobe Illustrator and printed via FineLine Imaging (Colorado Springs, CO). SU-8 photoresist and developer, silicon wafers, PDMS precursors, polymer casting resin, 3D printer and filament, disposable biopsy punches with plungers, and Tygon microbore tubing (0.508 ID x 1.524 mm OD) were purchased from Microchem (Newton, MA), Silicon Inc. (Boise, ID), Dow Corning (Auburn, MI), Smooth-On Inc. (Macungie, PA), Makerbot (Brooklyn, NY), Miltex (Plainsboro, NJ), and Cole-Parmer (Vernon Hills, IL) respectively.

2.3 Methods

2.3.1 Silicon Wafer Fabrication

New silicon wafers were acid cleaned in 1.0 M sulfuric acid for 30 minutes (rotary shaking at 250 rpm) followed by a 30 minute wash in ddH_2O. Wafers were then baked at 200°C for 15 minutes. Once the wafers returned to room temperature, SU-8 was spin coated onto the surface for desired channel depth. Microchip channel design was conducted on Adobe Illustrator, and these files were sent to Fineline Imaging (Colorado Springs, Colorado) for printing of negative photomasks (65,024 DPI). Microchannel masks were taped to a large glass slide and centered on top of the wafers before ultra-violet (UV) exposure. Pattered wafers were then washed in SU-8 developer and rinsed in IPA . Silicon wafers were silanized with TMCS before molding each batch of microchips through standard soft lithography using PDMS (Figure 2.1).

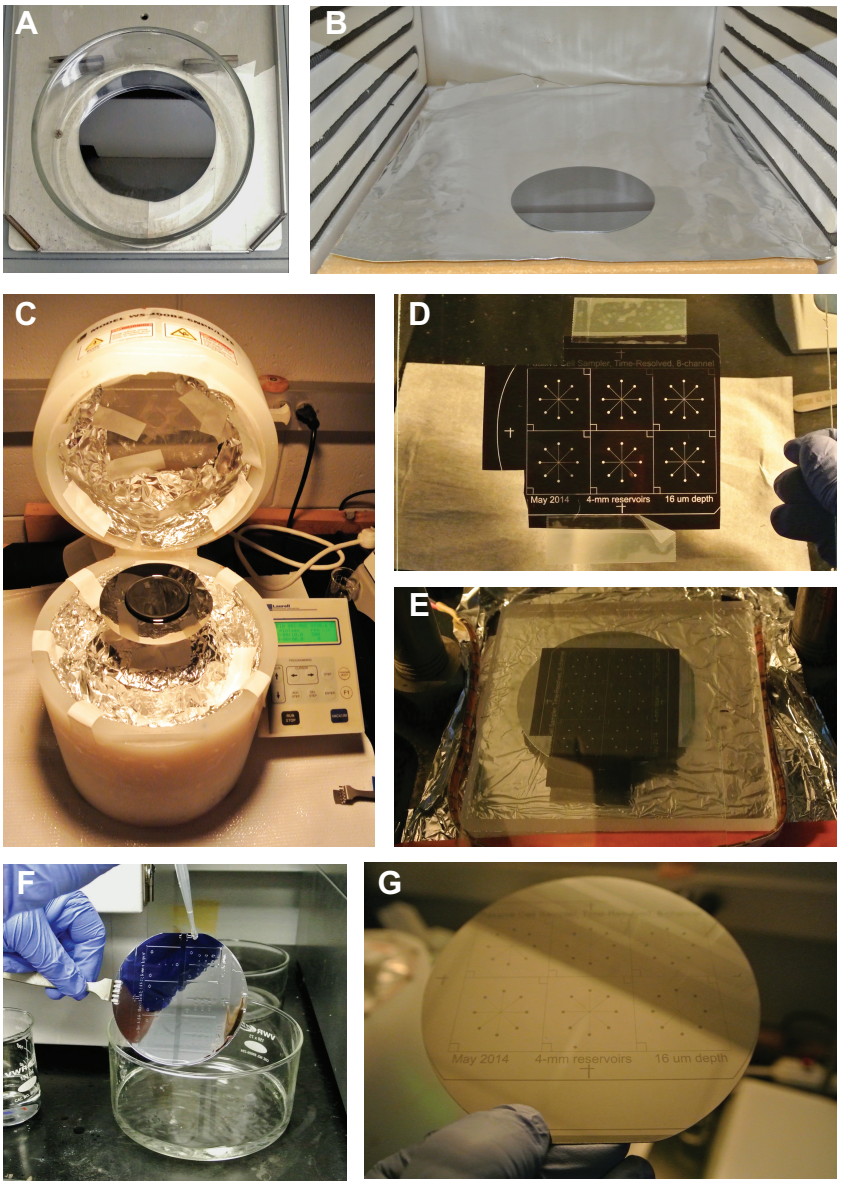

Figure 2.1: **Photolithography steps.** A) Wafer is acid cleaned on a rotary shaker. B) Wafer is baked at 200 C to remove residual water. C) Spin coating of SU-8 onto clean wafer. D) Microchannel transparency is taped onto a dust free glass slide. E) Wafer and design placed into UV lithography system for exposure step. F) Photoresist development step. G) Finalized SU-8 master wafer, ready for PDMS soft lithography.

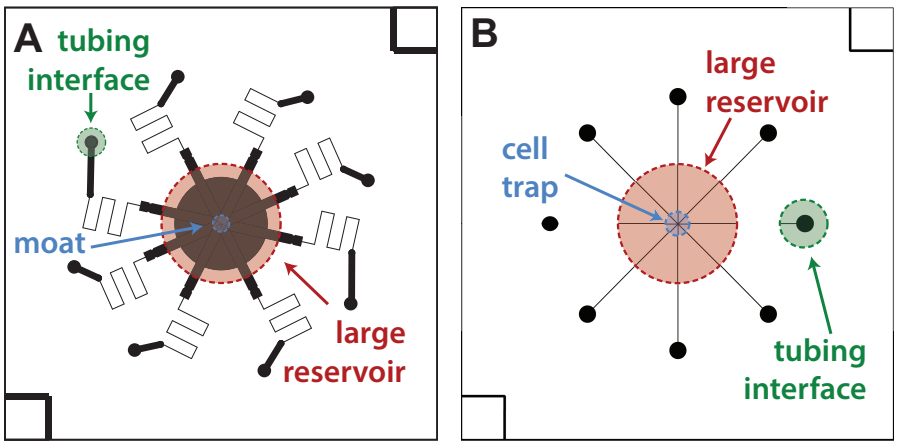

Figure 2.2: **Channel design for manual templates.** A) Isolated adipocyte chip design and B) islet or explant chip design. Large reservoirs are molded around the body of the template (red). For isolated adipocytes, the raised moat region (blue) connects the bulk media to the microchannels. Islets and adipose tissue explants can be placed directly onto devices in the cell trapping region (blue).

2.3.2 PDMS Microchip Device Design and Fabrication

2.3.2.1 Microdevice Fabrication for Hand Made Templates

For the first generation devices published by Godwin et al, two different heights of photoresists were patterned onto the silicon wafer master to function as the islet trapping region. Deep channels were 1.5 mm long, 600 μm wide, and 156 μm deep, where as shallow channels were 10.8 mm long, 60 μm wide, and 14.8 μm deep (Figure 2.2) [25, 26].

2.3.2.2 Microdevice Fabrication for 3D Printed Templates

In the straight eight-channel sampling device (Figure 2.2), the distance from the central channel intersection to each channel outlet was 7.5 mm, with 50 μm channel widths and ~16 μm typical channel depths designed to passively control flow rates. Six 1.0-in^2 designs (6.45 cm^2) were fit into one 4.0-inch diameter silicon wafer, generating a 2.0 inch by 3.0 inch (38.7 cm^2) rectangular photo-patterned region. For parallel curing of six devices, silicon wafers were cut to leave only the 2.0 x 3.0 in^2 rectangular channel designs. Small amounts of epoxy (5-minute set, Gorilla Glue) were applied to the bottom side of the wafer which was then

gently placed into the wafer alignment container (see Figure 2.9). Once the epoxy had set, wafers were silanized, and PDMS was added to the alignment container. 3D-printed interface templates (made of PLAF) were simply snapped into place on the container and allowed to cure at 50 °C for a minimum of 2 hours. Interface templates were then removed from the box, followed by the PDMS molds. The PDMS substrate, patterned with both micrometre-scale channels and millimeter-scale fluidic interfaces, was then diced into individual devices, and each device was bonded irreversibly to glass floor substrates (glass microscope slides) using a plasma cleaner (Harrick Plasma). Devices, such as the one shown in Figure 2.11, were then ready for cell culture, stimulation, and sampling applications.

PDMS precursors were mixed in a plastic weigh boat (10:1, base:curing agent) and stirred with a wooden spatula until sufficiently mixed. Uncured PDMS was then degassed until the polymer was bubble free. Double sided tape was placed onto the bottom of a cleaned silicon master wafer and attached to a square of aluminum foil. Edges of the foil were wrapped around the wafer and PDMS was poured on top of the encased wafer.

If interfacing templates were to be incorporated into the microchip design, the templates were placed into the degassed PDMS and aligned over the wafer channels. The wafer, templates, and PDMS were then placed into an oven to cure the polymer. Final placement adjustments of the templates were made and the PDMS was allowed to cure for ∼2 hours at 50°C (below the PLAF glass transition temperature of ∼60-65°C). Foil, templates, and PDMS were carefully removed from the wafer. Templates were extracted from the PDMS by running an X-acto knife or blunt ended tweezers between the template and PDMS. Razors were used to trim the bulk PDMS down to individual chips, while biopsy punches were used to punch inlet and outlet ports into the microchannels. Individual chips and glass slides were then washed and dried with methanol and N_2 gas. Clear Scotch tape was applied and removed from the surfaces of the channels and the glass slide. Glass and channel surfaces were plasma oxidized and then bonded to each other. If chips were to be used for cell

secretion experiments, BSA buffered solutions were added to the freshly bonded chips and the entire system was incubated for at least one hour before cell use.

2.3.3 Manually Fabricated Interface Templates

2.3.3.1 PDMS Mold for Ridgid Polymer Template

1 mm diameter holes were punched in a 1 mm thick slab of PDMS. The slab was then plasma oxidized and covalently bonded on a clean microscope slide. A 2-3 mm diameter plug was then punched out of a separate piece of PDMS and plasma oxidized to the 1 mm slab, centered between the 1 mm holes. 4-5 mm wells were punched in thicker PDMS ($\sim$2 cm height) and cut into individual pieces with small enough widths to rest on top of the thin PDMS slab without hanging off the sides. The thicker slab was then placed over the center of the 1 mm holes and 2-3 mm plug for a reversible seal (not plasma oxidized) to complete the mold (Figure 2.3A).

2.3.3.2 Polymer Template Fabrication

Pre-polymer solutions of Smooth-Cast (part A and part B) were measured into individual 1.7 mL sample tubes and degassed for 10 minutes. 100 μL of each part (1:1 by volume) were mixed in a PCR tube and degassed for a second time. This mixture was then carefully pipetted into the 1 mm holes in the base of the mold. The remaining volume of part A and part B ($\sim$1 mL) was mixed and degassed alongside the partially filled mold. The mixed polymer was then pipetted into the bulk of the mold and degassed a final time. Templates were allowed to cure overnight at room temperature. Once hardened, the body of the PDMS and template were carefully lifted off of the thin PDMS slab. An X-Acto^{TM} knife or blunt ended needle was used to peel the template from the PDMS mold (Figure 2.3B).

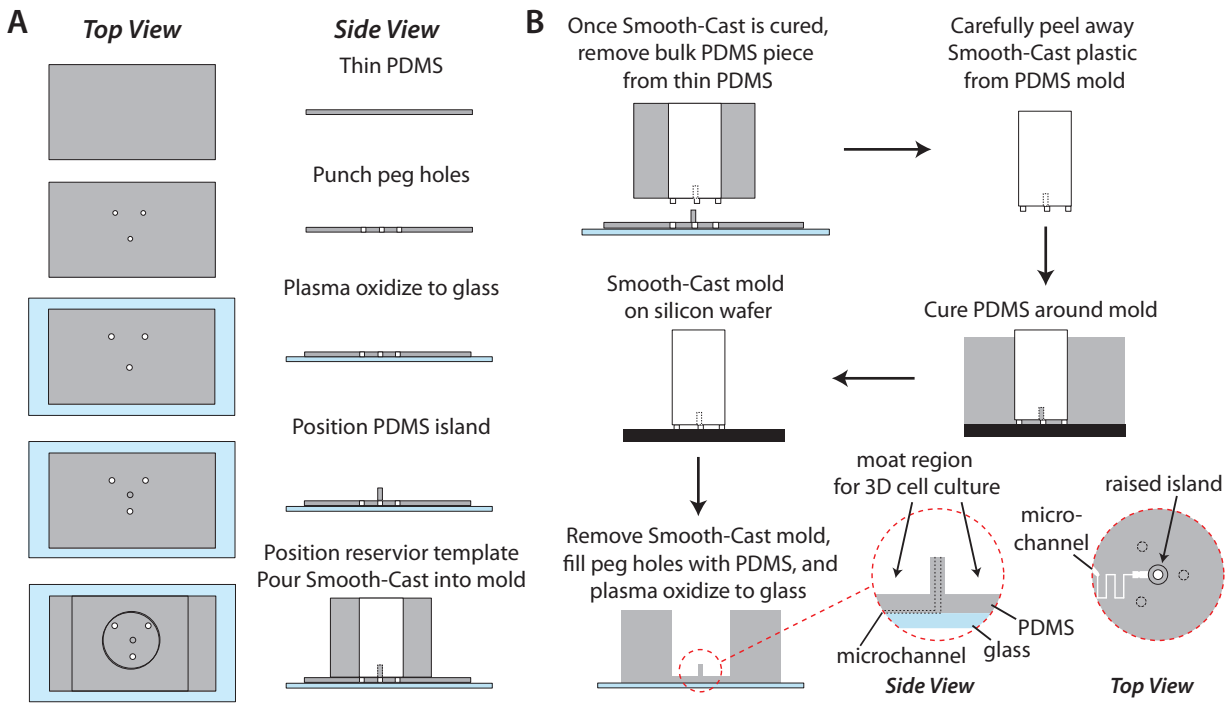

Figure 2.3: **Manual fabrication method for the Smooth-Cast 310 interface template.** A) The PDMS mold for the insert served as an initial proxy for the final device, including the raised island and moat region customized for culture of primary adipocytes in collagen. B) The resultant template was used to define a customized macro-to-micro interface to microfluidic channels for secretion sampling. Reproduced in part from [26] with permission of The Royal Society of Chemistry.

2.3.4 3D Printed Interface Templates

All 3D printed templates and devices were designed in SketchUp 3D modeling software, error checked in NetFab, and printed on a MakerBot Replicator 2 (100 μm layer resolution in the z-direction) with polylactic acid filament (PLAF, 1.75 mm diameter). When appropriate, surface smoothing of the printed objects was accomplished via exposure to THF vapor. 30 mL of THF was poured into a glass dish and heated to 80°C while covered. Printed objects were attached to a secondary lid via copper wire. Once the THF condensation level reached the top 25% of the dish, the lids were exchanged allowing the 3D printed objects to be suspended just above the liquid THF, where they were kept under THF vapor for 60 s. After treatment, pieces were rinsed with ddH_2O and allowed to degas for approximately 60 min at room temperature before use.

For surface characterization of the 3D printed objects, 10 x 10 x 5 mm^3 test pieces were printed. Control pieces were left untreated, while test pieces were treated with THF as previously described. After rinsing and degassing of the pieces, both were cured into a batch of PDMS. Once cured, the test pieces were removed from the PDMS, and the impressions of the templates were analyzed. Cross-sections of the impressions were sliced with a razor blade and mounted onto a glass microscope slide. Images were captured on a Nikon Ti-E inverted fluorescence microscope at 10X magnification, operating in wide-field transmittance mode.

2.3.5 Pancreatic Islet Isolation and Secretion Sampling

Pancreatic islets were isolated from C57BL/6 male mice as described previously [77, 78]. After isolation, islets were placed in RPMI media (10% FBS, 11 mM glucose) at 37°C and 5% CO_2 to incubate overnight. Islets were then transferred from RPMI media to low glucose imaging media (3 mM) at 37°C and allowed to acclimate for 1 hour. Following the low glucose starve, islets were transferred to a microchip containing either low glucose imaging media (3 mM) or high glucose imaging media (11 mM). Vacuum was applied manually to each

microchip channel for 5 minutes via a 100 mL glass syringe to achieve flow rates of ∼40 μL h^{-1}. After collecting sample for 40 minutes, tubing and plugs were removed from the outlet wells, and the sample volume was extracted using a pipette. Islet secretion samples were transferred from channel output wells to PCR tubes, diluted to 40 μL in BMHH, and stored at -20°C until quantification using a murine insulin ELISA kit (EZRMI-13K, Millipore).

2.3.6 Adipocyte Digestion and Microfluidic Culture

Collagenase type I was dissolved in phosphate-HEPES buffer (10 mg/ 8 mL) and placed in a water bath at 37°C. Epididymal fat pads were removed from C57BL/6J male mice as described previously [26, 15] and transferred to 4 mL of pre-warmed phosphate-HEPES buffer. Fad pads were transferred into a 2 mL snap cap tube, weighed, and minced for 2 minutes via surgical scissors. Collagenase was then added to the tube at 2 mL for every 1 g of fat. The suspension was pipetted up and down several times with a P1000 pipette. Tubes were placed in a rocking water bath (37°C and 120 rpms) for 30 minutes. Every 10 minutes during this time, the suspension was removed from the water bath and quickly pipetted up and down 3-5 times. 210 μm Spectra mesh was taped in a cone shape manner inside a funnel. The funnel tip was placed in the opening of a 5 mL glass test tube. Digested fat tissue was poured over the filter, followed by 3-4 mL of phosphate-HEPES buffer. Cell suspensions were centrifuged for 6 minutes at 900 rpm and 4°C. Infranatant was removed with an 18G 1.5 inch needle and small syringe. Cells were washed with 3-4 mL of phosphate-HEPES buffer, centrifuged at 4°C, and washed an additional time with phosphate-HEPES buffer. After the second wash, infranatant was removed and replaced with 3-4 mL of fat serum media. Freshly washed cells were then incubated for 30 minutes at 5.0% CO_2 and 37°C. Immediately before the incubation was complete, a collagen solution was prepared (4.5 mL collagen, 450 μL 10x MEM, 3-5 μL of 1.0 M NaOH). Cells were pipetted off the top of the serum media and into a 2 mL snap cap tube. The collagen mixture was then added to the cell solution at 45 μL of collagen to 10 μL of cells. Cell suspensions were thoroughly mixed

via pipetting and immediately plated (55 μL/microwell). Between every well plating, the stock cell suspension was re-mixed. Wells were gently shaken by hand after addition of the cell suspension (Figure 2.4). For all isolated adipocyte experiments on hand made templated devices, cells were plated in the same manner but at a ratio of 10 μL of cells to 30 μL of collagen mix (Figure 2.4). Once plated, all wells were incubated for 60 minutes at 5.0% CO_2 and 37°C. Serum media was then pipetted in each well and cells were returned to the incubator to rest overnight.

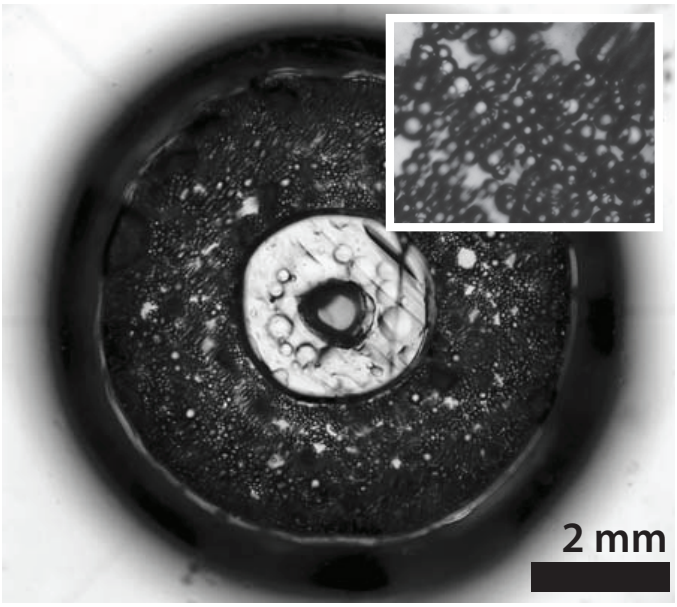

Figure 2.4: **Isolated adipocytes on microdevice.** Adipocytes cultured on 8-channel microfludic sampling devices. Top-down view image of digested and reconstituted adipose tissue cultured on a microdevice made with a 3D printed interface template. Inset shows zoomed version of adipocytes in collagen.

2.3.7 Adipocyte Explant Culture on Microdevices

Epididymal fat pads were removed from C57BL/6J male mice as described previously [26, 15, 79] and transferred to 4 mL of pre-warmed phosphate-HEPES buffer. Fat pads were transferred to a 60 mm petri dish containing a few milliliters of fresh phosphate-HEPES buffer. Excess vasculature and other non-adipose tissue was excised via micro surgical scissors. 2 and 3 mm sterile biopsy punches were used to remove alliqots of the fat tissue. As explants were punched, they were transferred with surgical tweezers into a glass tube with 3-4 mL of phosphate-HEPES buffer. Explants were centrifuged at 1000 rpm for 3 minutes. Infranatant was removed with an 18G 1.5 inch needle. 3-4 mL of phosphate-HEPES buffer

was added back to the tube. Cells were centrifuged and washed in this fashion one additional time with phosphate-HEPES buffer and 2 additional times with fat serum media. After the final rinse, explants were transferred to individual wells on a sterile 96-well plate containing 200 μL of serum media in each well. The 96-well plate was incubated for 30 minutes at 5.0% CO_2 and 37°C. 3D printed explant traps were placed into each well and the plate was returned to the incubator. Explants were maintained for up to 7 days in the incubator with serum media replacement twice a day.

2.3.8 Passive Microfluidic Flow Control

2.3.8.1 Islet Secretion Sampling

For islet secretion sampling, samples were collected into reservoirs while simultaneously applying vacuum. First, 1.5 mm holes were punched through the center of 3 mm PDMS plugs, and Tygon microbore tubing was inserted into the 1.5 mm holes. The plugs (with tubing) were then inserted into 3-mm diameter holes that were punched at the outlet of each channel. As depicted in Figure 2.5B, these plugs fit snugly into the outlets and were positioned a few centimeters from the bottom of the device to allow accumulation of secreted components into the reservoirs. Each time a new chip was used, the plugs were re-inserted into the new microdevice.

2.3.9 Isolated Adipocyte Secretion Sampling

After overnight incubation, isolated adipoctyes were washed with fresh serum media and allowed to incubate for 1 hour at 37°C and 5% CO_2. Cells were then washed and incubated for 3 additional hours in serum free media. Serum free media was replaced with fresh serum free media, tubing was inserted into each outlet well, and vacuum was applied briefly to ensure flow into each channel. Vacuum was removed and sampling media was added to the cells. Immediately after media application, vacuum was reapplied to the channels at a flow rate of 40 μL per hour for one hour. Cells exposed to serum free media served as the

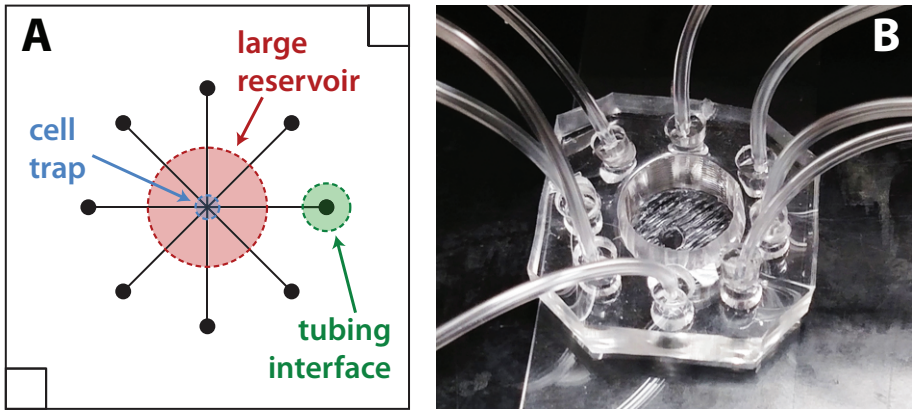

Figure 2.5: **Microfluidic device design for endocrine tissue stimulation and sampling.** A) 8 channel microfluidic design. For clarity, only one channel output (green) is labeled. B) PDMS microfluidic chip with 3D-templated fluidic reservoir, cell trap, and PDMS plug-to-tubing interfaces.

control where as treatment cells were exposed to 100 nM insulin in serum free media. At the end of the hour, vacuum was removed and the secretion samples were transferred into PCR tubes for storage at -20°C until further use. Secretion samples were analyzed via murine adiponectin ELISA.

2.3.9.1 Explant Secretion Sampling

For the larger sample volumes collected from adipose tissue explants (50 to 75 μL), secreted components were collected directly into the tubing and stored in PCR sample tubes. Eight separate pieces of tubing were directly interfaced to smaller (1.5 mm diameter) punched outlets at the end of each channel. Each of the 8 pieces of tubing was connected either directly to a syringe or to a custom 3D printed vacuum manifold and collection device (Figure 2.6).

Manifolds were printed with a single opening for applying vacuum which was pneumatically linked to eight openings to connect tubing from the device. 1.5 mm tubing fit snugly into the manifold openings, but an airtight seal required addition of silicon caulk. 8-strip PCR sample tubes and a customized 3D printed holder were used to collect the adipose tissue secretion samples. Strip lids were replaced by 3D printed lids with vacuum and sample ports. 8-strip tubes were placed in a printed holder which was mechanically clamped

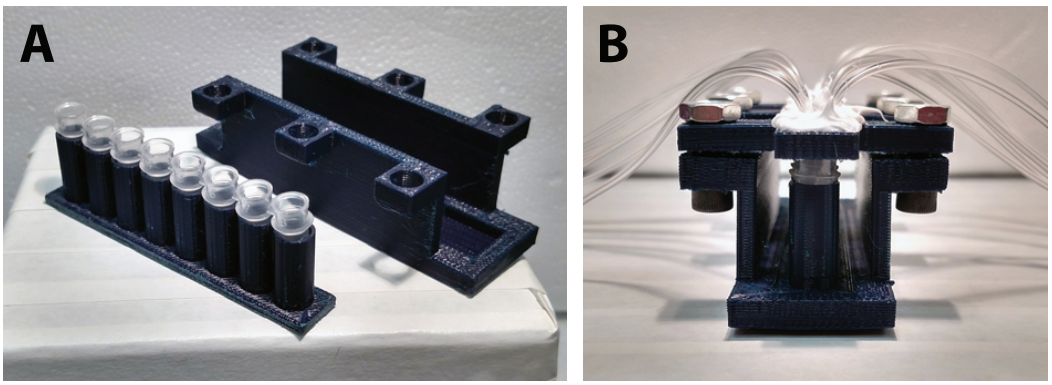

Figure 2.6: **Interfacing for endocrine tissue stimulation and sampling.** A) Disassembled and B) assembled 8-strip sample collection device. Each tube was interfaced with both a vacuum line and a sample line from the microchip to facilitate sequential temporal sampling

to maintain an airtight seal between the 8-strip tubes and the printed lids. Sample tubings were interfaced directly to the ends of the microfluidic channels while the single vacuum tube was connected to the syringe. Vacuum was applied to the entire system, driving solution from the cell culture region, through the tubing, and into the PCR tubes for collection.

2.3.10 Time-Resolved Glycerol Secretion from Adipose Explants

Prior to microfluidic sampling, explants were washed in high glucose/high insulin buffer (HGHI; serum free DMEM, 19 mM glucose, 2 nM insulin) and then transferred into the inlet well on the microfluidic chip, which also contained HGHI. A 3D printed adipose tissue trap (Figure 2.14) was added to the reservoir to hold the explant in place on the chip while also allowing fluid flow. Vacuum was applied to each channel via a 60 mL syringe, resulting in flow rates of $\sim$2 μL min^{-1}. Explants were exposed to HGHI for 30 min, and secretions were collected in a single channel over this time period. Explants were then quickly washed, and bulk solution was replaced with low glucose/low insulin buffer (LGLI; serum free DMEM, 3.5 mM glucose, 50 pM insulin). LGLI-treated cell samples were collected every 10 min after the buffer change for 30 additional min. At the end of the sampling experiment, vacuum was removed, and samples were transferred to 1.7 mL collection tubes. Samples were stored in a

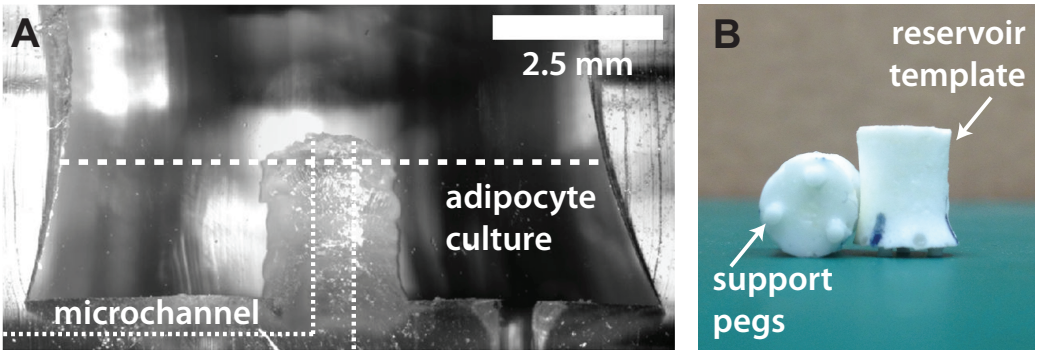

Figure 2.7: **Hand fabricated inserts for isolated adipocyte culture.** A) Cross section of typical device with raised moat to prevent collagen and cells entering the microchannels. B) Hand fabricated templates where support legs define the vertical distance between channels and the reservoir.

freezer at -20°C until quantification through glycerol assay kits (MAK117, Sigma). Samples were processed as per the manufacturers instructions for the fluorescent glycerol assay.

2.3.11 8-Channel Device Crosstalk Testing

During crosstalk tests, 50 nM and 100 μM fluorescein (in BMHH with 0.1% BSA) were used as low and high fluorescent tracers in the chip. Vacuum was applied to each channel in series, collecting solution for 5 min per channel. The first three samples were collected with 50 nM fluorescein in the cell culture reservoir. During the fourth sampling interval (20 min time point), 0.5 μL of 100 μM fluorescein solution was spiked near the channel input well. The remaining four samples were collected to test crosstalk between channel switching. Collected samples were analyzed in 96-well plate format using a Beckman Coulter DTX 880 multimode microplate reader.

2.4 Results and Discussion

2.4.1 Hand Fabricated Interface Templates

Manually fabricated templates were produced individually from a single PDMS master mold to decrease variability. 1 mm tall peg feet established the membrane thickness between

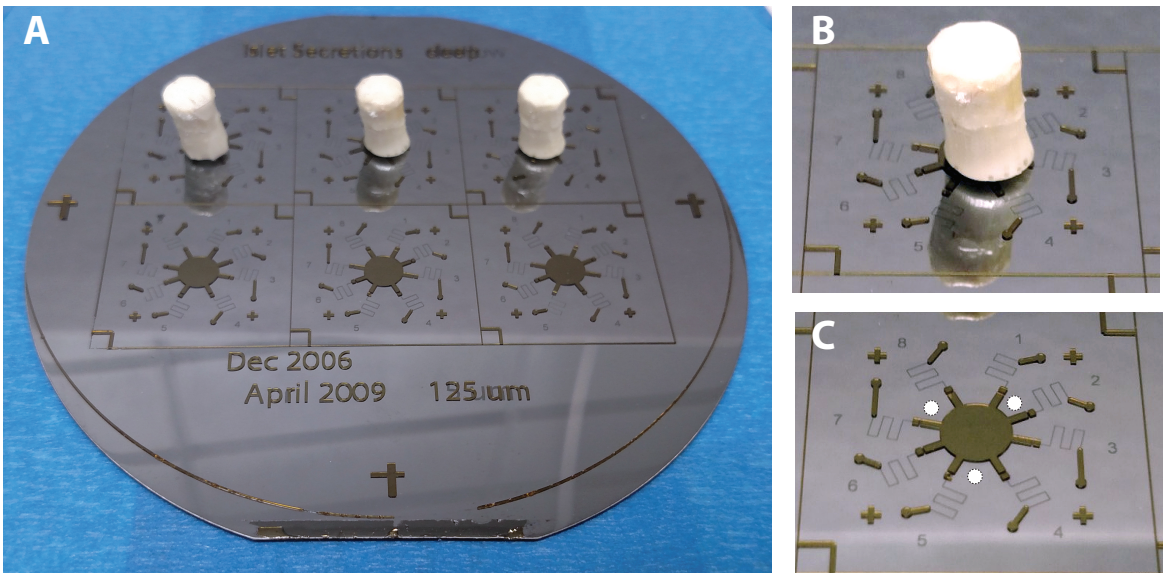

Figure 2.8: **Hand fabricated insert alignment.** A) Hand fabricated inserts aligned on a wafer without PDMS. Inset B and C emphasize the placement of the inserts on top of the wafer design and the wafer design without the insert respectively. The white circles on inset C represent where the three feet on the base of the insert would be placed for casting.

the microfluidic channels and the fluidic reservoir. The raised region of PDMS was formed by the 1 mm wide and 2 mm tall depression in the bottom of the insert (Figure 2.7). To connect the fluidic reservoir with the microchannels in the PDMS, an access point was punched into the 1 mm island. Punching through a 1 mm plug of PDMS proved difficult and led to a high number of fabrication failures (i.e. ripping of the plug). In future iterations of the inserts, slightly wider raised regions were used. As stated previously, there were also minor issues with the fabrication and use of these inserts in PDMS. Only one template could be made at a time, taking <1 day to be ready for use. Even though the same master mold was used for template fabrication, there was slight batch to batch variability. The size of the templates made them difficult to align properly and stay in position in the uncured PDMS (Figure 2.8). Because they were lightweight, the templates could easily shift during the curing process. Ultimately, this first generation of fluidic reservoir templates worked sufficiently for both the use in islet and isolated adipocyte chips. However, in order to improve ease of use and application, these were eventually replaced by 3D printed inserts.

2.4.2 3D Printed Interface Templates

3D printed interface template designs consisted of 6 reservoir-templating columns (for islets: 7.5 mm diameter; for adipose explants: 11.0 mm diameter), spaced to align over the center of the 8-channel crossing points in each separate device on the wafer master (Figure 2.9). Connected via a 2 x 3 in^2 PLA rectangle with lateral footings, the columns were maintained 1.0 mm from the wafer surface. This 1.0 mm gap disconnected the fluidic reservoir region from the channels. Inlet ports could then be conveniently punched through the reservoir to the central channel crossings (islets: 1.5 mm, adipocyte explants: 3 mm). The inlet port served as a confinement chamber for the cells on the chip, as in our previous work [26, 25]. By sequestering the cells in a smaller chamber, bulk solution in the large reservoir could easily be changed without significant disturbance of the cells. Limiting the dead volume surrounding the cells allows for rapid exposure to stimuli as well as comprehensive sampling [25]. In later iterations of the design, viewing ports were incorporated in the backing, and an interlocking system was designed to eliminate the need for hand alignment (Figure 2.9). A base was included, with a 2 x 3 in^2 region to insert and permanently bond the SU-8 patterned wafer. Wafers were cut to fit within the base dimensions. A removable wall with 9 mm height was printed to fit into the base and serve as the walls of a container for PDMS curing. Notched regions of the base allowed the PDMS templating piece to lock into place, which prevented movement of the templates as well as eliminating the need for hand alignment.

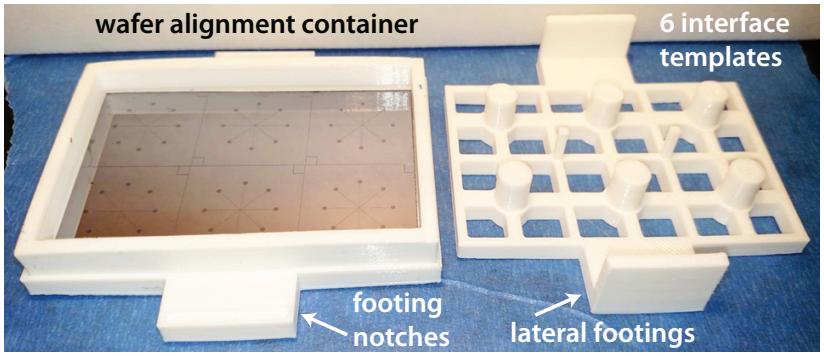

Figure 2.9: **Wafer alignment container.** Image of a 3D-printed alignment container and a 6-well template for sculpting PDMS central reservoirs above SU-8 patterned microchannels.

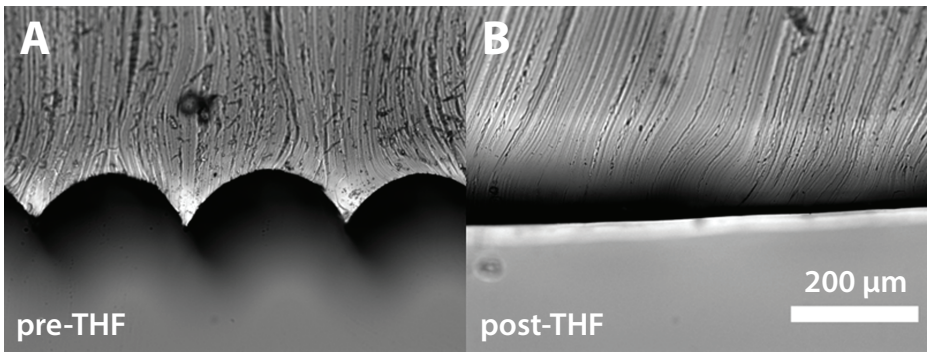

Figure 2.10: **THF smoothing of 3D printed devices.** A) Cross-section of PDMS cured around an untreated 3D template and B) a template treated with THF vapors for 1 min.

2.4.3 3D Template Surface Treatment

As shown by the cross-section of templated PDMS in Figure 2.10A, native 3D printed parts retain grooved surfaces due to the layering process involved in fused deposition modeling, the most common mode of operation in desktop 3D printers. When necessary, THF treatments can be used to smooth the surface of the PLAF material. Under controlled conditions, THF vapor partially dissolves the PLAF surface, resulting in a smoothed surface that can serve as a template for PDMS (Figure 2.10B). While it is possible to cast PDMS with untreated PLA templates, THF-based surface smoothing improves the release process and eliminates the presence of excessive PDMS microstructures. All 3D printed parts used herein were treated with THF vapors before use.

2.4.4 Fluidic Interfacing for Passive Flow Control

A cross-section of a typical device is shown in Figure 2.11. For temporally-resolved sampling, devices were operated passively by serially applying vacuum to each of the 8 outlet channels. As discussed in section 2.3.8.1, the method accommodates for sample collection for volumes less than 10 μL in the case of islet sampling on-chip; for the adipose tissue sampling, volumes averaged 20 μL, which was more easily collected and removed from directly connected tubing. Akin to our previous work, this approach greatly simplifies the operation of the analytical system, using a hand-held syringe and exploiting inherent fluidic resistances

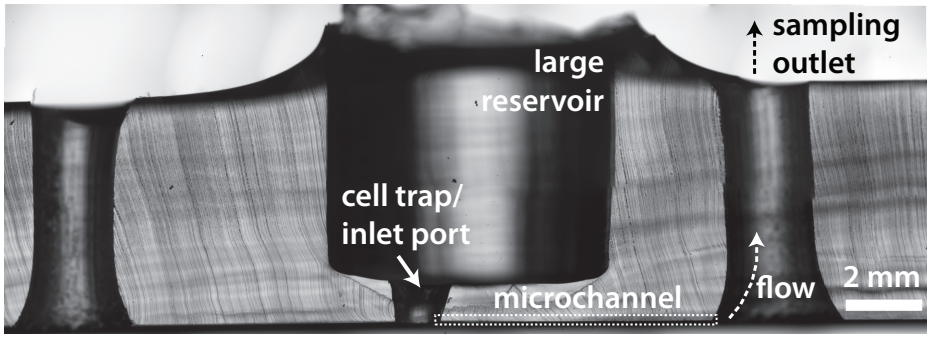

Figure 2.11: **Cross-section of a typical PDMS microdevice.** For clarity, only one microchannel sampling path is labeled.

of the microchannels for flow control [26, 25]. In this work, we used similar passive control and added the capability of temporally-resolved secretion sampling. Again, ease-of-use and device disposability are major advantages compared to other approaches that use syringe pumps or electroosmotic flow control. Devices were consequently inexpensive and disposable after a single use.

2.4.5 Evaluating Channel Crosstalk

It is well established that native PDMS is highly susceptible to non-specific adsorption of proteins and dyes such as fluorescein [80]. In order to minimize this effect, all devices were pre-treated with BSA buffer to not only better mimic cell sampling conditions but also to function as blocking mechanism for nonspecific binding of fluorescein. This pre-treatment has been shown to effectively eliminate non-specific adsorption to PDMS channels and reservoirs [25].

Since this 8-channel device was designed for simple, passive flow control, no valves were used to open or close the channels. It was thus necessary to evaluate the possibility of crosstalk between sampling channels during temporal sampling. Fluorescein solutions were used to track flow during operation of five separate devices. Operation of each device was matched with that of temporal sampling experiments, and solution was diverted from the central reservoir to a different outlet channel and reservoir every 5 minutes. Samples

collected in outlet reservoirs were not removed for analysis until all 8 channels were tested, allowing evaluation of diffusive crosstalk during the runs. Figure 2.12 shows that fluorescence levels in the reservoirs sampled during the first 15 minutes (3 channels) were statistically equal to the 50 nM fluorescein standard ($p > 0.1$). Once vacuum was applied to the fourth sampling channel (20 minutes time point), 0.5 μL of 100 μM fluorescein was spiked into the cell chamber to mimic cellular release. As shown in Figure 2.12, this spike was observed in the expected outlet collection reservoir as a 16-fold increase in fluorescence signal. Samples collected at time points following the spike showed a 6-fold decrease from the maximum fluorescence, indicating residual amounts of concentrated fluorescein in the bulk solution. Fluorescence signals from these 4 final samples were statistically equal and did not show a decay curve response that would indicate carry-over.

These results indicate minimal crosstalk during operation of the device and suggest that leakage through channels to outlets was insignificant. With all five devices, the 16-fold increase after the spike suggested that a large portion of the spiked fluorescein was swept into the appropriate collection channel (20-minute collection). Any crosstalk after this spike would have exhibited a decay curve in subsequent samplings, which was not observed. Furthermore, passive leakage through the channels would have increased the fluorescence of the first three samples (5-15 minute collections) above the 50 nM standard during the 40 minute experiment, yet no such increase was observed. Overall, this experiment validated the passive, 8-channel device design as adequate for temporal sampling of cellular secretions without significant crosstalk. This validation experiment is further supported by cellular release profiles discussed in sections 2.4.8.1 and 2.4.8.2.

2.4.6 3D Printed Adipose Tissue Traps

While tissues such as islets are denser than water and can be simply added to millimeter scale reservoirs as in (Figure 1.10), adipose tissue buoyancy poses a significant challenge for interfacing to microfluidic channels [26, 57]. As in section 2.3.6, we previously addressed

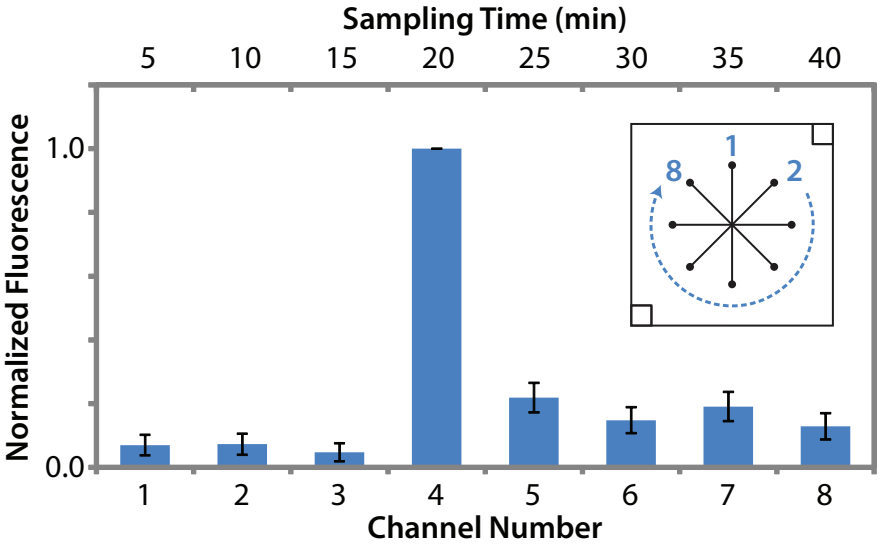

Figure 2.12: **Channel crosstalk during time resolved sampling was determined as insignificant using fluorescein as a flow tracer (n = 5 devices).** 50 nM fluorescein was added to the large central reservoir. 0.5 μL of 100 μM fluorescein was spiked into the smaller, cell-trap reservoir at the start of the 20 min sampling time to mimic cellular release. Inset channel design is labeled with channel numbers.

this problem using hand-fabricated templates to create a moat where dispersed primary adipocytes could be anchored down in collagen, adjacent to sampling channels [26]. However, explants do not require the use of collagen as a physical anchor for the cells. Adipose tissue explants, permitted the use of similar, albeit larger, interface designs compared to islet sampling devices. To counteract adipose tissue buoyancy, novel 3D-printed traps were designed and fabricated. Figure 2.14 shows the design and use of these customized adipose tissue trapping accessories. Due to the rapid prototyping capabilities, it was possible to quickly design custom traps for varying reservoir designs (Figure 2.14B) that were ideal for trapping 2 mm adipose tissue explants. As shown in the image (Figure 2.14B) and 3D renderings (Figure 2.14A), the traps included parallel beams of PLA (0.50 mm width, 0.50 mm spacing) that were suspended between the sides of the cylindrical support, which was custom fit to the reservoir size. These traps were used in the secretion sampling experiments to follow, a trapped explant is shown in Figure 2.14C and they highlight the inherent flexibility

of using customized 3D printed templates and accessories for application to multiple classes of tissues.

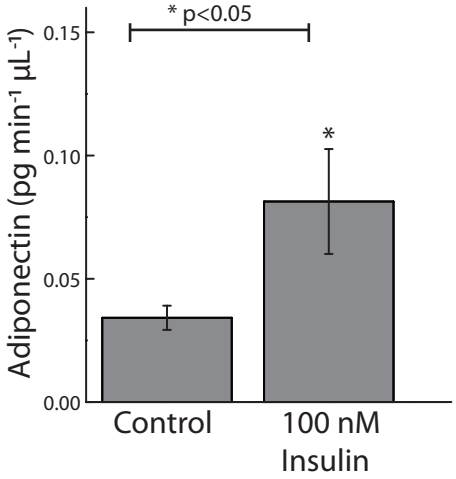

Figure 2.13: **Adiponectin secretion from isolated adipocytes.** At higher concentrations of insulin, adipocytes secreted significantly higher levels of adiponectin when compared to the control cells ($p<0.05$.)

2.4.7 Adiponectin Secretion from Isolated Adipocytes

Increased insulin has been established as a stimulant for adiponectin secretion. Isolated adipocytes were cultured in collagen on microfluidic devices containing raised moat regions, and adiponectin levels were quantified from 1 hour secretion samplings at 0 nM and 100 nM insulin. Adipocytes treated with insulin secreted around twice as much adiponectin as compared to untreated cells ($p<0.05$). The raised moat region allowed for on-chip cell culture in collagen without blockage of the microchannels. Proof of concept was established for the moat device design as well as on-chip isolated adipocyte culture (Figure 2.13).

2.4.8 Time-Resolved Sampling of Endocrine Tissue

It is well known that increases in serum glucose levels in vivo trigger the release of insulin from pancreatic islets. Additionally, the levels of glucose and insulin have a profound effect on fat storage and release in adipose tissue. Interfacing of these two tissue types, islets and adipose, to microfluidic channels presents challenges that are fundamentally unique for each tissue. Accordingly, these tissues were considered ideal for validation of the flexibility of our method using 3D printed interface templates.

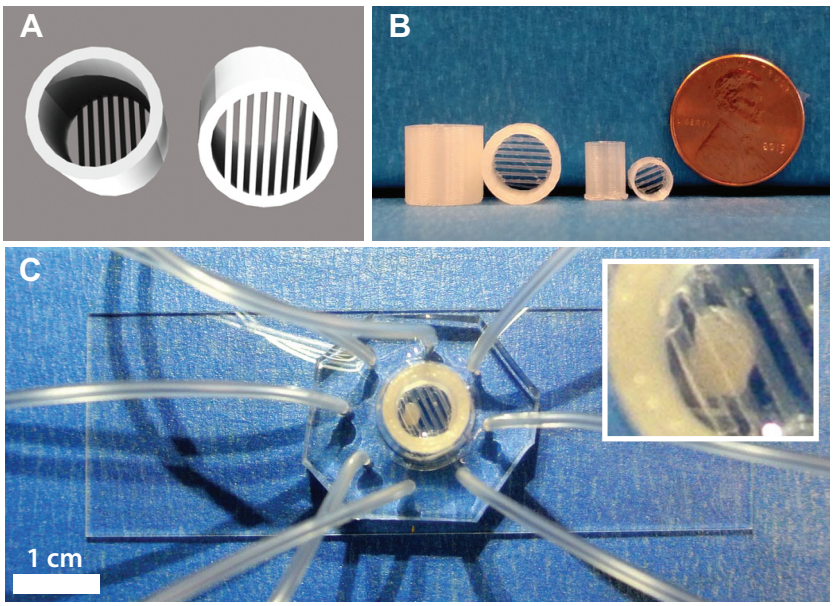

Figure 2.14: **Adipose tissue buoyancy was counteracted using 3D printed trapping accessories.** A) Explant traps sized for microfluidic devices (leftmost two) and 96-well plates (middle two). B) 3D rendering of explant traps, with parallel beams of PLA (0.50 mm widths) designed to hold adipose explants. C) A 2 mm explant was sequestered well below solution level and into the smaller inlet port near microchannel inlets.

2.4.8.1 Insulin Secretion from Islets

To monitor glucose-stimulate insulin secretion with our devices, groups of <10 islets were exposed to either 3 mM or 11 mM glucose, and secretions were sampled every 5 minutes by alternating vacuum between channels 1-8. As shown in Figure 2.15, quantification of secreted insulin via immunoassay (ELISA) demonstrated that islets exposed to 11 mM glucose secreted insulin at significantly higher rates than those at basal glucose ($p < 0.05$), as expected. It is also noteworthy that this data provides further evidence for the lack of crosstalk between individual channels.

2.4.8.2 Glycerol Secretion from Explants

To highlight the flexibility of the method, devices and accessories were also customized for adipose tissue interfacing to address cell buoyancy issues (see Figure 2.14 and section 2.4.6). An 8-strip tube holder was likewise designed and 3D printed for convenience in

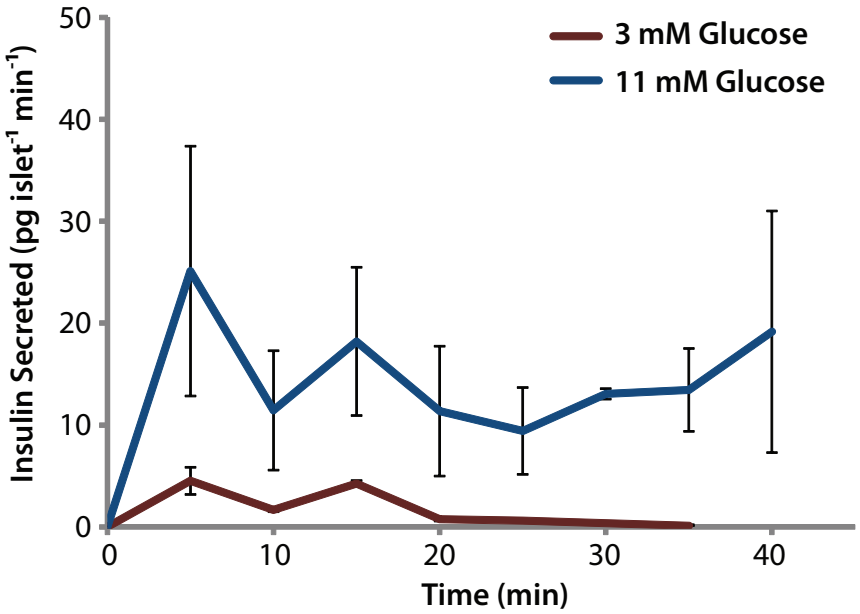

Figure 2.15: **Time resolved insulin secretion sampling.** The insulin secretion rate from primary murine islets was clearly increased ($p<0.05$ for all points) in the presence of higher glucose levels, and the expected initial spike of insulin was observed. Five groups of <10 islets were assayed at high glucose, and two groups were assayed at low glucose (total of 7 microdevices used).

sample collection from the larger explants (see Figure 2.6). To assay endocrine function, varying glucose and insulin levels were applied to these cells. Epididymal white adipose tissue (eWAT) explants were initially treated with HGHI to maximize triglyceride storage within lipid droplets in the cells. A single sample from this treatment was collected in one channel over 30 min to provide a baseline glycerol secretion rate. Once the explants were exposed to LGLI, samples were collected in 10-min intervals. As shown in Figure 2.16, this treatment induced rapid glycerol release from the adipocytes, signifying internal triglyceride breakdown. Glycerol release rates continued to increase after exposure to LGLI, as expected. To our knowledge, this represents the first example of microfluidic temporal sampling of murine eWAT explants in the literature.

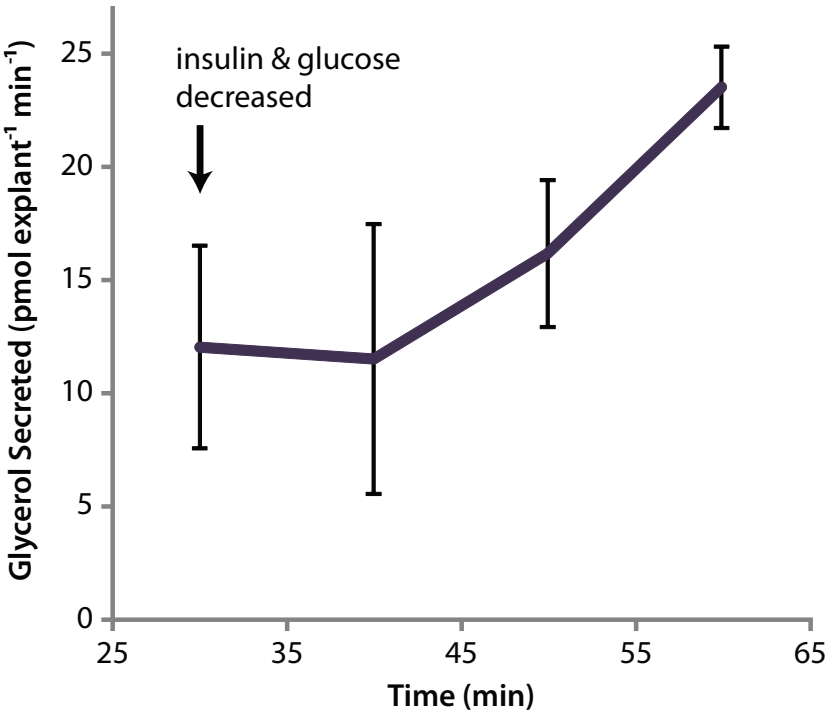

Figure 2.16: **Time resolved glycerol secretion sampling.** Buoyant eWAT explants (2 mm) were trapped with 3D printed accessories and interfaced to a 3D templated device. After 30 min of treatment in HGHI solution, the explants were switched to LGLI solution, and the glycerol secretion rate was observed to increase, as expected. Three eWAT explants were evaluated on three separate microdevices.

2.5 Conclusions

We have presented a robust method for macro-to-micro interfacing of endocrine tissue to microfluidic systems utilizing manually fabricated polymer templates and 3D-printed interface templates. Cylindrical templates were used to create millimeter scale fluidic reservoirs within the bulk PDMS substrate above microchannels. Fluidic interfaces and any necessary accessories could be customized to the tissue of interest. Resulting devices were validated for primary endocrine tissue sampling; glucose-stimulated insulin secretion was assayed from pancreatic islets, and glycerol secretion from adipocytes was sampled and quantified. The application to varying tissue types demonstrates the inherent flexibility of using 3D printing and rapid prototyping. While the results herein are focused on passively-operated microfluidic devices, it is certainly feasible that similar 3D printed interface templates could be used

for interfacing fluidics and/or pneumatics to actively valved devices. By emphasizing the potential to sculpt bulk PDMS above microchannels using 3D printed templates, this work also alludes to the possibility of interfacing other preparative or analytical techniques to microfluidic systems. For example, optical or electrical components could feasibly be integrated into the bulk PDMS to match with channel designs in a highly reproducible manner. Ultimately, these interfacing methods will be limited by the resolution of desktop 3D printers, but it is expected that a number of other applications could be devised.

Chapter 3

Homogenous Fluorescence Assay for Real-Time Monitoring of Fatty Acid Uptake in Primary Adipose Tissue

3.1 Introduction

Metabolism of triglycerides (TG) and free fatty acids (FFA) takes place predominantly in adipocytes [22, 81, 3, 20, 19]. In times of excess energy intake, white adipocytes synthesize TG from FFA and store them in a large lipid droplet which accounts for 85-90% of the cell volume [22, 3, 20]. When the body requires more energy, TG are hydrolyzed via lipolysis and FFA are secreted back into the blood stream. While a variety of tissues can store TG, only adipose tissue can uptake TG without compromising their tissue integrity [22]. Additionally, adipocytes are the only cell type which can secrete FFA and glycerol into circulation. Synthesis and storage of TG and FFA play a vital role in energy homeostasis, and imbalances of these processes have been associated with obesity, diabetes, and other metabolic disease states [22, 81, 3, 20, 19].

While the biochemical mechanisms of lipolysis are thoroughly understood, exchange and transport of FFA within and between adipocytes is still relatively unclear. Membrane proteins such as fatty acid transport proteins have been shown to facilitate FFA exchange, but due to limitations in currently available FFA detection methods, limited dynamic studies have been done [82, 83, 84, 85, 86]. In 2005, real time monitoring of FFA uptake was reported using a commercially available fluorescence based assay (QBT, Figure 3.1) [82]. The QBT assay utilizes fluorescently labeled dodecanoic acid (cell permeable FFA analogue) and a proprietary fluorescence quencher (cell impermeable). Stock solutions of the assay contain excess of the quencher so that minimal fluorescence is observed. When FFA analogues are taken up into the cells, they are no longer in close proximity to the quencher, and therefore

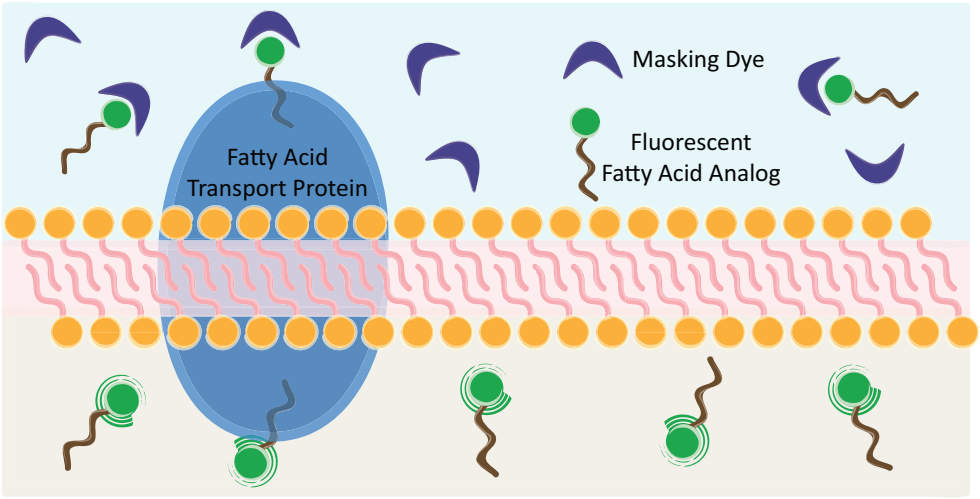

Figure 3.1: **Cartoon Representation of QBT Assay Mechanism.** Excess masking dye (purple) quenches fluorescent output from FFA* (green) when outside the cell. FFA* can be transported into cells through transport proteins (blue), but the masking dye cannot permeate the cell. Once inside, fluorescence from FFA* is no longer quenched and intensities within the cells begin to rise.

fluorescence can be seen within the cells. Since the quencher is present in excess and is impermeable to the cells, background fluorescence is limited. Unlike traditional cell stains, this assay does not require cell fixation or washes - making it ideal for dynamic imaging studies. Liao et al [82] monitored FFA uptake rates with this assay on 3T3-L1 cells under varying media insulin concentrations. Rapid FFA uptake was observed in <30 s. Because this assay is both rapid and homogenous, it seemed highly applicable for on-chip dynamic monitoring of FFA uptake in 3T3-L1 cells, isolated adipocytes, and adipose explants.

Initially, our goal was to directly apply the QBT assay to on-chip studies, but the high cost and short reagent lifetime associated with the product made it difficult for translation to microfluidic platforms. The assay is shipped lyphilized and the entire stock vial must be reconstituted in buffer before use. Once re-hydrated, the mixture is guaranteed to last only up to 5 days. Currently the smallest stock available for purchase is two 10 mL vials and costs $ 160.00 (moleculardevices.com price as of June 2016). The company suggests the use of 100 μL per sample on 96-well plates, totaling around $ 0.80 per well. For microfluidic purposes, not nearly this much volume is needed per chip, and a significant percentage of the stock

is wasted if it is not used within 5 days. In an attempt to prolong the product shelf life, aliquots of freshly reconstituted stock were placed in a -80°C freezer; however, even at these conditions, assay performance was significantly impeded. At this point, the QBT assay was deemed non-deal for microfluidic applications due to the high stock volumes and short shelf life, but the principle concepts behind the assay served as inspiration for development of a similar assay synthesized in-house.

FFA naturally bind to the protein albumin, increasing the solubility of FFA in aqueous environments. When secreted from adipose tissue into the blood stream, nearly all FFA bind to albumin in the blood, and the albumin acts as a transport protein for the FFA outside the cells [83, 87, 88]. Combining this naturally occurring interaction with the principles of the QBT assay kit, we developed a fluorescent, homogenous FFA uptake assay. Since bovine serum albumin (BSA) does not enter adipocytes, quenchers could be covalently attached to the protein and thus prevented from quenching fluorescence within the cells. FFA analogues with covalently attached fluorescent dyes (FFA*) could bind to the BSA-quencher conjugates (BSA-Q) outside the cells, limiting background fluorescence and allowing for fluorescence imaging applications. As FFA* are taken up into the cells, fluorescence increases within the cells only. The BSA-Q based assay performs in a similar manner as the QBT assay, but exhibits significantly improved shelf life and lower costs. Herein, the synthesis and application of the BSA-Q assay will be described in further detail to emphasize its importance in reference to microfluidic platforms.

3.2 Experimental

3.2.1 Reagents and Materials

Fatty acid free BSA was obtained from Akron Biotech (Boca Raton, FL). Lauric acid sodium salt was obtained from Spectrum Chemical (New Brunswick, NJ). Insulin, D-glucose, 4−2−hydroxyethyl−1−piperazineethanesulfonicacid (HEPES), nystatin, fluorescein, tetrahydrofuran (THF), KH_2PO_4, and NaH_2PO_4 were purchased from Sigma-Aldrich (St. Louis,

Missouri). Bovine serum albumin (BSA), fetal bovine serum (FBS), NaCl, $CaCl_2 \bullet 2H_2O$, disposable culture tubes, sterile 96-well plates, nalgene rapid-flow filter units and bottle top filters (PES membrane, 0.2 μm pore size, sterile), polypropylene mesh (210 μm), sterile DPBS, and blunt ended needles were purchased from VWR (West Chester, Pennsylvania). Penicillin-streptomycin, Minimal Essential Media (MEM) non-essential amino acids solution 100X, sodium pyruvate, L-glutamine, collagenase P, collagenase type I, and Dulbecco's Modified Eagle Medium (DMEM), $MgSO_4 \bullet 7H_2O$, 10K molecular weight cut-off Slide-A-Lyzer MINI dialysis devices, BODIPY FL C12 fatty acid analogue (505/512 nm), and BODIPY C12 fatty acid analogue (558/568 nm) were purchased from ThermoFisher Scientific (Grand Island, New York). Black hole quenchers with a succinimidyl ester active group (BHQ) 3 (612 nm max absorption) and 10 (516 nm max absorption) were purchased from Biosearch Technologies (Petaluma, CA). Trimethylchlorosilane (TMCS) was purchased from Alpha Aesar (Ward Hill, MA). Channel masks were designed using Adobe Illustrator and printed via FineLine Imaging (Colorado Springs, CO). SU-8 photoresist and developer, silicon wafers, PDMS precursors, 3D printer and filament, disposable biopsy punches with plungers, and Tygon microbore tubing (0.508 ID x 1.524 mm OD) were purchased from Microchem (Newton, MA), Silicon Inc. (Boise, ID), Dow Corning (Auburn, MI), Makerbot (Brooklyn, NY), Miltex (Plainsboro, NJ), and Cole-Parmer (Vernon Hills, IL) respectively.

3.2.2 Synthesis of BSA-Quencher

Activated BHQ-3 and BHQ-10 were dissolved in DMSO immediately before use. Fatty acid free BSA (FAF-BSA) was dissolved in sterile DPBS. FAF-BSA (typically lysine residues) and activated quenchers were allowed to react for 2 hours at room temperature, protected from light, with mild rocking. This solution continued to react overnight at 4°C, protected from light. Reaction solution was then transferred onto dialysis membranes (10K Slide-A-Lyzer) and purified as per manufacture's instructions using DPBS as the counter buffer.

Purified product (BSA-Q) was aliquoted and stored at -80°C until further use. Electrospray ionization mass spectroscopy (ESI-MS) was performed on the BSA-Q.

3.2.3 FFA* and BSA-Q Titration

Solutions containing 0 - 2 μM FFA* and 0.2 μM BSA-Q or native BSA were analyzed on a Beckman Coulter Multimode plate reader using FITC and TRITC profiles. Reagents were diluted in PBS buffer (pH 7.3). Samples were prepared in triplicate on the plate and triplicate fluorescence measurements were performed on each sample.

3.2.4 Adipocyte Explant Culture on Microdevices

Epididymal fat pads were removed from C57BL/6J male mice as described previously [26, 15, 79] and transferred to 4 mL of pre-warmed phosphate-HEPES buffer. Fat pads were transferred to a 60 mm Petri dish containing a few milliliters of fresh phosphate-HEPES buffer. Excess vasculature and other non-adipose tissue was excised via micro surgical scissors. 3 mm sterile biopsy punches were used to remove alliqots of the fat tissue. As explants were punched, they were transferred with surgical tweezers into a glass tube with 3-4 mL of phosphate-HEPES buffer. Explants were centrifuged at 1000 rpm for 3 minutes. Infranatant was removed with an 18G 1.5 inch needle. 3-4 mL of phosphate-HEPES buffer was added back to the tube. Cells were centrifuged and washed in this fashion one additional time with phosphate-HEPES buffer and 2 additional times with fat serum media. After the final rinse, explants were transferred to individual wells on a sterile 96-well plate containing 200 μL of serum media in each well. The 96-well plate was incubated for 30 minutes at 5.0% CO_2 and 37°C. 3D printed explant traps were placed into each well and the plate was returned to the incubator. Explants were maintained for up to 7 days in the incubator with serum media replacement twice a day.

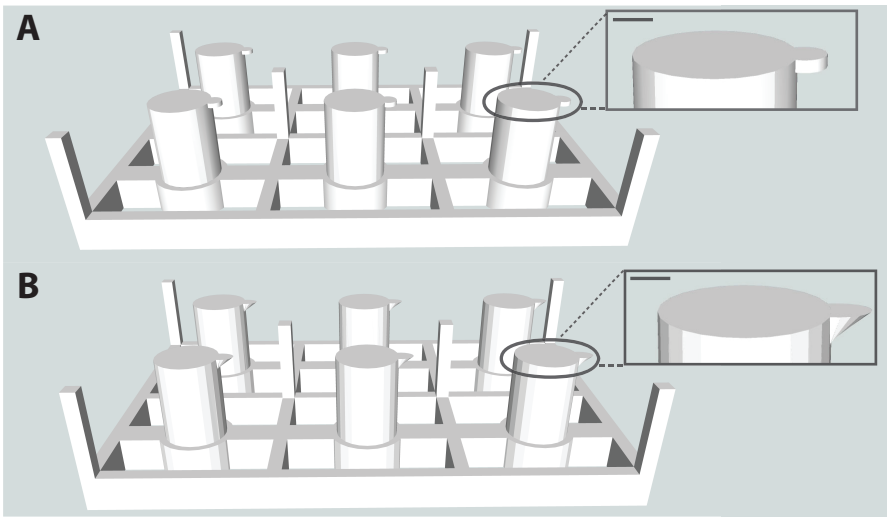

Figure 3.2: **3D rendering of template for explant imaging.** 9 mm diameter columns suspended 500 μm from channels were designed for explant imaging. A) A disc shaped foot and B) a tapered disc foot were added to the end of the column to generate a confinement chamber for the explants. Insets show zoomed in view of foot shape (scale bar represents 2 mm).

3.2.5 3D Printed Templates

3D printed templates were designed as previously described in section 2.3.4. Templates aligned so that 6 columns, 9 mm in diameter, were centered over each 1.0 in^2 design block on the silicon wafer (Figure 3.2). Peg legs on the four corners and middle of the template maintained the columns 500 μm from the channel designs. The corner legs were shaped to be slightly smaller than the alignment markers on the channel designs for ease of alignment. Footed templates were printed in the same manner, but with extrusion settings to include temporary support beams. Explant traps as described in section 2.4.6 were printed with varying outer diameters to fit the new template column width.

3.2.6 Microfluidic Device Fabrication

Passive microfluidic devices were fabricated as previously described in section 2.3.2.2. 3D templates were aligned in uncured PDMS (Figure 3.2, Figure 2.11), and baked at 55 °C (below the glass transition temperature of PLAF) for at least 1 hour. Once cured, templates

were carefully removed, and all inlet/outlet wells were punched (1.5 mm diameter outlet, 3.5 mm explant well for non-footed templates). Vias between the footed explant capture region and outlet channels were ablated using a CO_2 laser system (5 ms exposure time and 61% power). Immediately after ablation, chips were thoroughly rinsed with methanol to remove debris generated from the laser blast. Channels were cleaned and dried with methanol, N_2 gas, and Scotch tape prior to air plasma oxidation. Once bonded reservoirs and channels were treated with BSA solution for at least one hour, Tygon tubing (1.5 mm OD) was inserted into outlet wells. Approximately 90% of the BSA solution was removed from the reservoir before transferring explants into the device.

Multilayer devices were fabricated using channel designs as shown in Figure 3.3. Control channel (black) wafers were generated with SU-8 photoresist where as AZ photoresist was used for the fluidic channels (blue). For the thicker fluidic channels, PDMS was mixed 5:1 (base:curing agent) and baked at 50°C for 4 hours. Cured PDMS was removed from the wafer, inlet and outlet wells were punched, and individual 1 in^2 chips were excised. PDMS mixed 20:1 was spin coated onto control wafers and partially baked at 65°C for 40 minutes. Fluidic chips were aligned over the partially cured control wafer so that valves crossed over the corresponding channel regions. After all six fluidic chips had been placed onto the control channel wafer, the whole system was further baked at 65°C for 4 hours to complete layer to layer bonding.

3.2.7 Fluorescent Explant Imaging

Serum free media used with the QBT system was formulated to use fatty acid free BSA while excluding glucose and phenol red. Serum free media used with the BSA-quencher system was formulated to exclude glucose, phenol red, and BSA. Dilutions of glucose, insulin, free fatty acids, and BSA-Q were done in serum free media. Low glucose and insulin media (LGLI) consisted of serum free DMEM, 3.5 mM glucose, 50 pM insulin; whereas high glucose and insulin media (HGHI) consisted of serum free DMEM, 19 mM glucose, 2 nM insulin.

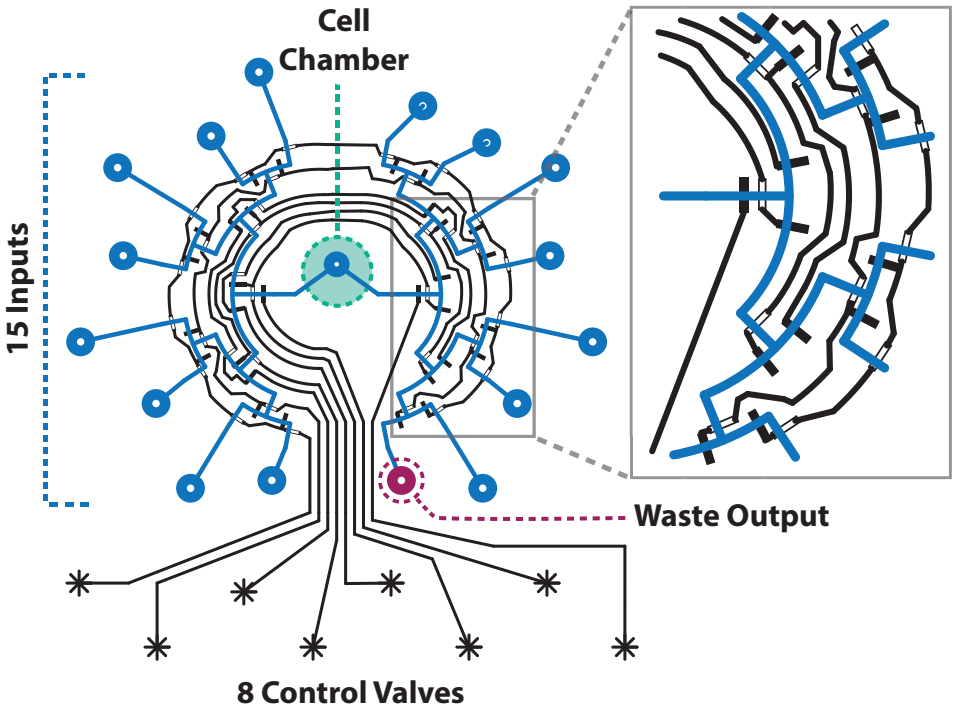

Figure 3.3: **Multilayer channel design for μMUX chip.** 16 total channels available for input/outputs. For explant analysis up to 15 inputs (blue) were used at once and the remaining channel served as a waste output (purple). Fluid channels are shown in blue and control channels are shown in black. Valves on control channels were aligned over fluid channels for accurate flow control (as shown in inset). Explants were contained in a central well (green).

After explants were removed from storage serum media, they were washed 3X with fresh serum free media and pre-treated in LGLI and 2.0 μM unlabeled FFA. Explants were then washed again with serum free media and placed on microfluidic chips containing fresh serum free media in the cell reservoir chamber. For passive chips, 3D printed traps were then placed on top of the explants, whereas in valved chips, a platinum wire mesh held the explant in place.

Dilutions of FFA* and BSA-Q were done in LGLI and HGHI. All solutions were kept at 37°C and protected from light. 2.0 μM FFA* and 1.0 μM BSA-Q were applied to cells

for treatments and imaging for all samples unless specified otherwise. For treatments with FFA uptake inhibitor (sulfo-N-succinimydal FFA derivative [89]), explants were exposed to 200 μM inhibitor for 30 min between application of green FFA* and red FFA*. Fluorescent images were captured using a Nikon-Ti fluorescent microscope through FITC, TRITC, and DAPI profiles. Image analysis was done via ImageJ and Microsoft Excel.

3.3 Results and Discussion

3.3.1 BSA-Q Validation

A homogenous, fluorescence assay for FFA uptake has been developed. Lauric acid FFA* with BODIPY dyes (505/512 nm and 558/568 nm) was paired with BSA modified with covalently attached quenchers (max absorption at 516 nm and 612 nm). In solution, FFA* molecules bind to BSA-Q, thereby largely quenching fluorescence in free solution. If BSA-Q is replaced with native BSA, the quenching effect is lost, and fluorescence intensity is significantly higher (Figure 3.4). These preliminary experiments validated proof-of-concept for general assay performance. In order to establish assay application for biological samples, this system was then applied to adipocyte explants for real-time analysis of FFA uptake.

3.3.2 Fluorescent Imaging for Monitoring FFA* Dynamics

Explants were imaged on a passive, 8-channel chip and on an actively valved μMUX to monitor FFA* uptake in low glucose and insulin conditions and high glucose and insulin conditions. Figure 3.5 A-D portrays isolated adipocytes (A) and explants (B-D) stained with LipiTOX/DAPI (A-B), BSA-Q assay (C), and QBT assay (D). The adipocytes contained within the explants show similar cell size distributions as isolated adipocytes. Since explants are undigested portions of adipose tissue, they retain much higher cell density than isolated adipocytes. This property is advantageous for microfluidic applications, because 2-3 mm scale explants contain thousands more cells than reconstituted adipocytes occupying the same volume. The adipocytes in explants are packed tightly together and maintain tissue

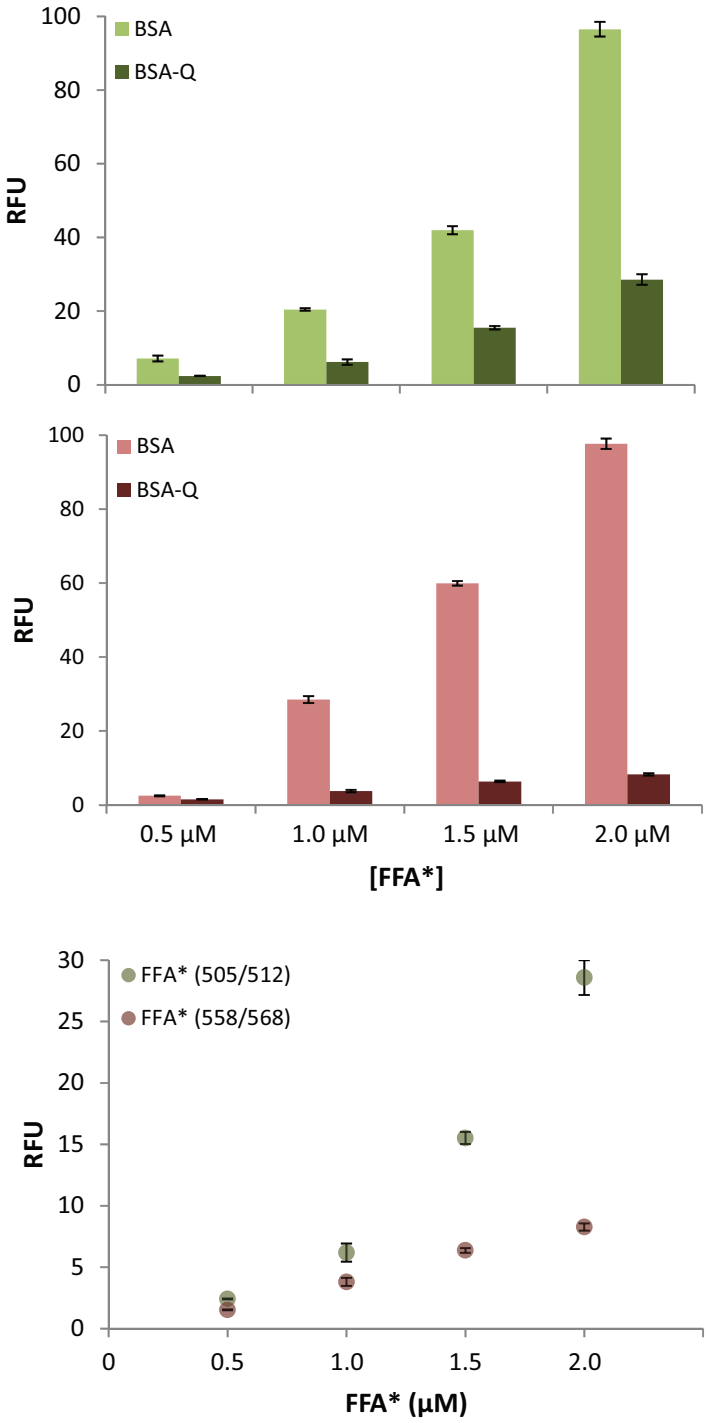

Figure 3.4: **FFA* titration with BSA-Q.** $FFA^\star_{(505/512)}$ (green) and $FFA^\star_{(558/568)}$ (red) were titrated into solutions containing 0.2 μM BSA-Q or 0.2 μM plain BSA. Fluorescence intensity between plain BSA and BSA-Q samples were statistically different at all concentrations of FFA*. The bottom graph shows the fluorescence intensity data for BSA-Q samples only where FFA* 505/512 and FFA* 558/568 were quenched greater than 70% and 80% respectively.

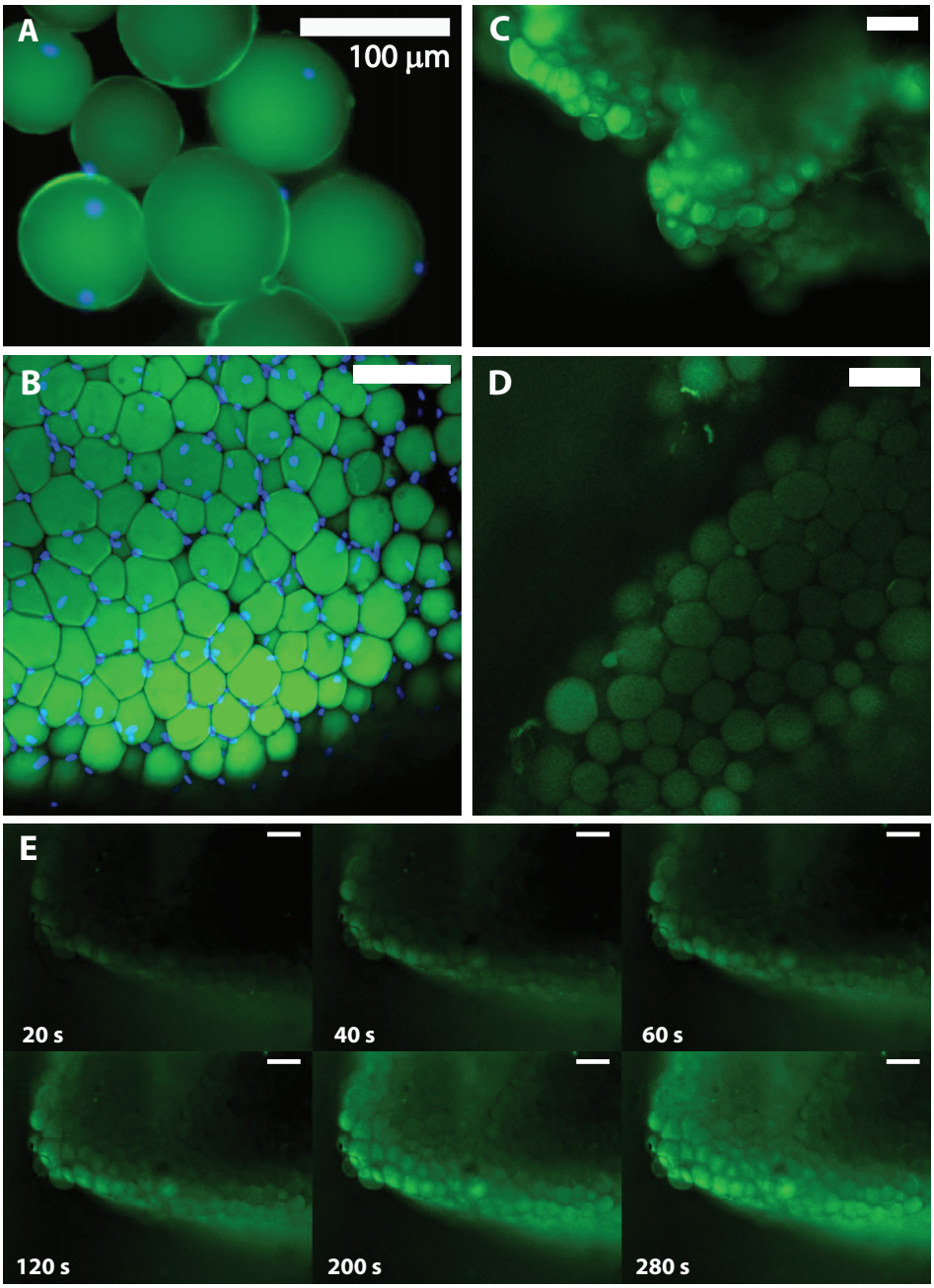

Figure 3.5: **Fluorescent imaging of isolated adipocytes and explants.** All scale bars represent 100 μm. A) Fixed isolated adipocytes and B) an explant which have been stained with LipiTOX (neutral lipid stain) and DAPI (nucleus). Explant after exposure to C) BSA-Q assay and D) QBT assay. E) Time lapse montage of FFA* uptake into explant with BSA-Q in free solution. Edge cells uptake FFA* first and FFA* can be observed in the bulk of the cell after prolonged exposure. For video of real-time imaging of FFA* uptake refer to the following website: `http://www.auburn.edu/academic/cosam/faculty/chemistry/easley/research/brooks/video001.htm`

matrices as well as other cell types, so that FFA uptake and transfer between cells better mimics *in vivo* tissue conditions. For these reasons, explants were utilized for dynamic FFA uptake studies.

3.3.2.1 Passive Devices

The homogenous BSA-Q assay allowed for real-time monitoring of rapid FFA* uptake and release. Constant microfluidic flow of the solution bathed the explants with assay solution so that all surfaces were continuously exposed to fresh media. High cell densities of the explants caused a wave effect to be seen in fluorescence uptake. While the surface adipocytes are in constant contact with FFA*, more centrally located adipocytes are not instantly exposed to the media. Adipocytes along the edge of the explants uptake FFA* more rapidly than inner cells, which was initially observed as fluorescent ring around the explant (Figure 3.5E). Over time, FFA* can be seen permeating central adipocytes, and fluorescence is observed in the bulk of the explant. Most likely, this effect is due to FFA* exchange between adipocytes.

The mechanism for FFA transport between adipocytes is not fully understood. In order to gain further insight for this process, a known FFA transport inhibitor was applied to explants. Both FITC and TRITC channels were recorded for the entirety of these experiments. Explants were first exposed to green FFA* in LGLI for 10 min to demonstrate normal FFA uptake before application of inhibitor. Cell media was switched to LGLI containing either 0 μM (control) or 200 μM inhibitor (sample) for 10 mins followed by a quick wash with fresh media to remove any residual inhibitor. Red FFA* in HGHI was then added to the cells. Green FFA* uptake was observed in both control and sample explants before inhibitor treatment. Red FFA* uptake was significantly reduced in explants exposed to inhibitor as compared to the control (Figure 3.6). Pairing the BSA-Q assay with inhibitors allows for dynamic interrogation of FFA transport in live explants. While this inhibitor has been previously established to reduce FFA transport, this work represents the first real-time

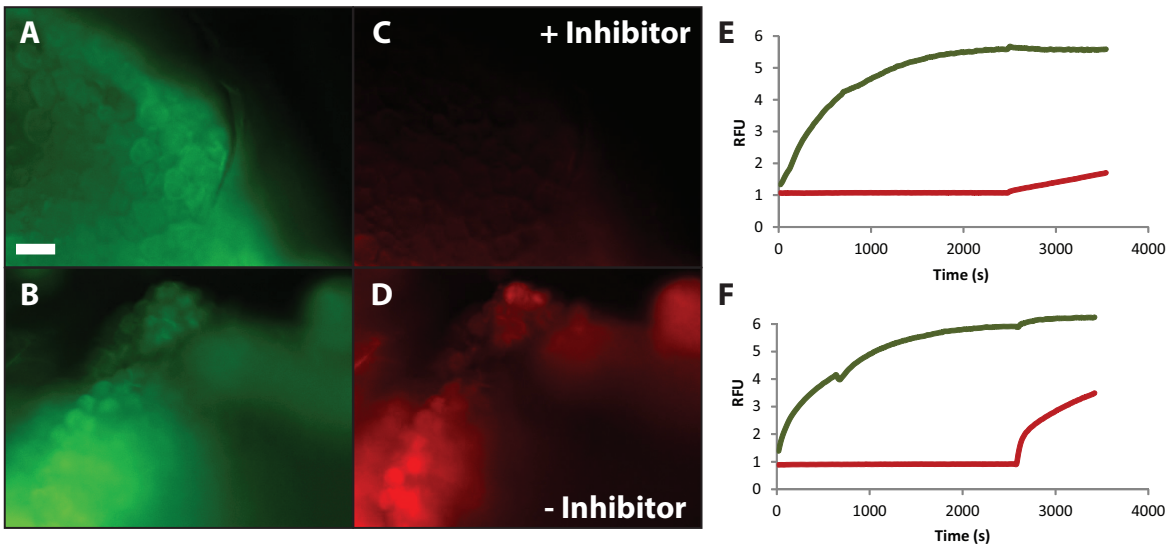

Figure 3.6: **FFA* uptake in explant on passive device.** Explants were bathed in green FFA* (A), exposed to media containing either 0 μM (D) or 2 μM (C) FFA uptake inhibitor, followed by a final treatment of red FFA* (C-D). Fluorescence time traces represent total intensity of explants in both the FITC and TRITC channels (E-F). Scale bar represents 100 μm.

application of the drug on explants. Further experiments involving this inhibitor as well as fluorescent labeled analogues of the inhibitor are planned for the immediate future. Fluorescently labeled inhibitors could provide information such as where on the cells the inhibitor binds and if the inhibitor is cell permeable or not.

Due to the passive nature of this device, media exchange was performed by hand via a P-200 pipette. Chip simplicity allowed for quick fabrication times and passive operation; however, manual solution changes limited the number of stimulatory solutions that could be applied to the sample, as well as the imaging speed. Devices were taped to the microscope inside of a stage top incubator. When manual solution changes needed to be done, the lid to the incubator had to be removed and the condenser optics had to be moved temporarily. Solution changes were done in under a few seconds, but much care needed to be taken when removing and replacing the incubator lid. The microscope stage does not have a lock to physically prevent it from shifting positions when changing the media, which can cause the viewing window to be slightly shifted. To monitor dynamic fluorescence fluctuations in cells

over time, it is imperative to remain focused on the same cell groupings throughout the entirety of the experiment. While taking extra time to replace the incubator lid decreased shifting of the stage, those few seconds prevent continuous imaging. In a dynamic study where signal changes can be seen in under 60 s, losing even 20 s between application of stimulation and imaging could mean the loss of important kinetic data. In order to accommodate rapid solution changes of up to 15 stimulatory inputs, explant imaging was then transferred onto an automated, valved micro device (μMUX).

3.3.2.2 μMUX Devices

The μMUX chip consisted of 16 input/output channels and 8 control channels. Control channels interfaced to solenoids controlled by a LabView application that was designed in house. 15 of the inputs were utilized for sample application via 1 mL syringes interfaced to tygon tubing (Figure 3.7) and the remaining channel functioned as the waste output. Cell media could be removed and replaced in <10 s without the need for pipetting or opening of the stage incubator. Figure 3.8 represents preliminary analysis of an adipose explant on the μMUX device. LGLI and HGHI were applied to the cells while alternating FFA* and unlabeled FFA. Rates of FFA* uptake were observed to be faster in HGHI than LGLI. FFA uptake rates have been shown to correlate with fluctuations in glucose and insulin levels in the media. Low glucose and insulin within the media simulates fasting conditions where triglycerides are broken down into FFA. High glucose and insulin mimics postprandial conditions where accessible energy sources are elevated and excess FFA are taken up and stored in the cells as triglycerides. When unlabeled FFA was applied to cells, fluorescent levels within the cells decreased. Unlabeled FFA were taken up into the cells replacing a fraction of the FFA* and a reduction in fluorescence intensity was observed as some FFA* were released.

Glucose and insulin levels were then applied in an incremental fashion to observe FFA* fluctuations over step-wise changes in media. High FFA* uptake rates can be seen at initial

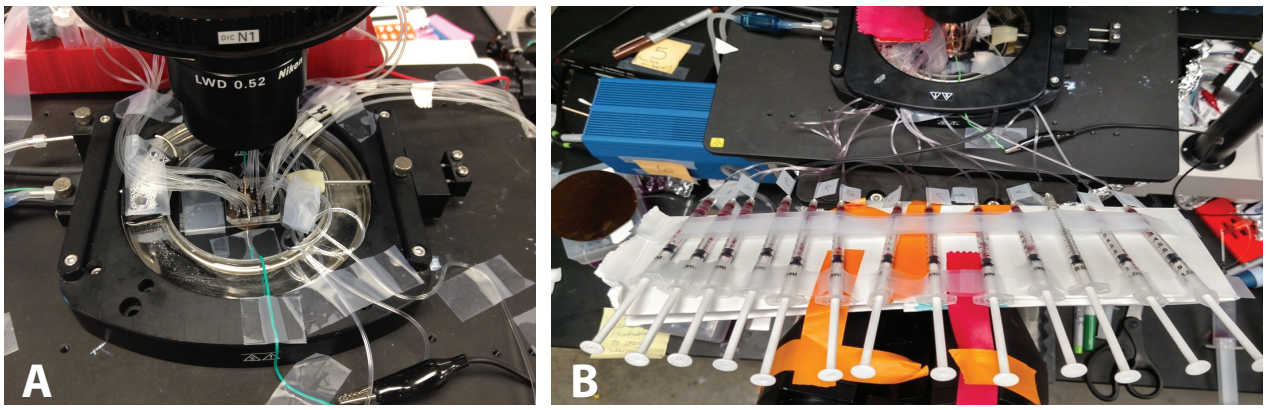

Figure 3.7: **μMUX Device in Use.** A) μMUX chip in stage top incubator. B) Sample syringes connected to input channels.

high glucose and insulin time points, and lower rates are observed at low glucose and insulin (Figure 3.8). As glucose and insulin levels are increased, uptake rates began to increase.

While this chip design required extra fabrication steps and more expertise during operation, dynamic data could be collected faster and with a wider variety of stimulatory solutions than the passive device. Current data analysis and rate curve fitting techniques for this method are focused on edge cells of explants, but further work is ongoing to develop appropriate methods of image analysis and data fitting for all cells of the explant, which will need to account for cell-to-cell diffusive transport. Ideally, this assay could be applied to explants for quantitative comparisons of uptake rates between cell clusters within a single explant as well as between separate explants. Explants have been observed to have lower uptake rates in low glucose and insulin and higher rates in high insulin and glucose, but the absolute slopes of the rate are not directly comparable for quantitative analysis between individual explants. This could possibly be overcome through alternative image analysis systems and normalization techniques.

3.4 Explant Confinement Templates

During imaging of explants on both passive and valved chips, top loading trapping mechanisms described in Chapter 2 were employed to anchor explants in the cell culture

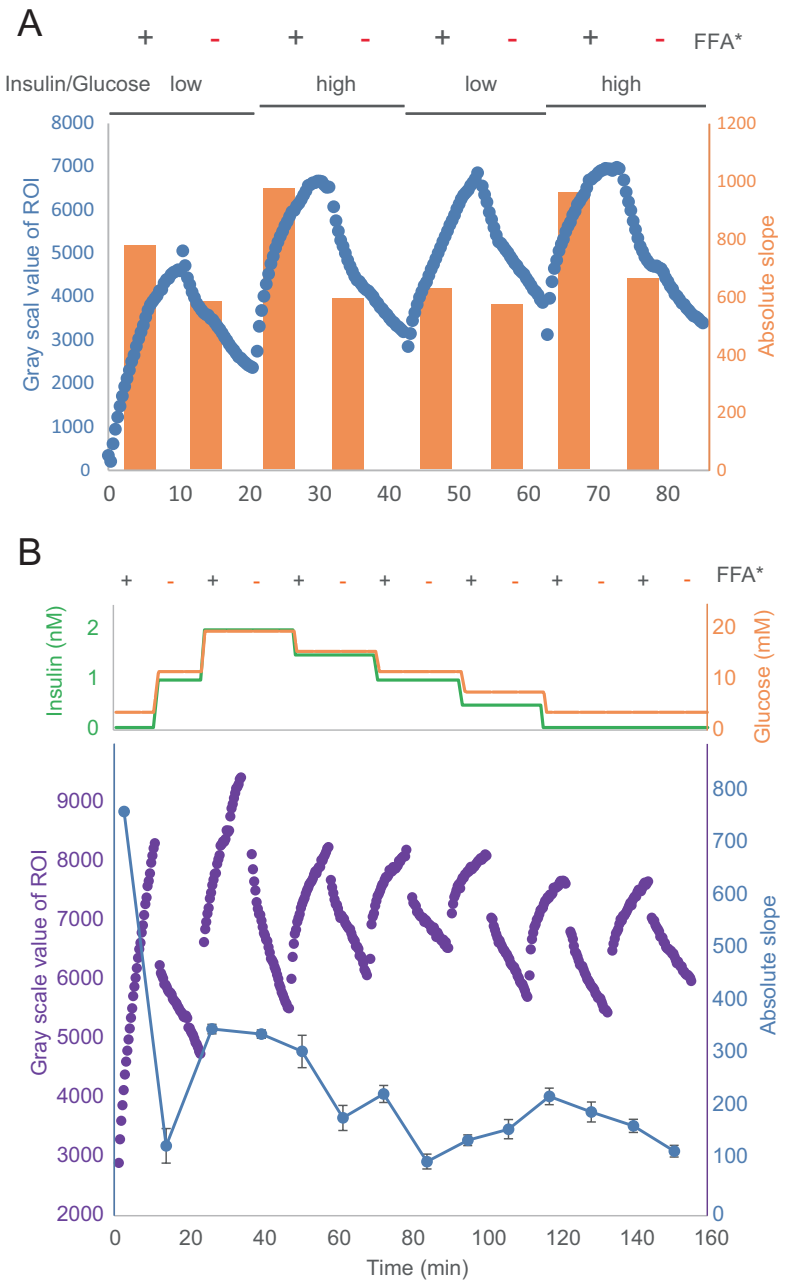

Figure 3.8: **FFA uptake in explant on μMUX.** A) FFA* uptake with alternating inputs of HGHI and LGLI and B) FFA* with stepwise increases in glucose and insulin. Each treatment was monitored over 10 min increments where the uptake/release of FFA* and unlabeled FFA were observed for each treatment. A) Grey scale intensities of the edge cells are represented in blue and show the overall uptake over time. The absolute slope of uptake rates is shown in orange. B) The top graph represents the stepwise additions of glucose (orange) and insulin (green). Grey scale intensities of the edge cells are represented in purple and show the overall uptake over time. The absolute slope of uptake rates is shown in blue.

well. When solutions were changed, explants did not move significantly in the x and y directions, but fluttering was observed in the z direction. In some cases, edges of explants would flutter but return to their original position; however, often the edges would move slightly causing issues with image analysis. Footed templates (Figure 3.2) were designed so that small outcroppings were located at the tip of the cylindrical post which forms the large reservoir in PDMS. Explants could be placed in the footed well and confined to this region for the duration of imaging experiments. 3D printed explant traps were also placed in the large well to ensure explants could not shift in the x-y directions. By confining explants in all directions, the observed fluttering was decreased during solution changes. PDMS devices were fabricated using two footed template designs - round and tapered (Figure 3.9). Rounded confinement chambers limited the volume available for the explant more so that the tapered design; however, round templates proved more difficult to remove from cured PDMS. Tapered templates released from PDMS much easier than the round designs and produced fewer chips with microtears in the device. Addition of these footed regions for explant confinement can be applied to not only these devices, but also other explant devices used within our lab. 3D design software allows for rapid design changes and easy incorporation of tapered feet onto other template designs.

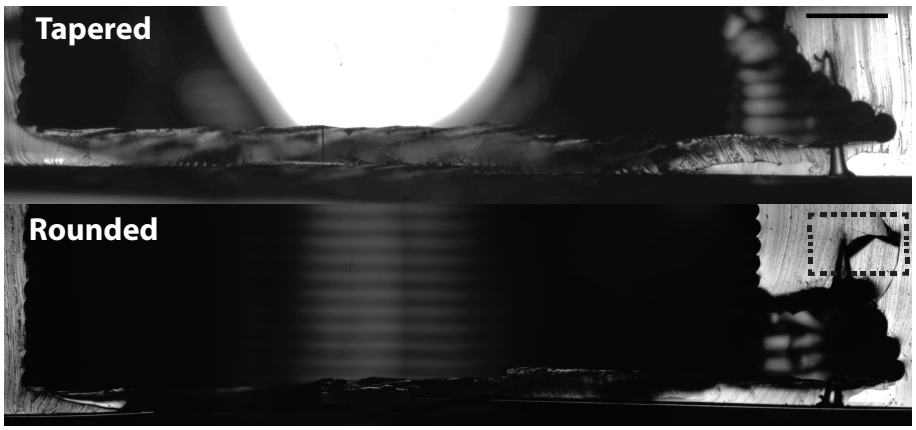

Figure 3.9: **Cross section of explant confinement chips.**Tapered (top) and disc (bottom) shaped templates were used to cast explant chips. Laser ablation points interface the bulk reservoir with microchannels. Scale bar represents 1 mm.

3.5 Conclusions

A homogenous assay for real time fluorescence imaging of fatty acid uptake/release in live tissue has been developed, and proof of concept of the assay was applied to adipose tissue explants on microfluidic platforms. Currently there is a commercially available assay (QBT) which functions in a similar manner, but due to its short shelf life (<5 days) and high minimal purchasing volumes (10 mL), it is not economical for microfluidic platforms. The labeled quencher BSA in the BSA-Q assay can be aliquotted, frozen, and maintain functionality for at least 6 months, and likely longer. The QBT assay requires 100 μL of assay solution per sample on a 96-well plate. For microfluidic purposes, the assay volume required for the BSA-Q assay can range between 30 - 300 μL. A single 100 μL sample of QBT assay costs \$0.80. Using this volume and taking into account the price per mole of FFA* and black hole quenchers for the BSA-Q assay, the cost of a single sample is <\$0.03 - roughly 25X cheaper than the QBT assay. Our in house assay is cheap, easy to use, and has significantly longer shelf life than the commercially available version. Synthesizing a custom assay allows for greater range of application with lower associated costs. Herein FFA* with ex/em of 505/512 and 558/568 are utilized, but alternatively labeled FFA* are commercially available as well as quenchers with varying absorption ranges. If alternative fluorophores or multiplexing is desired, these aspects can easily be built into the assay.

Application of the BSA-Q assay was demonstrated on adipose explants on both a passive and actively controlled microfluidic devices. Passive devices were fabricated via 3D templating as described in Chapter 2 with minor template design alterations. Outcroppings on the tip of the column templates formed explant trapping regions to prevent tissue movement during time lapse imaging. Minimal stimulatory solutions could be applied to explants on the simple passive devices, whereas the valved chip accommodated for up to 15 inputs. While the valved device required more complex fabrication and flow control, it allowed for automated solution changes so that a wide range of stimulatory solutions could be rapidly applied to the explants - a feature not attainable on the passive device.

Dynamic fluctuations in FFA uptake were observed on both passive and valved devices. FFA uptake rates correlated to media glucose and insulin levels such that in HGHI uptake rates were increased when compared to LGLI. This correlation matches FFA uptake response to fasting and feeding conditions *in vivo*. The BSA-Q assay paired with microfluidic devices geared toward explant imaging opens up possibilities for dynamic explant studies using not only glucose and insulin, but also stimulation via β-ARs, α_2-ARs, and FFA transport inhibitors. Improved image and data analysis will be required before quantitative data can be generated for explant to explant comparisons.

Chapter 4

Development of Proximity Assays for Picomolar Range Quanititation of Endocrine Hormones

4.1 Introduction

Obesity and other metabolic diseases have become prevalent worldwide health issues. Gaining further insight on adipose tissue and its endocrine functions can help improve understanding on these conditions and possible treatments. As stated before in Chapter 1, with the development of microfluidic devices for on chip endocrine cell culture, we were able to sample secretions from these cells, but standard protein assay methods were not well matched with microfluidic sample volumes. The gold standard for protein quantization is ELISA, but these assays are costly and require >10μL sample volumes for each well. Several aptamer and antibody based assays have been developed in the Easley lab to function as viable alternatives to ELISA with improved ease of use, reduced cost and assay time, comparable limits of detection (LOD), as well as lower sample volume [90, 91, 92, 93]. This chapter will focus mainly on proximity ligation assays (PLA) with additional discussion of electrochemical proximity assays (ECPA).

Specifically proximity ligation immunoassays for detection of leptin and insulin have been developed. Using as little as 3 μL of sample, these assays can detect as low as 40 pM leptin and 100 pM insulin. The sensitivity and selectivity of the proximity ligation assay thus allows for detection of low levels of protein while reducing sample volume requirements. These attributes, along with the homogeneous detection, make proximity ligation a very useful bioanalytical technique that is better suited for microfluidic analysis. However, two disadvantages of this technique are the time associated with optimizing assay conditions as

well as incompatibility with serum samples. Our electrochemical and temperature scanning assays are capable of protein analysis in whole and diluted blood [90, 92].

4.1.1 Immunoassays

Immunoassays utilize the strong and highly specific binding affinity between antibodies (Ab) and their target antigens (Ag) in order to gain quantitative information on biomarkers such as peptides, proteins, hormones, antibodies, receptors, and even whole cells and single units of bacteria [94, 95, 96, 97, 98]. Due to the inherent specificity of the Ab-Ag interactions, immunoassays have the unique capacity to detect Ag in complex biological matrices. The very first publication on immunoassays was in 1959 by Berson and Yalow who sought to develop a method for detection of insulin in human serum [99]. While this work opened up novel platforms for immunological studies, the rate of immunoassay development was strongly hindered by the limited availability of polyclonal antibodies from manufacturers [100]. In 1975, Kohler and Milstein described the first account of monoclonal antibody production which established methods to indefinitely produce antibodies through hybridoma cell lines with much higher yields than traditional polyclonal methods [101]. Monoclonal antibodies allowed for more rapid development of novel immunoassays utilizing a wide variety of readout methods.

4.1.2 ELISA

Detection of proteins and peptides has historically been performed using larger volume assays (>100 μL) employing the strong binding affinity of antibodies specific to the protein of interest. The current gold standard for detection and quantization of proteins is the enzyme-linked immunosorbent assay (ELISA) (Figure 4.1) [102]. This well-plate based, heterogeneous assay typically utilizes a primary antibody absorbed to the plate which captures the target protein to the plate surface. Secondary antibody is then added which binds

to a second epitope of the target protein. Horseradish peroxidase (HRP) is typically bio-conjugated to the second antibody. Substrate mix is added to the sample wells, and HRP reacts with the substrate molecule to generate a color change. After this reaction has run for about twenty minutes, a stop solution is added to quench the HRP-substrate reaction. Excluding the final stop reaction addition, multiple wash steps are done between each step. By washing the wells, any unbound antibodies or proteins will be washed away, reducing potential background signal. Target protein levels are then detected via absorbance readings correlating to the enzymatic amplification [103, 104, 105]. The two main advantages of the ELISA stem from the high specificity of dual antibody capturing methods and enzymatic signal amplification.

By incorporating an enzymatic color change reaction, for each protein added, many substrate molecules are consumed producing a stronger color change. Signal amplification is a common method integrated into assays in order to improve detection limits by attenuating low signal into detectable ranges [106, 107]. Dual antibody recognition increases the specificity of an assay allowing for decreased LODs. ELISA can be tailored to fit almost any target protein by choosing an antibody pair for the desired target molecule. As long as a protein has at least 2 antibodies that bind to separate epitopes on the protein, it can be detected with ELISA [108]. Because of this specificity and the heterogeneity of ELISAs, complex samples such as whole blood and serum can be accurately tested without strenuous sample cleanup.

While ELISA offers many advantages, there are several drawbacks to this method. ELISAs cannot easily be scaled down. The assay plate comes in a standard 96-well format and the reagents should be used in one sitting. If only a few samples needed to be run at one time, a majority of the plate would go to waste. With costs averaging around $500, each well represents at least $5. Factoring in duplicate or triplicate measurements, a single sample can easily cost $15 to run. Additionally, the assay turnaround time for ELISAs is $\sim$6-8 hours. Long assay time is not ideal if point of care type detection is desired. Furthermore, most

ELISAs require at least 10 μL per sample well, which can prove too large for many types of precious samples. Clearly there is a need to establish assays with similar characteristics and LODs as ELISA, but with lower assay cost, run time, and sample volume.

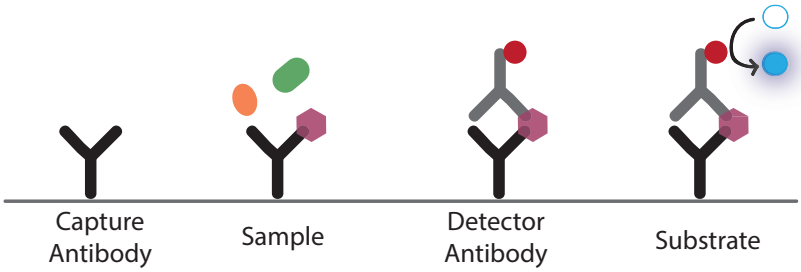

Figure 4.1: **Sandwich ELISA.** Capture antibodies are attached to well plate surface. Sample solution is incubated with capture antibody followed by wash steps to remove excess sample. Detector antibodies are then added to complete the sandwich complex around the sample, followed by additional wash steps. Substrate solution is added to generate the enzymatic color change. Stop solution inhibits substrate generation for absorbance measurements.

4.1.3 Small Volume Immunoassays

By reducing the volume of sample needed to perform assays, the number of replicates that can be done on a single sample can be increased. This is incredibly important, especially in reference to biological studies. For example, if a study aimed to use ELISA to analyze murine protein levels in the blood over a 24 hour period, very few samples could be taken from the mouse and they would be $\geq$ 10 μL. On average, an adult mouse has a circulating blood volume between 1.5-2.5 mL. When collecting multiple samples of blood from the animal, up to 1.0% (10 μL) of the total circulating blood can be safely taken every 24 hours [109]. This volume strictly limits the types of assays that can be performed on the sample. However, if comparable small volume assays are developed, the sample volume restriction becomes less of an obstacle, and a wider variety of study options are available. When sample volume is reduced, the amount of target molecules in the sample is also reduced. Techniques such as pre-concentration of samples or signal amplification must be used in order to maintain relevant LOD. As discussed herein, one specific class of small volume

assays utilizes the proximity effect in order to increase the local concentration of target protein bound to antibodies, facilitating small volume analysis.

Small volume immunoassays typically incorporate sandwich type binding in order to increase assay specificity for the target protein. Much like the ELISA design, these assays include two affinity probes which bind to separate epitopes of the target protein. One characteristic that differentiates small volume assays from ELISA is that they are predominantly homogeneous, non-surface bound techniques. Instead of coating a plate surface with capture antibodies, affinity probes are typically antibodies covalently bound to single strands of DNA. Since DNA can be easily designed and fabricated, this aspect adds versatility to assay designs [110, 111].

4.1.4 Proximity Effect

When separate pieces of an affinity complex are in the same solution, lowering the amount of space between the pieces increases their local concentration, making the binding event more favorable. It has been previously estimated that if a solution containing 1 nM of two pieces of complimentary ssDNA were confined to a 1.7 fL volume sphere, then the radius between the two strands would be ∼700 nm. If the ssDNA pieces were affinity ligands for the same target molecule, upon binding, both probes would be brought into close proximity to each other. The distance between bound probes could be reduced from 700 nm to around 10 nm. Confining the probes increases the local concentration to above 400 μM, or 400,000X fold higher than their unbound concentration. This phenomenon is a result of entropic stabilization and is known as the proximity effect [111].

Increasing the local concentration of affinity probes is a key concept employed with small volume proximity assays [110, 111, 112]. A common method to incorporate the proximity effect into an assay is through the attachment of single stranded pieces of DNA to the affinity ligand. These oligonucleotides (oligos) can be easily modeled and designed to bind to each other or to a third, connecting oligo. DNA strand melting temperatures (T_m) are

used as an indicator for complex stability. Stronger complexes require higher temperature to denature the double stranded DNA. With short, complimentary oligonucleotides, typical T_m are lower than 22 °C, meaning that at room temperature, DNA hybridization will not occur [113]. Without the proximity effect, the unhybridized oligonucleotides represent potential background formation. However, if assays are performed above the T_m, background formation will be reduced. This same concept can be applied to affinity probes bound to the oligos. When the target protein is not present, the DNA hybridization has a lower stability and Tm, making the background formation less favorable than signal. If the target protein is present, the overall stability of the signal complex is greatly enhanced. Each of these concepts stems from the local concentration change of the proximity effects on the system. Manipulation of the proximity effect opens the door to a new class of immunoassays know as small volume proximity assays.

4.1.5 Proximity Ligation Assay

One of the first examples of a small volume proximity immunoassay is the proximity ligation assay (PLA) [114, 110, 115]. Here the sequence of oligonucleotides linked to each of the two antibodies are specifically designed so that they do not bind to each other, but instead both bind to distinct regions of a third piece oligo known as the connector. This connector is intentionally designed to have weak binding energy at the assay temperature, making analyte-independent connection unfavorable. When the protein of interest is present, each of the antibodies will bind to their perspective epitopes, bringing the oligo pieces in close proximity to each other. The connector piece of DNA can now favorably bind to the two antibody tails, forming the complete proximity complex (Figure 4.2). DNA binding properties can be computationally estimated using nucleic acid modeling software (NUPACK) [116]. Designing the connector and antibody oligos to have a weak binding affinity for each other limits the probability of the complex forming without the target protein present.

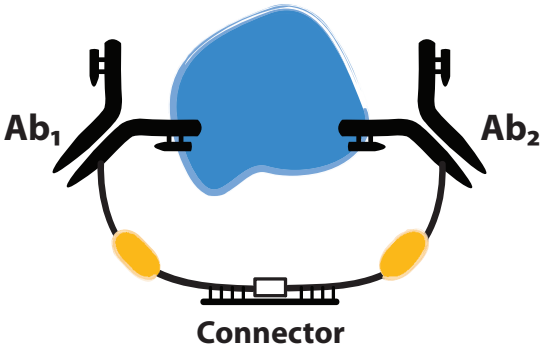

Figure 4.2: **PLA proximity complex.** Single stranded DNA oligos are attached to 2 antibodies which bind to separate epitopes on the target protein. A connector oligo binds to both ends of the antibody-oligos forming the complete proximity complex. The white box represents the region where ligation of the two antibody-oligo strands takes place. Yellow ovals represent PCR primer binding regions.

The basic proximity complex formed in PLA is very similar to that of other types of proximity assays. What distinguishes each type of assay is their unique signal readout methods. As its name would suggest, PLA incorporates the ligation of the two antibody oligo tails. When the two oligos hybridize to the connector, DNA ligase enzymatically ligates the ends together (white box shown in Figure 4.2), forming one coherent strand of DNA. This process effectively translates protein signal into nucleic acid output. After ligation, the newly formed oligo can be exponentially amplified via polymerase chain reaction (PCR) [110, 112].

4.1.5.1 Polymerase Chain Reaction

PCR relies on thermal cycling and enzymatic DNA amplification. Samples are initially heated to denature double stranded pieces of DNA. As the samples are cooled, short primer oligos can bind to specific target regions of the unhybridized oligo strands. DNA polymerase can then bind to the primer regions of the template strand and begin rebuilding its complimentary strand. The procedure for PCR follows the cycle of denaturing, primer annealing, and enzymatic extension for around 30-50 cycles, which produces billions of copies of the target sequence. PCR amplifies the target sequence of DNA, but the final PCR product does not shed any light onto the beginning quantity of DNA or the intermediate amplification

cycles [117, 118]. Real time quantitative PCR (qPCR) on the other hand, generates amplification curves via fluorescence output and can be used to quantify the amount of starting template DNA [119].

4.1.5.2 Real-time Quantitative Polymerase Chain Reaction

Nonspecific fluorescent dyes such as SYBR green can be used to quantify DNA amplification in real time as well as specific oligo strands with fluorescent dyes bound to them (Figure 4.3). Nonspecific dyes intercalate favorably to double stranded DNA. In free solution the dyes emit limited levels of fluorescence. However, once intercalated, the dye emits a strong fluorescence signal indicating the presence of double stranded DNA [120, 119]. A potential drawback with nonspecific dyes is that they intercalate with any double stranded DNA and not just your target sequence. Specifically designed fluorescent probes, known often as Taqman probes, function similarly to DNA primers. Taqman probes are short oligos with a fluorophore and quencher pair attached to each end of the oligo. The probe binds to the template strand in a separate region from the primers. When DNA polymerase begins to extend along the template strand, it will cleave any extra pieces of DNA in its path. As the polymerase extends, it will also digest the Taqman probe, releasing the fluorophore and the quencher. Once the fluorophore is in free solution, the fluorescence of the sample will increase. As the template DNA is amplified, the fluorescence levels will continue to increase. When PCR reaction components begin to deplete, fluorescence levels will plateau due to overwhelming amounts of DNA being generated [118, 119, 121]. By tracking the relative fluorescence levels throughout each cycle, qPCR amplification curves are produced (Figure 4.4).

Amplification curve traces exhibit three main phases : baseline, exponential, and plateau (Figure 4.4) [122]. Initial fluorescence levels are low, so the first few cycles will have relatively the same intensity. Once the exponential phase is reached, fluorescence levels increase drastically. After 40-50 cycles, the rate of increase in fluorescence decreases resulting in the

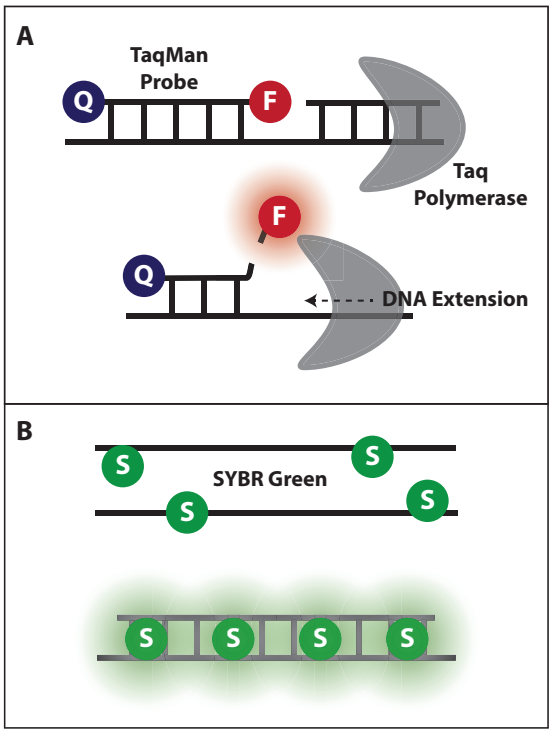

Figure 4.3: **Fluorescent dyes for real-time PCR.** A) Taqman probe dyes include a short ssDNA with both a fluorophore and quencher covalently attached. During the extension phase of PCR, Taq polymerase will cleave the probes. Once separated, the fluorophore is no longer quenched. B) SYBR green intercalating dyes are only minimally fluorescent when in free solution. Strong fluorescence is observed when this dye intercalates into dsDNA.

final, plateau phase. The starting amount of DNA template determines how quickly the exponential phase is reached. Samples with higher amounts of starting DNA will reach the exponential phase faster than samples with lower amounts of starting DNA.

Calibration curves can be generated with standard amounts of target DNA. In order to associate a specific value from the curves to an amount of DNA, a fluorescence threshold cutoff value is set. The PCR cycle number at which an amplification curve breaks through the threshold line is called the C(t) value or cycle threshold value (Figure 4.4) [122, 121]. Calibration curves are then graphed in terms of concentration vs. C(t) values. The more target DNA present, the more proximity complexes are formed and ligated, which directly correlates higher DNA concentrations to higher starting amounts of DNA and therefore lower C(t) values. In PLA, DNA signal is directly translated into a protein signal when ligation occurs, and data can then be represented in terms of protein concentration vs C(t).

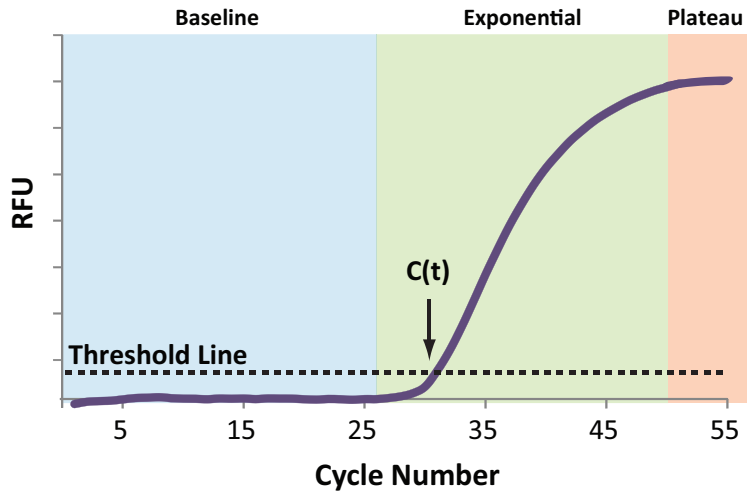

Figure 4.4: **Real-time Quantitative PCR amplification curve.** After each PCR cycle, the fluorescence of the sample is measured. For the first few cycles, there are limited copies of the target sequence and therefore lower fluorescence (baseline). The threshold line for a sample is slightly higher than the background. After 15-20 cycles, exponential amplification is observed by a sharp and steady increase in fluorescence. The cycle number at which the fluorescence level breaks through the threshold line is considered the cycle threshold or C(t) number. This value can be used to compare samples and establish calibration curves.

4.2 Experimental

4.2.1 Reagents and Materials

Oligonucleotides were purchased from Integrated DNA Technologies (IDT; Coralville, Iowa) and methylene blue-conjugated DNA (MB) was obtained from Biosearch Technologies (Novato, CA). Insulin antibodies 3A6 and 8E2 were purchased from Fitzgerald Industries (Acton, MA). Leptin and leptin antibodies were purchased from Peptrotech (Rocky Hill, NJ). Antibody-oligo conjugation kits were purchased from Solulink (San Diego, CA). Insulin, D-glucose, 4−2−hydroxyethyl−1−piperazineethanesulfonicacid (HEPES), tris(2-carboxyethyl) phosphine hydrochloride (TCEP), nystatin, KH_2PO_4, and NaH_2PO_4 were purchased from Sigma-Aldrich (St. Louis, Missouri). Bovine serum albumin (BSA), fetal bovine serum (FBS), NaCl, $CaCl_2 \bullet 2H_2O$, disposable culture tubes, nalgene rapid-flow filter units and bottle top filters (PES membrane, 0.2 μm pore size, sterile), polypropylene mesh (210 μm), and

blunt ended needles were purchased from VWR (West Chester, Pennsylvania). Penicillin-streptomycin, Minimal Essential Media (MEM) non-essential amino acids solution 100X, sodium pyruvate, L-glutamine, collagenase P, collagenase type I, and Dulbecco's Modified Eagle Medium (DMEM), and $MgSO_4 \bullet 7H_2O$ were purchased from ThermoFisher Scientific (Grand Island, New York).

4.3 Methods

4.3.1 Proximity Ligation Assay

Antibody probes were diluted with 1X PBS, 1% BSA, pH 7.3. Leptin and insulin standards were diluted with 1X PBS 0.1% BSA pH 7.3. Connector oligo was diluted with 10 mM TRIS buffer, pH 7.2. For insulin PLA, antibody probes (1 nM, 0.5 μL each) and protein sample (3 μL) were added to PCR tube for 60 minute incubation at room temperature. Connector oligo (400 nM, 1 μL) was then added to the mixture and incubated for 30 minutes at room temperature. For leptin PLA, antibody probes (200 pM, 0.5 μL each) and protein sample (3 μL) were added to PCR tube for 30 minute incubation at 37°C. Connector oligo (80 nM, 1 μL) was then added to the mixture and incubated for 30 minutes at room temperature. For all dilutions of antibody probes and protein samples, larger volume pre-mixes were prepared.

Ligation and real-time PCR components were added to each sample for a total volume of 50 μL. The PCR mixture consisted of the reagents listed in table 4.3. The ligation mixture was incubated for 5 minutes at room temperature. After ligation, the samples were loaded onto the real-time PCR instrument (CFX96 Real-Time System, BioRad). The ligase was inactivated and the polymerase was hot-started via a 10 minute step at 90°C. The temperature cycling for the remaining reaction time was 95°C for 15 sec and 60°C for 60 sec done for 50 cycles.

Name	DNA Sequences for PLA 5'-3'
Leptin Antibody Probe 1	/5AmMC6//iSp18/ TACCACACACCTACCTCCACCTCTCCT-CATCCAACTGCTTGAAGCG
Leptin Antibody Probe 2	/5Phos/ CGACATGTCGTCTCTCACCTCACTCACCACAAC-CACCAACCACACCAC /iSp18//3AmMC6T/
Leptin Connector	TATCGACATGTCGCGCTTCAAGCTTA
Leptin Forward Primer	TACCACACACCTACCTCCACCTCT
Leptin Reverse Primer	TGGTGTGGTTGGTGGTTGTG
Leptin Zen Probe	AAGCGCGACATGTCGTCTCTCACCTCA
Insulin Antibody Probe 1	/5AmMC6//iSp18/ CCCAACCCAACCAACCCAACCCTCAACC-CAAATCAACATTTAATCG
Insulin Antibody Probe 2	/5Phos/ GCGCCGGCGCACCCAACTCAACCCTCCCTCCCTCC-CACCTCCCACCTA /iSp18//3AmMC6T/
Insulin Connector	AAAGCGCCGGCGCCGATTAAATGAAT
Insulin Forward Primer	AACCCAACCAACCCAACCC
Insulin Reverse Primer	TAGGTGGGAGGTGGGAGG
Insulin Zen Probe	CAACCCAAATCAACATTTAATCGGCGCCG

Table 4.1: **DNA sequences for PLA.** All sequences listed 5' to 3'. 5AmC6: 5' amino modifier C6. iSp18: internal 18-atom hexa-ethyleneglycol spacer. 3AmC6T: 3' amino modifier C6 dT.

Name	DNA ECPA Sequences 5'-3'
Leptin Antibody Probe 1	/5AmMC6//iSp18/ CCCACTTAAACCTCAATCCACGCGGAUU-UGAACCCUAACG
Leptin Antibody Probe 2	TAGGAAAAGGAGGAGGGTGGCCCACTTAAACCTCAATCCA /iSp18//3AmMC6/
Leptin MB-DNA	CCACCCTCCTCCTTTTCCTATCTCTCCCTCGTCACCAUGC /MB-C7/
Insulin Antibody Probe 1	/5AmMC6//iSp18/ CCCACTTAAACCTCAATCCACGCGGAUU-UGAACCCUAACG
Insulin Antibody Probe 2	TAGGAAAAGGAGGAGGGTGGCCCACTTAAACCTCAATCCA /iSp18//3AmMC6/
Insulin MB-DNA	CCACCCTCCTCCTTTTCCTATCTCTCCCTCGTCACCAUGC /MB-C7/

Table 4.2: **DNA sequences for ECPA.** All sequences listed 5' to 3'. 5AmC6: 5' amino modifier C6. iSp18: internal 18-atom hexa-ethyleneglycol spacer. 3AmC6T: 3' amino modifier C6 dT. MB-C7: methylene blue

4.3.2 Pancreatic Islet Isolation and Secretion Sampling

Pancreatic islets were isolated from C57BL/6J as described previously (section 2.3.5). After overnight incubation, islets were transferred to a microwell containing 3 mM glucose in BMHH. Islets were starved at low glucose for 1 hour at 37°C. Groups of 5 islets were then pipetted into PCR tubes containing 40 μL of 3 or 11 mM glucose in BMHH. After an additional hour at 37°C, secretion samples were removed from the PCR tubes and frozen until further use.

4.3.3 Electrochemical Proximity Assay

4.3.3.1 Preparation of Gold Electrodes

Gold electrodes (2 mm diameter, CH Instruments, Inc., Austin, TX) were cleaned in freshly prepared H_2SO_4/H_2O_2 (3:1, V:V) piranha solution for 20 minutes. Polishing of electrodes was performed using a 0.05 μM aluminum oxide slurry (Buehler, Lake Bluff, IL)

Reagent	Concentration in 50 μL
10X Buffer	1X
dNTPs	0.18 mM
ATP	73 μM
Primers	0.45 μM
Zen Probe	45 nM
$MgCl_2$	1.9 mM
T4 DNA Ligase	26.8U
Amplitaq Gold DNA Polymerase	1.5U

Table 4.3: **Real-time PCR reagents.** Concentrations listed are in 50 μL total volume.

in water for 10 minutes followed by 10 minutes of sonication in ethanol. Electrodes were placed with gold surfaces facing up, and fresh piranha solution was dropped carefully onto the surface. After 10 minutes of exposure to the piranha solution, electrodes were rinsed with ddH_2O. Electrochemical cleaning was performed in 0.5 M H_2SO_4 through a series of oxidative and reductive scans.

Thiolated DNA and MB DNA was reduced in TCEP for 120 minutes at room temperature and protected from light. Reduced thiolated DNA was diluted to 2 μM and MB DNA was diluted to 1 μM in HEPES/$NaClO_4$ buffer (10 mM HEPES and 0.5 M $NaClO_4$, pH 7.0). Electrodes were incubated in thiolated DNA overnight (protected from light), rinsed with ddH_2O, and immersed in 3 mM 6-mercaptohexanol for 40 minutes (protected from light).

4.3.3.2 Electrochemical Methods

A standard 3 electrode system consisting of a Ag|AgCl(s)|KCl(sat) reference electrode (Bioanalytical Systems), a platinum gauze flag counter electrode (0.77 cm^2), and a gold working electrode (potentials relative to the reference electrode). All electrochemical measurements were conducted using a GAMRY Reference 600 electrochemistry workstation. All measurements were done in HEPES/$NaClO_4$ buffer unless otherwise specified.

Parameter	
V_{int}	-0.45 V
V_{final}	-0.10 V
Frequency	60 Hz
Pulse Size	50 mV

Table 4.4: **Electrochemical parameters for insulin ECPA.**

4.3.4 Insulin ECPA

Electrodes were prepared as described previously (section 4.3.3.1). Proximity complexes were applied step wise to the electrode surface. 10 μL of Antibody 1 (50 nM) was pipetted onto the gold electrode surface and incubated for 3 minutes, followed by a 15 second rinse in HEPES/$NaClO_4$ buffer and drying with N_2 gas. Electrodes were then suspended in insulin or biological samples for 3 minutes followed by a 15 second rinse in HEPES/$NaClO_4$ buffer and drying with N_2 gas. 10 μL of Antibody 2 (50 nM) was pipetted onto the gold electrode surface and incubated for 3 minutes. The gold, counter, and reference electrodes were then placed directly into a fresh solution of MB-DNA. Square-wave measurements were conducted upon initial insertion of the gold electrode to the MB-DNA solution as well as after the electrode had been incubated in the solution for 3 minutes under the parameters listed in table 4.4. For time resolved sampling, pancreatic islets were transferred to a small glass vial (37°C) containing 300 μL of BMHH with 3 mM or 11 mM glucose. Electrodes were suspended directly in the cell media. For serum analysis, samples were undiluted in a small glass vial and remained on ice during experiments.

4.3.5 Leptin ECPA

Electrodes were prepared as described previously (section 4.3.3.1). Leptin standards were diluted in 1X PBS (0.1% BSA). 10 μL of Antibody 1 (50 nM) was pipetted onto the gold electrode surface and incubated for 3 minutes, followed by a 30 second rinse in HEPES/$NaClO_4$ buffer and drying with N_2 gas. 20 μL of protein sample was pipetted onto the gold electrode surface and incubated for 3 minutes, followed by a 30 second rinse in

Parameter	
V_{int}	-0.45 V
V_{final}	-0.10 V
Frequency	75 Hz
Pulse Size	90 mV

Table 4.5: **Electrochemical parameters for leptin ECPA.**

HEPES/$NaClO_4$ buffer and drying with N_2 gas. 10 μL of Antibody 2 (50 nM) was pipetted onto the gold electrode surface and incubated for 3 minutes. The gold, counter, and reference electrodes were then placed directly into a fresh solution of MB-DNA. Square-wave voltammetrySWVSquare-Wave Voltammetry measurements were conducted upon initial insertion of the gold electrode to the MB-DNA solution as well as after the electrode had been incubated in the solution for 3 minutes under the parameters listed in table 4.5.

After the electrochemical measurement had been made on a sample, electrodes were enzymatically regenerated for up to 19 times per electrode. Gold electrodes were immersed in uracil-DNA excision mixture for 7 minutes at 37°C followed by a quick buffer rinse before use in following measurements.

4.4 Results and Discussion

4.4.1 Proximity Ligation Assay Optimization

Once optimal conditions for PLA have been determined, these parameters can simply be reused for sequential runs with each Ab-probe and target protein. However, many iterations of preliminary runs are required to determine optimal probe design and concentration, sample and assay volume, incubation conditions, dynamic range, and ligation time. When Fredriksson et al presented the first proximity ligation assay, they took much care in experimentally probing these parameters. Initial PLA experiments done in the Easley lab very closely mimicked the experimental conditions of Fredriksson et al and Gullberg et al [110, 112], but these conditions proved inadequate for optimal performance of leptin and insulin PLA. The major contributing factors were differences in probe dissociation constants

(K_d). Even between our leptin and insulin probes, there were slight assay adjustments that needed to be made in order to obtain peak performance.

The original protocol for PLA is as follows: 1) Incubate 1 μL of sample with 4 μL of antibody probe mixture (20 pM each probe) for either 1 hour at room temperature or 15 minutes at 37°C. 2) Add 45 μL of amplification and ligation mixture containing 400 nM connector oligo, ligase, and PCR premix. 3) Ligate for 5 minutes at room temperature. 4) Transfer to PCR machine for heat denaturation of ligase and thermal cycling for amplification. The major alterations made to this protocol included probe concentration, incubation timing, and sample volume. 1 nM Ab and 400 nM connector were determined optimal for insulin PLA, whereas 200 pM Ab and 80 nM connector were used for leptin PLA. Instead of adding connector with the ligation and amplification mix, an intermediate incubation step was added so that the connector could interact with the probes and sample for longer in the 5 μL total volume. Separating and increasing the incubation time with the connector improved the signal to noise ratio and LOD. Both insulin and leptin PLA were successful with 1 μL samples, but higher error was observed when pipetting such small volumes. By switching to 3 μL samples, assay error was reduced while improving the dynamic range.

4.4.1.1 Probe Design

DNA binding and interactions can be estimated with molecular modeling software, and Fredriksson et al determined that for the oligo portions of the Ab-probes, ~40 nucleotides length was ideal. They also state that the length could be increased without significant effects on the assay. While this could prove useful for larger proteins, longer oligos are more costly and have lower manufacturing efficiencies. Long, flexible linkers can be added internally into oligo sequences to increase overall length without changing nucleotide count (iSp18).

Increasing connector oligo length can produce false positives due to non-target DNA hybridization; however, short connectors do not have high enough T_m to hold the complexes

together and can also act as primers. In both cases, background ligation and amplification can occur. Connector lengths totaling around 20 bases with roughly half of the connector binding to each arm of the proximity complex provide efficient complex formation with limited background. Asymmetrical connectors have been proven by our group to increase assay dynamic range as well as improve signal/background [123]. Additionally, connector concentration can be varied to minimize background formation. Ratios of connector concentration to probe concentration <1 reduce overall signal and background by forcing the connector to be the limiting reagent. Alternatively, excess of connector oligo in assay solution allows almost all of the proximity probes to be bound to a single connector. Without the target protein present, connector oligos will stay bound to separate arms - limiting ligation and therefore background.

Limiting antibody probe concentration reduces reagent use and background formation. The K_d of antibodies should also be factored into the probe concentration. Below the K_d, the likelihood of proteins binding to a single probe is reduced, which in turn limits the assay signal. An important point to note here is that in all cases background reduction should be an active goal. Since PLA is an amplified readout, signal and background are exponentially increased during PCR. While it may seem counter intuitive to reduce both the ligated signal and background, very little starting signal is needed to analyze the sample simply because of exponential amplification through PCR.

4.4.1.2 Insulin and Leptin Proximity Ligation Assays

After optimization of PLA conditions for both insulin and leptin, protein standards were used to generate PLA calibration curves (Figure 4.5). It is important to note that the assay was consistent enough that each of the triplicate calibration curves was run as individual qPCR experiments on separate days. While assay consistency is advantageous, it would have been easier and quicker to run all replicates simultaneously. This touches on a disadvantage of PLA in that the assay has a limited capacity for high throughput analysis.

On a conventional thermocycler, 96-wells can be amplified and monitored simultaneously; however, when exceeding more than 15-20 samples in PLA there was observable signal drift. When adding the ligation and amplification mix, it is imperative that all of the pre-mixture is added relatively quickly to the samples. If a full 96-well plate is to be analyzed via PLA, even with an 8-channel pipette, the addition of pre-mixture would be too slow. The first row or two of samples would be exposed to the ligase for around a minute longer than the final samples. Higher ligated product would be present in the initial samples, but not due to higher target protein content. This issue could be solved by robotic sample handling, but this accessory was unavailable in our studies.

4.4.1.3 Proximity Ligation Assay Specificity

As further validation of assay performance, leptin probes were tested with solutions of 200 pM insulin, 0.1% BSA, and 200 pM leptin. Due to the highly specific nature of antibodies, no significant response was expected for non target proteins. Of these three proteins, the only samples to show a C(t) value different from the blank contained leptin. Both insulin and BSA readouts were statistically different from the leptin samples, with $p < 0.006$ as seen in Figure 4.6.

4.4.1.4 Proximity Ligation Assay for Samples with Complex Biological Matrices

After optimizing PLA for simple protein standards, the next goal was to use PLA for protein analysis in cell secretions and serum. Since PLA is a homogenous assay, more complex sample matrices could potentially pose an issue for the assay. While the dual antibody probes should maintain high specificity, non-target DNA in the samples could potentially interact with the DNA portion of the probes and connector. Non-specific hybridization could lead to higher background formation, hindering the limit of detection. Enzymes, specifically DNAses, are present in serum. These enzymes could degrade the probe oligos and limit the

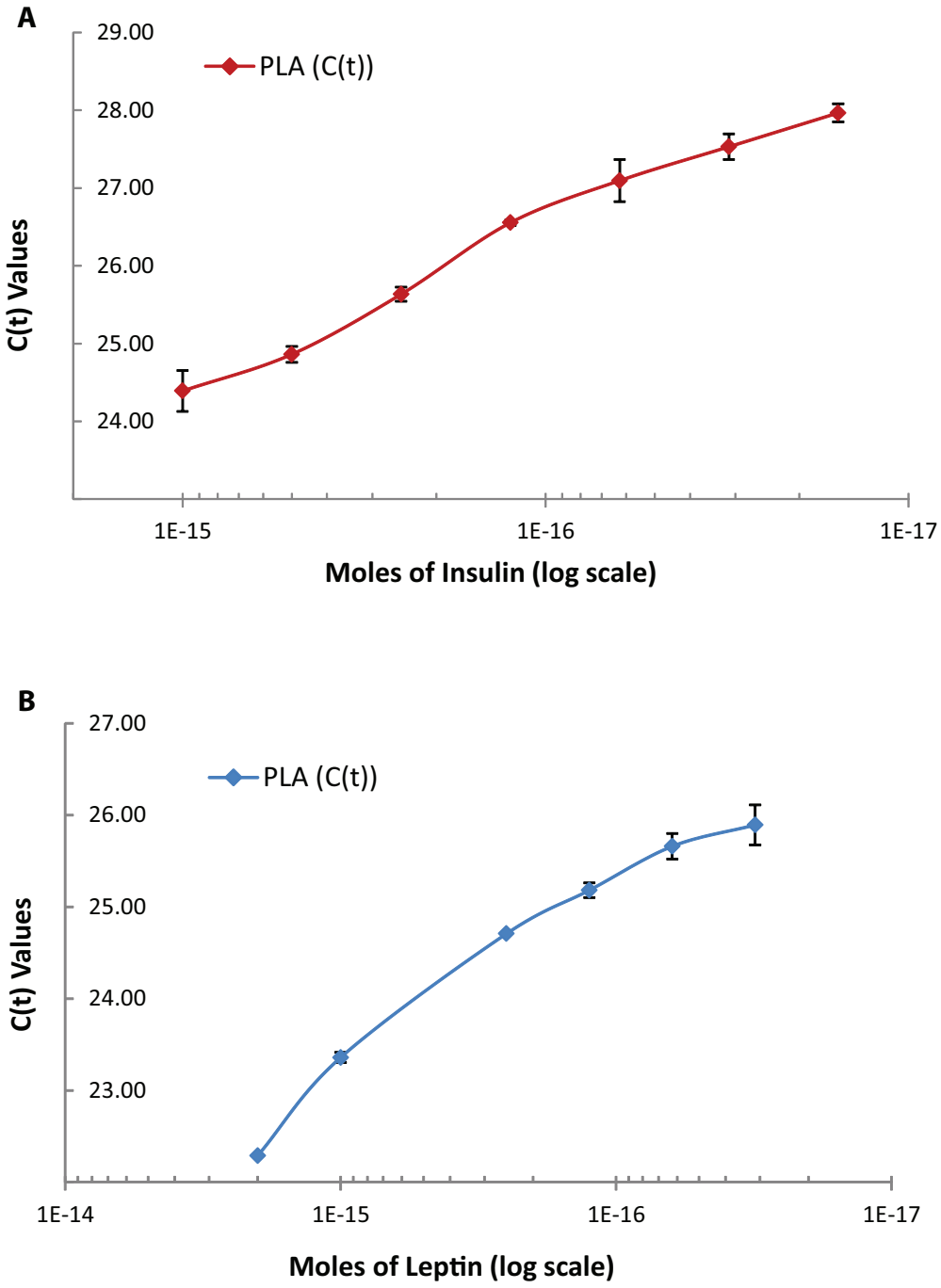

Figure 4.5: **PLA Calibration Curves.** A) Insulin and B) leptin PLA calibration curves. Average of triplicate real-time PCR experiments for insulin and leptin using 3 μL protein standard in each iteration. Error bars represent standard error.

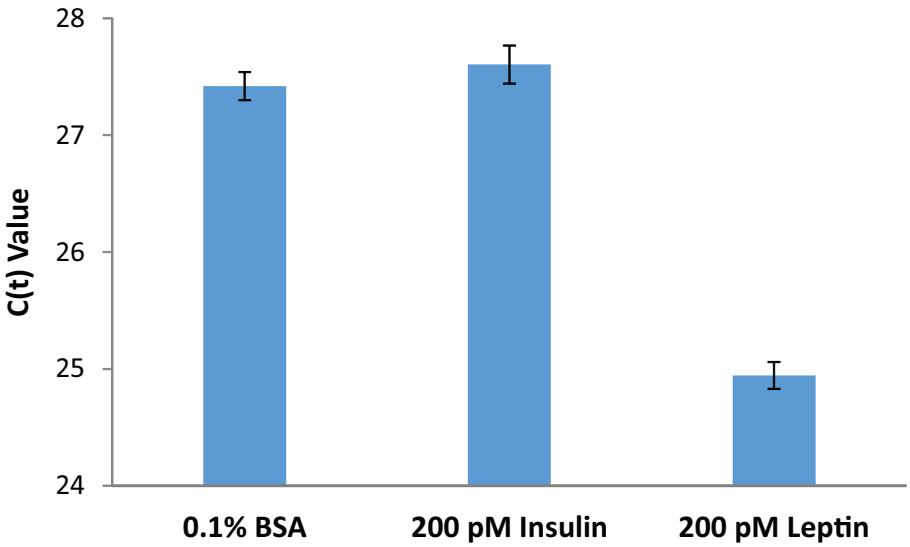

Figure 4.6: **Specificity of PLA.** 200 pM insulin, 200 pM leptin and 1.0% BSA samples were analyzed using leptin PLA probes. C(t) values above the control were observed only with leptin protein samples as expected for a specific leptin assay. Insulin and BSA C(t) values were not statistically different than the blank, but were significantly different than leptin ($p < 0.006$).

overall signal and performance of the assay. The following sections expand on PLA coupled with secretion and serum samples.

4.4.1.5 Insulin Secretion Samples from Pancreatic Islets

A simple tube assay was performed on groups of 5 pancreatic islets treated with low (3 mM) or high (11 mM) glucose. When exposed to higher glucose concentrations, islets should respond by increasing insulin output. Samples from the tube assay were run via insulin PLA. The low and high glucose groupings represent three biological replicates, i.e. three groups of islets. Insulin levels from the low glucose group showed significantly lower insulin output than the high glucose group ($p < 0.006$, Figure 4.7). Recall that lower C(t) values represent higher target protein levels.

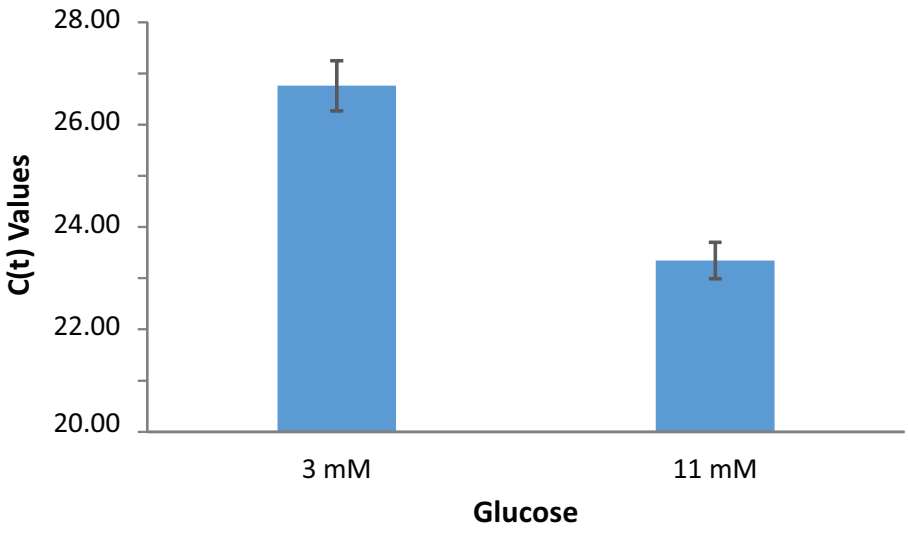

Figure 4.7: **Insulin Secretion Samples.** Secretion samples from groups of 5 islets stimulated in either 3 mM or 11 mM glucose for 1 hour (n = 3 per glucose treatment) Detected insulin amounts from the 11 mM glucose groupings were statistically higher than the 3 mM glucose grouping ($p < 0.006$).

4.4.1.6 Leptin Secretion from Isolated Adipocytes

Murine adipocytes were isolated, cultured on microfluidic devices, and sampled as described previously (section 2.3.6). Secretion samples from 1 h, 3 h, and 12 h increments were analyzed via leptin ELISA and PLA. In all sampling times, no detectable leptin secretions were found using either PLA or ELISA. This could be due in part from the relatively low cell count when using isolated adipocytes. Secretion samples from explants could be used in the future to further test this hypothesis. Explants have much higher cell density than isolated adipocytes and should therefore secrete overall higher levels of leptin.

4.4.1.7 Serum Samples

After validation of PLA with complex samples such as undiluted secretion samples, the next proof of concept for the assay was performance in serum samples. We received murine serum samples from a collaborator (Dr. Greene) which had previously been analyzed via ELISA for insulin or leptin content. Using this information, we wanted to compare PLA

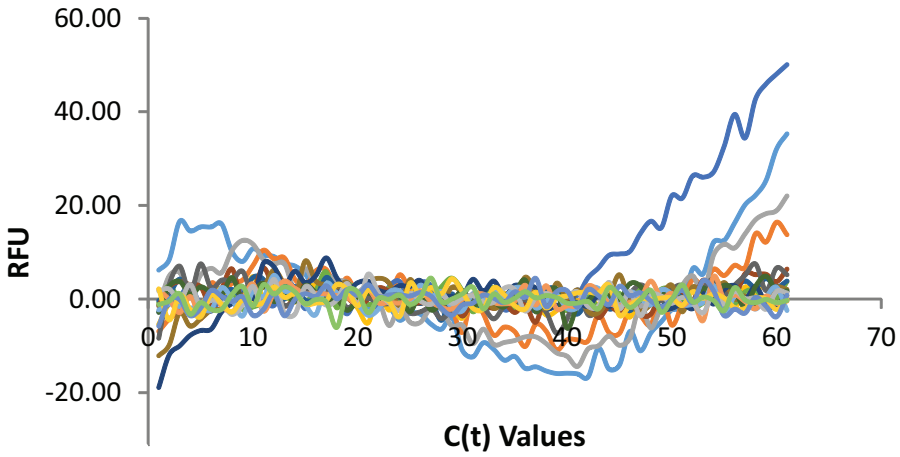

Figure 4.8: **Insulin PLA with Serum Samples.** Representative rt-PCR curves from PLA with diluted serum. In all cases, PCR amplification is inhibited and no useable data is generated.

readouts of the same samples with already known ELISA data. From the serum collection, samples were first chosen which fell within or above the dynamic range of the insulin or leptin PLA so that dilutions of the sample would still be detectable. Using the same PLA conditions, undiluted serum yielded no amplified PCR products. This result was not surprising in that undiluted serum contains many types of enzymes and DNAses which could easily degrade the antibody probes and ligated product. Serum samples were then diluted 1/2, 1/5, and 1/10 to reduce the enzyme concentration but keeping the target protein level above the LOD. In all cases no significant amplification was observed (Figure 4.8). In order to circumvent probe degradation, high concentrations of dummy DNA could be added to reduce DNAse activity on target DNA, EDTA could be added to the serum sample to reduce enzyme activity, probes could be transferred to beads for solid phase PLA with wash steps, or probes made from single stranded peptide nucleic acids (PNA) could be used. These avenues have not yet been completely exhausted. At this time, another student in our lab was optimizing an electrochemical proximity assay (ECPA) capable of serum analysis. We thus chose to move to ECPA analysis of leptin in following studies.

4.4.2 Electrochemical Proximity Assay

During the same time that PLA was being optimized in the Easley lab, an electrochemical proximity assay (ECPA) was also being developed. While the majority of the groundwork for ECPA was performed by Jiaming Hu, the biological validation of insulin ECPA was a collaborative effort. Following his work, we then developed leptin ECPA. The following sections will briefly overview ECPA with a focus on the biological applications and on leptin ECPA development.

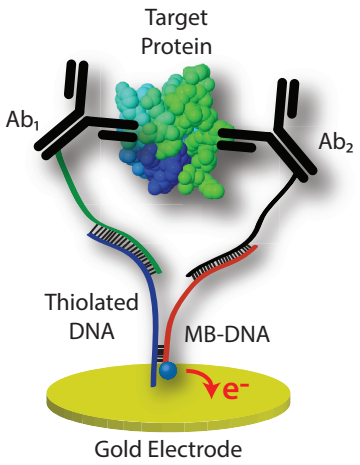

Figure 4.9: **Electrochemical Proximity Assay Complex.** Antibody oligo 1 (green) binds to thiolated DNA (purple) covalently attached to the gold electrode surface. When the target analyte is present, antibody oligo 2 (black) binds to the protein. MB-DNA (red) binds to both the antibody oligo 2 and thiolated DNA to form the complete proxiity complex.

ECPA utilizes a dual antibody capturing system, where the antibody probes are synthesized in the same manner as the PLA probes. A single strand of thiolated DNA is covalently attached to the surface of a gold electrode as a self-assembled monolayer and is complimentary to a short section of antibody probe 1. Antibody probe 2 binds to a short oligo with a covalently attached methylene blue (electrochemically-active species). The MB-DNA strand binds to both the antibody 2 oligo as well as the thiolated oligo on the electrode surface (Figure 4.9).

The proximity complex was built stepwise on the electrode surface so that wash steps in between additions were necessary. Antibody 1 is first added to a clean electrode coated in a monolayer of thiolated DNA. After a brief incubation, the electrode is quickly washed with buffer. The electrode is then dipped into a sample solution followed by a second washing.

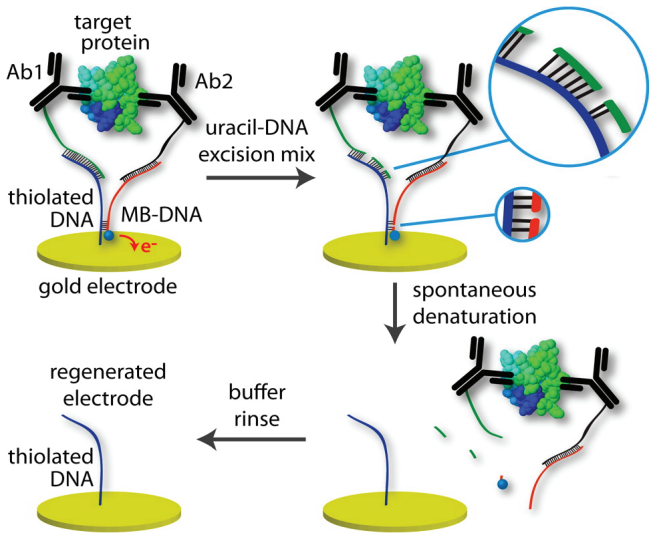

Figure 4.10: **Enzymatic regeneration of electrode surface.** Uracil-DNA excision mixture can cleave oligos near deoxy-uracils in Ab-1 oligo and the MB oligo. The complex stability is reduced and will spontaneously denature from the electrode. Regenerated electrodes are then ready for additional measurements after a quick buffer rinse. Reprinted with permission [92]. Copyright 2014 American Chemical Society.

Antibody 2 is added to the electrode for a final incubation period, and the whole system is then dipped into a solution of MB-DNA with its accompanying counter and reference electrode. Square wave voltammetry measurements are then conducted directly in the MB solution.

The first generation of ECPA was non-reusable, meaning that after a single measurement, electrodes had to be cleaned and activated before the next measurement. This process takes over a day of cleaning and incubation iterations. To speed up this process and facilitate higher throughput measurements, the second generation of ECPA was designed to have reusable electrodes (Figure 4.10). Uracils were incorporated into the MB-oligo and the antibody 1 oligo. After a measurement, electrodes could be dipped into a solution of uracil-DNA excision mixture which cleaved the DNA strands around the deoxy-uracils. Breaking the oligos into short fragments reduces the overall T_m of the system, allowing the oligos to simply be washed away with a quick buffer rinse. Electrodes were proven to function for up to 19 regenerations before significant fluctuations in assay performance were observed.

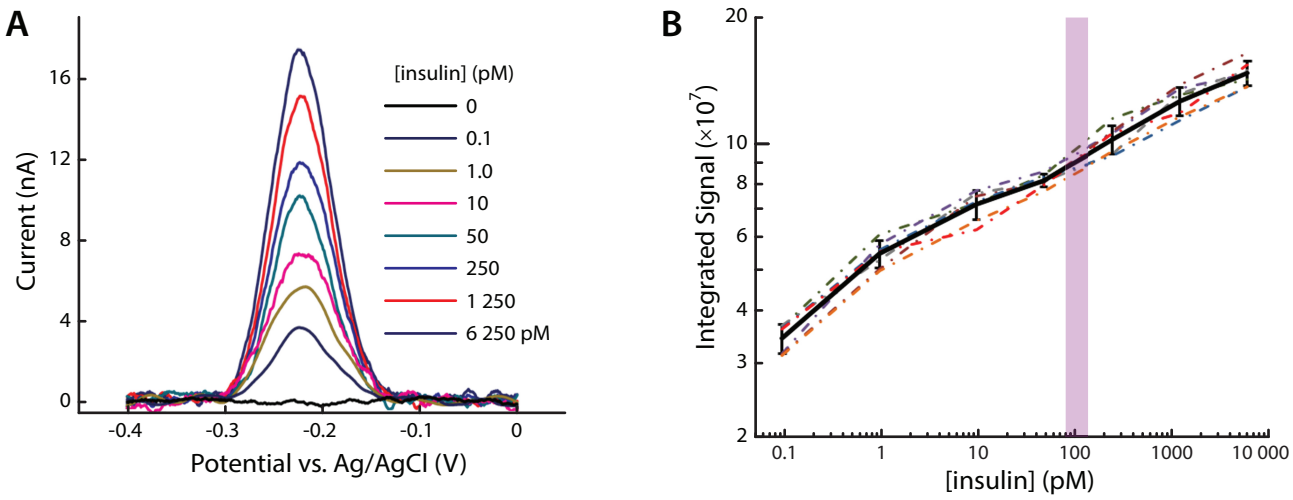

Figure 4.11: **Insulin ECPA Calibration Curve.** A) Current fluctuations corresponding to increasing insulin concentrations. B) Integrated signal for calibration curves generated through seven different electrodes. Reusable insulin ECPA had a LOD of 10 fM. Reprinted with permission [92]. Copyright 2014 American Chemical Society.

4.4.2.1 Insulin ECPA

Proof of concept for reusable, antibody based ECPA was established through insulin detection (Figure 4.11) [92]. Probes and sample were added in a cyclic fashion, and samples were held at 37°C to facilitate future applications with live cells. Calibration curves were generated with seven individual electrodes. Current output was integrated between -330 and -100 mV, with peak amplitude at -210 mV (MB redox peak). The LOD for insulin ECPA was 10 fM where the dynamic range extended up to 6.25 nM.

4.4.3 Temporally Resolved Insulin Secretion

Insulin secretion was temporally monitored directly from islets. Since antibody probes were added cyclically and not directly to the sample, electrodes could be dipped into solution with pancreatic islets and electrochemical measurements could be done in real-time. Islets from two different mice were kept at 37°C in a small glass vial containing low (3 mM) glucose and evaluated in groups of 5 and 15 islets. Two measurements were taken at low glucose,

followed by 5 measurements at high (11 mM) glucose. Insulin spikes were observed after switching from low to high glucose (Figure 4.12) .

4.4.3.1 Detection of Insulin in Serum

Insulin ECPA was performed on unspiked, 20-fold diluted murine serum samples which were collected in house. To prevent probe degradation from DNAses, serum samples were kept on ice during the entirety of the experiment. Standard addition methods were used for calculation of insulin concentrations (120 and 140 pM) (Figure 4.12C), which fell within previously published insulin serum values (113.8 $\pm$ 31.2 pM) [124]. These results were very promising, and we therefore switched our plans for serum sample analysis to be done on ECPA instead of PLA.

4.4.3.2 Leptin ECPA

In order to probe further into the dynamics of adipokine secretion, ECPA probes for leptin were synthesized. One of the advantages of ECPA is that the antibodies attached to the oligo probes can simply be changed to target the protein of choice. Preliminary testing of leptin ECPA with leptin standards shows electrochemical response with as little as 125 pM leptin (Figure 4.13). While this does not currently surpass the LOD for leptin PLA, further optimization and analysis is necessary to maximize the dynamic range and minimize the LOD. Even if the LOD for leptin ECPA cannot be significantly improved, it could still be considered a viable option for serum analysis which is currently unattainable for PLA.

4.5 Conclusions

Proximity assays for insulin and leptin were developed using qPCR and electrochemical readouts as detection methods. PLA allows for sample volumes as low as 3 μL, rendering it ideal for analysis of small volume secretion samples collected on microfluidic devices. Traditional immunoassays such as ELISA require >3X this volume and are costly in both

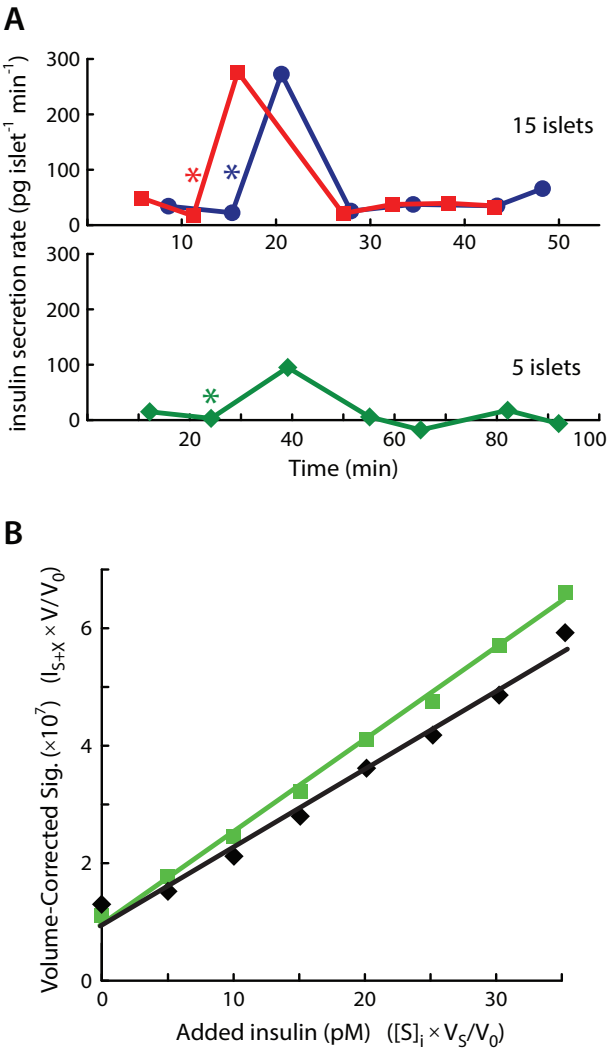

Figure 4.12: **Insulin ECPA for complex biological samples.** A) Real-time quantitation of insulin in secretion samples from murine pancreatic islets. Asterisks (*) indicate when glucose was changed from 3 mM to 11 mM. Insulin secretion levels at low and high glucose match well with previously published rates of up to (˜10-500 pg islet^{-1} min^{-1})[28, 57]. B) Quantitation of insulin in unspiked mouse serum (diluted 20-fold). Insulin serum levels in two different mice were calculated to be 120 and 140 pM. These levels match well with previously published murine serum concentrations where C57BL/6J mice were found to have circulating insulin levels of 16.4 ± 4.5 mU/mL (113.8 ± 31.2 pM)[124]. Reprinted with permission [92]. Copyright 2014 American Chemical Society.

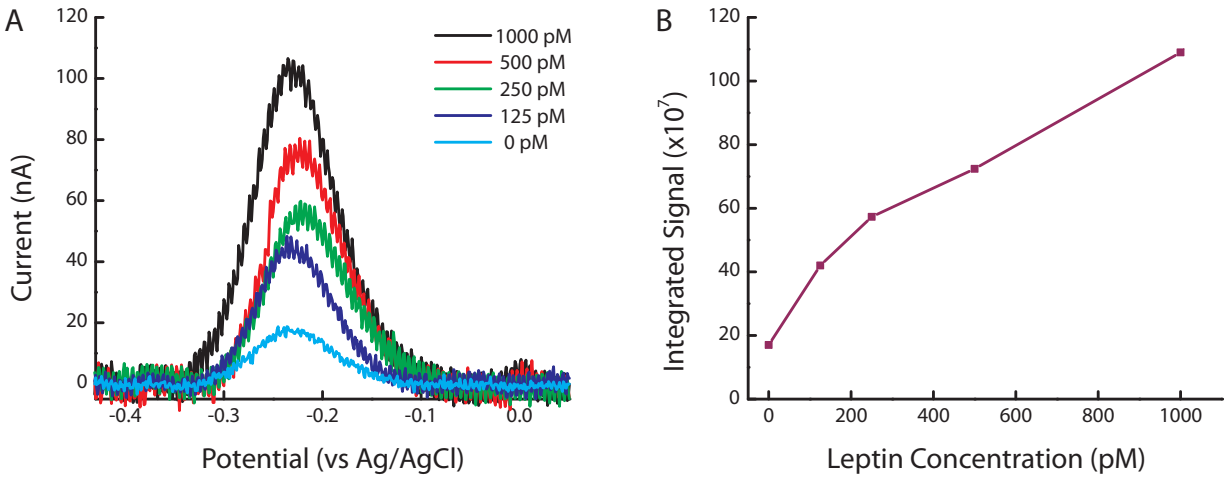

Figure 4.13: **Leptin ECPA calibration curve.** A) Current fluctuations correlating to increasing leptin concentrations. B) Integrated signal under current curves.

time and expense. Both PLA and ECPA have been proven sufficient methods for protein detection in undiluted secretion samples. While PLA currently is not compatible with serum samples, ECPA can be used for serum analysis. Both methods allow for antibody 'plug and play' so that minimal probe design alteration is needed to extend these methods to other target proteins. This quality is ideal for producing sensitive immunoassays targeting a variety of proteins. Not only can these assays detect single proteins, but there is also the possibility for multiplexing. By incorporating alternative fluorophores in Taqman probes or electrochemical tags with different oxidation peaks, multiple proteins could potentially be analyzed simultaneously.

Chapter 5

Analysis of Actinide Ligand-Metal Complexes Using Droplet Fluidics

5.1 Introduction

This chapter focuses on microscale platforms for UV-Vis analysis of metal-ligand complexes in organic solvents for potential detection of actinides and lanthinides. In previous sections of this work it has been established that an ongoing goal of our research is to not only fabricate microfluidic devices for our own immediate purposes, but to also improve fabrication and ease of use so that we can extend the advantages of microfluidic platforms to non-experts. The application of microfluidics to chemistry in organic solvents has been limited in comparison to aqueous chemistry, and the application to 5f chemistry even more so [40, 125, 126]. Herein a droplet generating microfluidic device and a PDMS based micro well plate (μWell) system have been developed to accommodate pyridine based solutions containing inorganic ligands which chelate metal ions and result in an observable color change [29].

Droplet generating microfluidic devices retain many advantages of standard microfluidics, while allowing the formation of discrete, monodispersed droplets at rates up to 100 kHz [30, 127]. By producing isolated units at high rates, a statistically relevant testing population can be generated in under a minute. A principle tenet of 5f chemistry is the reduction of waste generation. This reduction, coupled with reduced assay costs and statistically relevant droplet scanning, makes pairing 5f analysis with microfluidics ideal [127, 128, 129].

5.2 Experimental

5.2.1 Reagents and Materials

Pyridine (99.8%) and 2,3-diaminophenazine (98%) were obtained from Sigma-Aldrich. 3,5-di-tert-butylsalicyaldehyde (98%), copper (II) acetyacetonate (98%), and $UO_2(NO_3)_2{\cdot}6H_2O$ (98%) were purchased from TCI (Portland, OR), STREM (Newburyport, MA), and J.T.Baker respectively. Trimethylchlorosilane (TMCS) were purchased from Alpha Aesar (Ward Hill, MA). Channel masks were designed using Adobe Illustrator and printed via FineLine Imaging (Colorado Springs, CO). Krytox 157 FSL surfactant, HFE-7500 oil, Aquapel, SU-8 photoresist and developer, silicon wafers, PDMS precursors, and filament, disposable biopsy punches with plungers, and Tygon microbore tubing (0.508 ID x 1.524 mm OD) were purchased from Dupont (Willmington, DE), 3M (Maplewood, MN), Pittsburgh Glass Works (Pittsburgh, PA), Microchem (Newton, MA), Silicon Inc. (Boise, ID), Dow Corning (Auburn, MI), Miltex (Plainsboro, NJ), and Cole-Parmer (Vernon Hills, IL) respectively.

Cu [di-tert-butyl-salphenazine] and UO_2 [di-tert-butyl-salphenazine] ligand complexes were synthesized by Branson Maynard and Emily Hardy from the Anne Gorden research group. Synthetic details are included in [29].

5.2.2 Microfluidic Device Fabrication and Surface Treatment

Microfluidic devices were fabricated as described in section 2.3.2, using a droplet generating microchip design previously fabricated in our lab (Figure 5.1) [30]. Following plasma cleaning and sealing of the microchips, Aquapel was applied to each inlet channel and pulled through the entirety of the channels using vacuum. Methanol was washed through the channels, and the microdevices were placed into an oven at 65°C for at least 4 hours. For droplet formation, a solution of 1.8% w/w Krytox 157/HFE-7500 oil was used as the surfactant/carrier surfactant. Unpatterned slabs of PDMS (2 mm tall) were used for μWell devices.

Up to 30 wells (2.5 mm diameter) were punched into the PDMS. μWell chips were plasma oxidized, bonded, and treated with Aquapel in the same manner as the droplet device.

5.2.3 UV-Vis Imaging

UV-Vis spectra were collected via a benchtop Cary 50 Bio spectrometer in a 1 mm quartz cuvette containing 3 mL of sample. All on-chip imaging was performed using a CRAIC Technologies 20/20 PV microspectrophotometer. Exposure time was autodetected through the CRAIC Minerva 8.7.3.12 software. UV-Visible spectral data was collected from 200 to 800 nm.

5.3 Results and Discussion

5.3.1 UV-Vis Spectra of Complexes

Benchtop UV-Vis spectra collection required several milliliters of sample per single run. Microfluidic spectra were collected from picoliter scale sample droplets in a stopped-flow manner via the CRAIC imaging system. In the electronic spectra of [L] (Figure 5.2), two major features are observed in the UV-Vis range at 322 and 424 nm; ϵ = 2.4 x 10^4 and 1.8 x 10^4 L mol^{-1} cm^{-1} respectively. The free base [L] was obtained by acid stripping the UO_2[L] complex and used for further electronic spectroscopy characterization. Upon coordination of either metal center, these two peaks were shifted to higher energy, and two charge transfer bands arose. The middle energy feature (364 nm) in the UO_2[L] complex became a shoulder of the higher energy feature (336 nm). The predominant low energy feature in the UO_2[L] complex showed a maximum at 472 nm (ϵ = 1.9 x 10^4), with a shoulder at 520 nm. The Cu[L] complex, however, showed a predominant peak at 522 nm (ϵ = 1.9 x 10^4), with a shoulder at 460 nm. The growth of these low energy peaks was visualized in the metal titration spectra (Figure 5.3).

Similarities in peak maxima and shape between the macro and micro scale systems can be seen in figure 5.2. To overcome the reduction in path length (1 mm to 100 μm) between

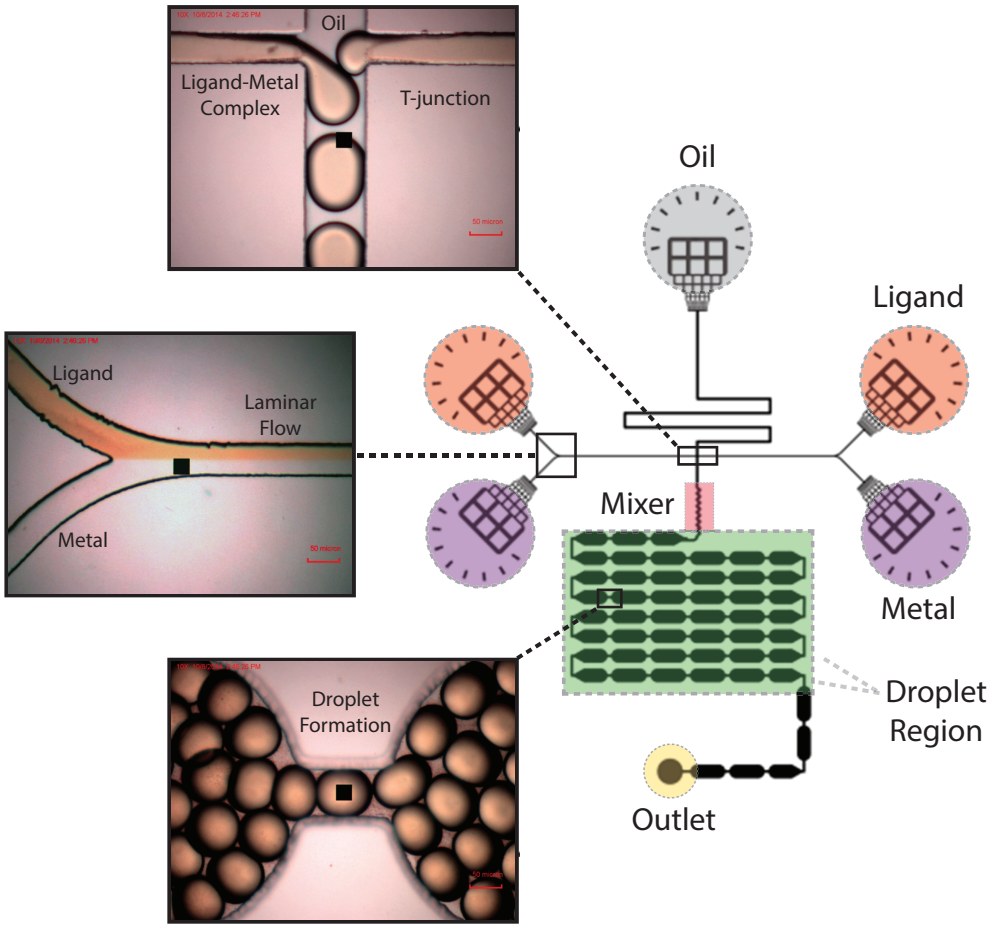

Figure 5.1: **Droplet generating device.** Channel design for microfluidic droplet device. Perfluorocarbon oil (grey) with surfactant promoted droplet generation. Ligand (red) and metal (purple) solutions flowed through the channel in a laminar fashion until reaching the T-junction where pyridine in oil droplets were formed. Mixing of the ligand and metal occurred in the serpentine passive mixing region (pink) and complex containing droplets were imaged in the droplet channel region (green). Waste was collected in tygon tubing connected to the outlet well (yellow).

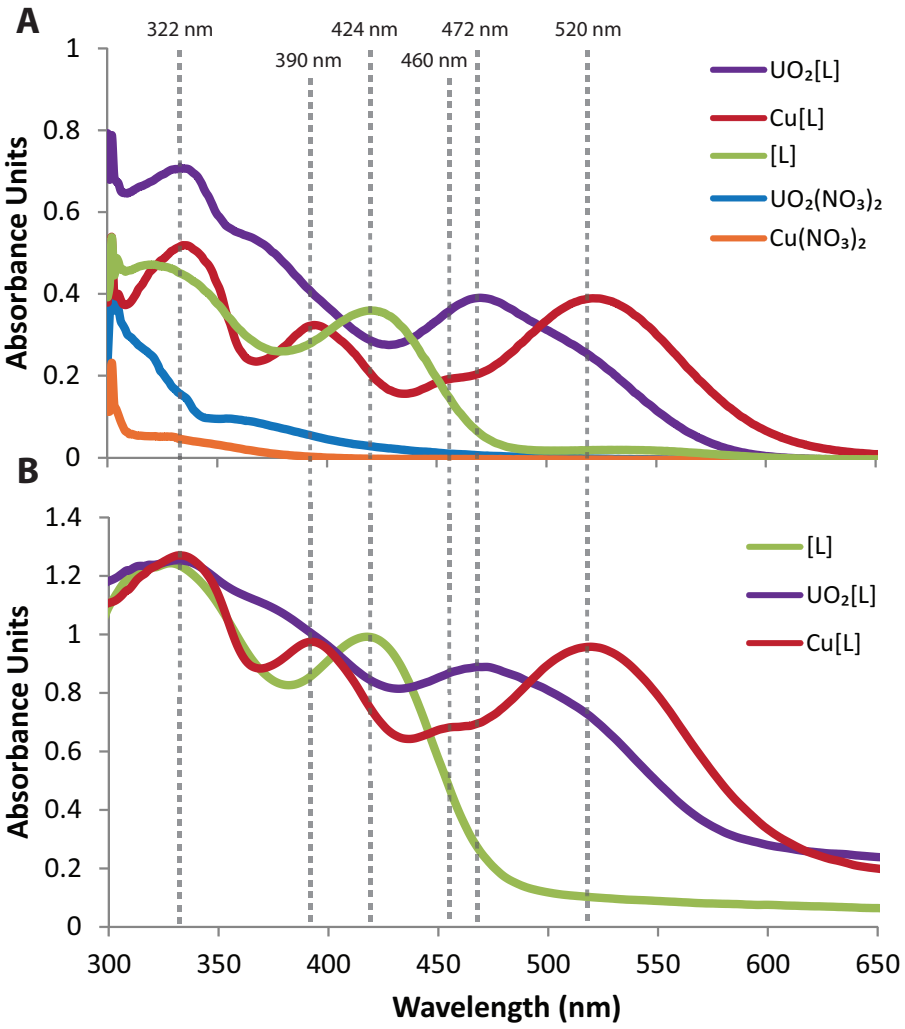

Figure 5.2: **Complex spectra on macro and micro scale.** A) UV-Vis spectrum of the metal starting materials [$Cu(NO_3)_2$, $UO_2(NO_3)_2$], [L], Cu[L], and UO_2[L] complexes in pyridine at 20 μM. B) CRAIC spectra of complexes collected on chip with 100 μm optical path length.

systems, higher sample concentrations were used in the microfluidic system; however, far less sample was used in the microfluidic system overall. Sample volumes of ∼3 mL were needed for the cuvette based system, whereas less than 50 μL was needed to fill microfluidic inlet wells for the droplet generating device. The cuvette represented only 1 sample environment, but hundreds of thousands droplets could be generated on-chip. Sample droplet volumes are in the picoliter range ($\sim 10^{-10}$) - a stark 10^6 reduction in volume in comparison to a cuvette based system.

Reduced reagent volume is advantageous for decreasing costs and generated waste in any type of experiment. This aspect is especially significant in reference to lanthanide and actinide compounds which are scarce, costly, and generate radioactive waste. PDMS μWell devices were fabricated to mimic a cuvette based system, but maintain small volumes (10 μL) (Figure 5.3). The aim of this system was to create a middle ground between macro scale cuvettes and microfluidic droplet generating devices. When synthesizing new ligand systems, many spectral measurements were carried out on the complex with varying metal centers and metal-to-ligand concentrations. During the initial testing and optimizing stages, it was not necessary to generate thousands of sample droplets on-chip to collect spectra. The μWell system was designed such that around thirty samples could be monitored at once in volumes as low as 10 μL, thereby reducing volumes needed for preliminary ligand analysis. Once optimal conditions were determined and specific ligand systems were chosen, they could easily be transferred to droplet devices for more in-depth analysis.

5.4 Conclusions

This chapter has provided proof of concept for detection of metal-ligand complexes within microfluidic droplets (pyridine droplets in perfluorocarbon oil) (Figure 5.1). UV-Vis spectra collected using the microdroplet system matched well with spectra from macro-scale measurements (Figure 5.2). Reducing sample volume by more than 6 orders of magnitude on this micro device with concurrent spectroscopic detection could have reverberating effects

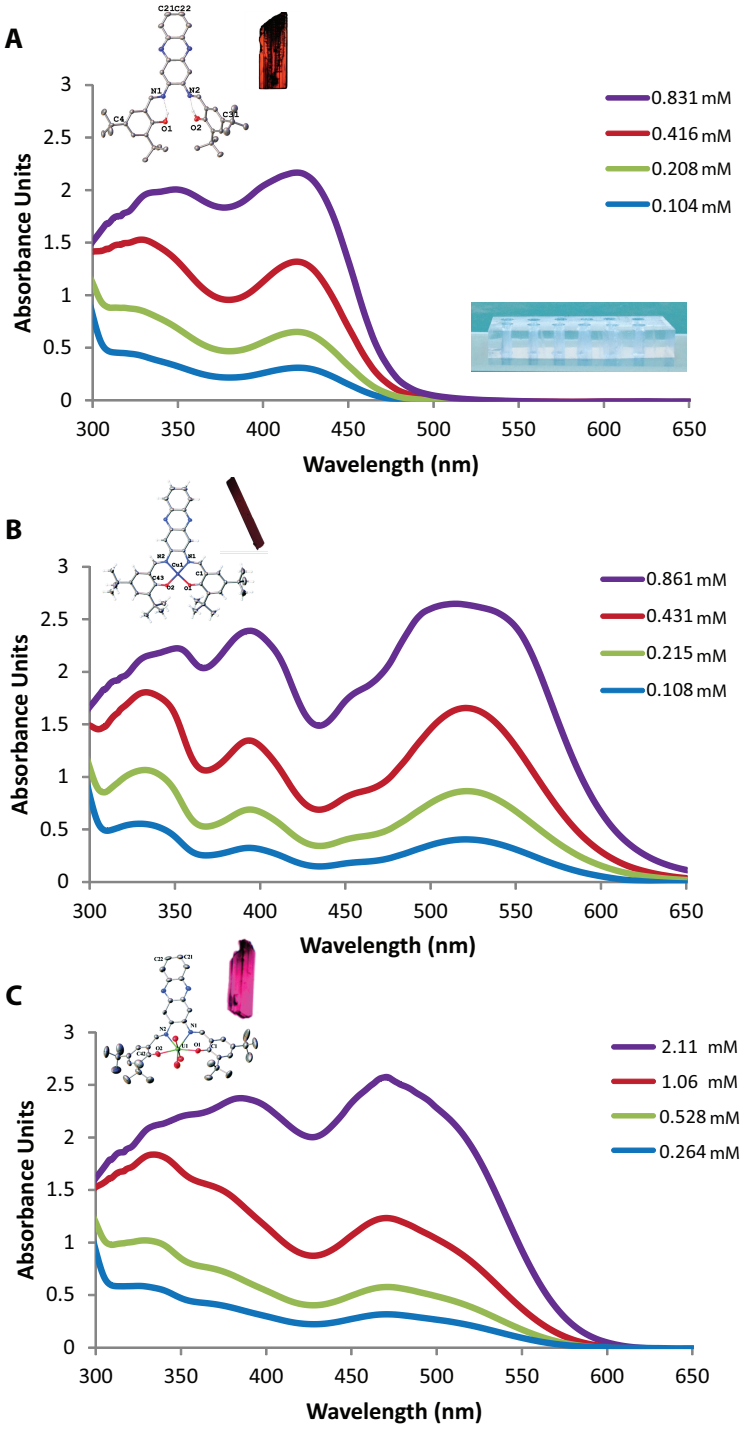

Figure 5.3: **Titration spectra of [L], Cu[L] complex, and UO_2[L] complex in μWells.** UV-Vis spectra of plain ligand (A), copper ligand (B), and uranyl ligand (C) collected from samples contained in the μWell plates. Insets for each grouping of data represent the ligand or complexed ligand structure. A typical μWell device is shown as an inset image in (A) where sample wells were 2.5 mm in diameter and held $\sim$10 μL.

within the field of environmental actinide sensing. By designing simple, easy-to-use microdevices, sample and waste volumes can be drastically reduced, while opening up the potential for on-site detection. The ability to reliably sense actinide elements at a release event and quickly respond could play a large role in altering the current standards of immediate response in field detection procedures. While current sensing methods for actinide elements have high selectivity and low limits of detection, they require high sample and reagent volumes as well as expensive instrumentation for assays that can take up to several days for analysis to be completed [130]. Our approach required less than 5 minutes to collect multiple spectra and determine sample composition in picoliter volumes. Admittedly, analysis was conducted using a relatively expensive, non-portable spectral microscope; yet miniturization of the UV-Vis spectral optics is certainly achievable in future generations of this system. This novel combination of droplet microfluidics with spectral detection using synthetic actinide sensors could help establish a foundation for research in microfluidic analysis of radioactive materials.

Chapter 6

Summary and Future Work

6.1 Summary

Herein microanalysis platforms have been designed for microfluidic cell culture and secretion sampling, real-time monitoring of FFA uptake, and metal-ligand binding kinetics. Proximity immunoassays and a fluorescent FFA assay were designed to accommodate small volume samples and on-chip imaging. 3D printed templates were utilized for simplified microdevice fabrication methods and allowed for culture of primary, murine pancreatic islets, isolated adipocytes, and adipose tissue explants. Designing minimalistic microanalysis platforms was an overarching goal of this work. Microfluidic devices can be used to interrogate systems in ways previously unattainable through macroscale methods; however, microanalysis methods are not being adapted into other realms of the scientific community. Complex microfluidic devices offer many advantages associated with liquid handling and high throughput analysis, but they are not readily usable to non-experts. By designing passive microfluidic devices which can easily be paired with a multitude of assays and imaging systems, this work has established microanalysis platforms that could be utilized by experts and non-experts alike.

6.2 Expanding 3D Template Interfacing for Bioanalytical Platforms

3D templates for primary endocrine tissue culture were presented in Chapters 2 and 3 for use with groups of islets, isolated adipocytes, and adipose tissue explants. As organ-on a-chip platforms have emerged, more focus has been invested in production of devices capable of culturing multiple cell types simultaneously. Current co-culture platforms for

islets and adipocytes do not focus on monitoring dynamic interactions between the cells, and the adipocytes used are typically not from primary sources. Through 3D templates, it is possible for fabrication of simple, passive co-culture devices. Figure 6.1 demonstrates a potential design for co-culturing primary pancreatic islets and adipose tissue explants. This system could be used for probing the dynamics of insulin secretion and subsequent FFA fluctuations from adipocytes.

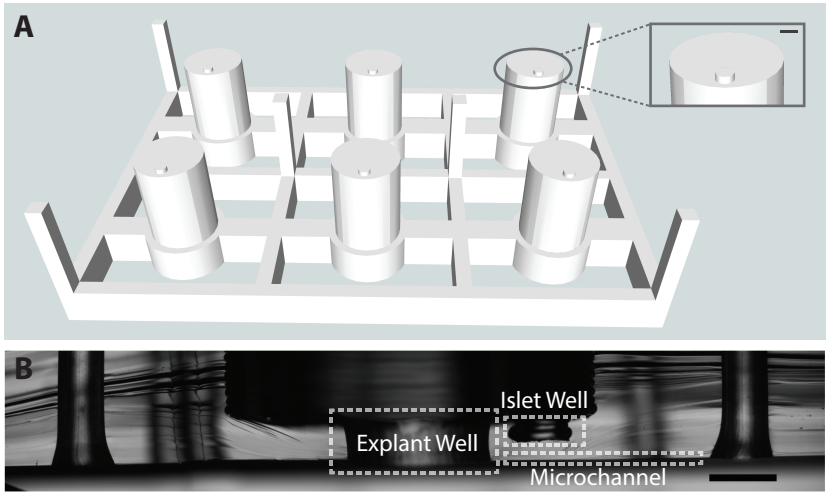

Figure 6.1: **Co-culture device design.** A) 9 mm diameter central template region with 1.5 mm diameter raised region which forms islet containment well (inset scale bar 1.5 mm). B) Cross section of PDMS device fabricated from this template. Scale bar represents 1.5 mm.

6.3 Accurate Adipose Explant Volume Measurement

Adipose explants and adipocytes are not easily analyzed quantitatively without disrupting the cellular environment. Tissue lysis, flow cytometry, and specialized image analysis systems are often used for counting individual, isolated adipocytes for normalizing secretion data or protein levels. Explants can be lysed for total protein, DNA/RNA, or specific biomarker analysis. However, when applying stimulatory solutions, protein and DNA/RNA levels can fluctuate in response to treatments. In order to improve biological data from the adipocytes, there is also a need for a more accurate method for normalization between

explant samples. With diameters in the 2-3 mm range, explants are too small for traditional volumetric measurements. Even larger explants would be difficult to measure due to their inherent buoyancy. To remedy this issue, a 3D printed sandwich volumetric measurement device has been designed for explant sizing and normalization (Figure 6.2). Glass slides have been glued into two sides of the 3D printed box. Viewing ports were designed in the sides of the box for explant viewing. Notches in the view ports represent 1 mm increments which can be used as a reference for sizing. Glass cover slips of a known thickness can be placed between the two box sides when closing the system to set an internal height. When explants are placed on the larger glass slides and the system is closed, images of the explant can be used for tissue area calculations. Since the height of the system has been constrained by the glass cover slips, the explant volume can then be calculated. Further work should be done to characterize this system. Measurements should be done on elastic material of known volume for proof of accuracy. Explants could be measured, lysed, and then analyzed for total protein to determine if there is a correlation between volume and protein levels. This method could be used to determine total volume of explants for normalization and direct comparison purposes. Additionally, to our knowledge, this is the first instance of accurate methodology for volume measurements of adipose explants.

6.4 Proximity Ligation Assays for Peptide Detection

Proximity ligation has been established as an accurate method for homogeneous detection of proteins; however, this method can only be applied to proteins large enough for two antibodies to bind simultaneously. Traditional PLA methods cannot be directly applied for detection of small proteins and peptides. Dynamic secretion studies of metabolically relevant peptides such as glucagon, somatistatin, and amylin could provide further insight to metabolic disease states. Solid phase, competitive PLA has recently been developed for small molecule detection with antibodies conjugated to magnetic beads [131]. Antibodies are covalently attached to the bead surfaces and target peptides are linked to oligos. Labeled

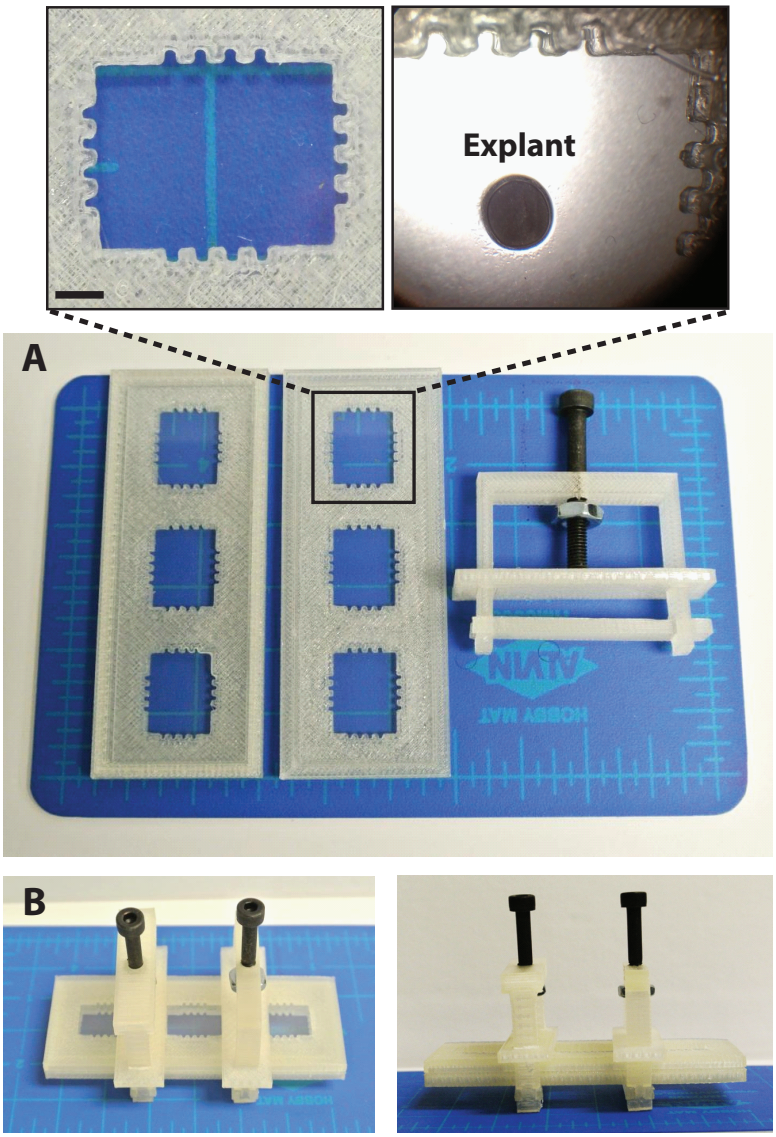

Figure 6.2: **Explant volume measurement device.** A) Disassembled explant volume measurement device. Two 3D printed walls with imaging ports are attached to standard size glass slides. Notches in view ports represent 1 mm increments for scale. Two printed clasps maintain pressure on system to hold slides and cells in place. Glass cover slips (not pictured) are placed between two glass slides to give closed system an exact internal thickness. Left inset shows zoomed in viewing port with 4 mm scale bar. A representative explant image is shown in the right inset. B) Assembled explant volume measurement device.

target peptides can form the proximity complex on bead surfaces. When target peptide is not present, the full proximity complex can form resulting in ligated product. As target peptide is added into the system, it can bind to the antibodies and block proximity complex formation resulting in lower amounts of ligated product. This variation of PLA could be applied to detection of peptides relevant for islet and adipocyte secretion studies.

Bibliography

[1] R. F. Dods, *Understanding diabetes : a biochemical perspective*. Hoboken, N.J.: John Wiley & Sons INC, 2013.

[2] F. M. Ashcroft and P. Rorsman, "Diabetes mellitus and the β cell: the last ten years.," *Cell*, vol. 148, pp. 1160–71, mar 2012.

[3] H. J. Harwood, "The adipocyte as an endocrine organ in the regulation of metabolic homeostasis.," *Neuropharmacology*, vol. 63, pp. 57–75, jul 2012.

[4] M. E. F. Vázquez-Vela, N. Torres, and A. R. Tovar, "White adipose tissue as endocrine organ and its role in obesity.," *Archives of medical research*, vol. 39, pp. 715–28, nov 2008.

[5] P. Wang, N. M. Fiaschi-Taesch, R. C. Vasavada, D. K. Scott, A. García-Ocaña, and A. F. Stewart, "Diabetes mellitusadvances and challenges in human β-cell proliferation," *Nature Reviews Endocrinology*, vol. 11, p. 201, feb 2015.

[6] S. Islam, *The Islets of Langerhans*. Springer Verlag, 2010.

[7] T. K. Bratanova-Tochkova, H. Cheng, S. Daniel, S. Gunawardana, Y.-J. Liu, J. Mulvaney-Musa, T. Schermerhorn, S. G. Straub, H. Yajima, and G. W. Sharp, "Triggering and Augmentation Mechanisms, Granule Pools, and Biphasic Insulin Secretion," *Diabetes*, vol. 51, pp. S83–S90, feb 2002.

[8] S. Misler, Z. Zhou, A. S. Dickey, A. M. Silva, D. M. Pressel, and D. W. Barnett, "Electrical activity and exocytotic correlates of biphasic insulin secretion from β-cells of canine islets of Langerhans: Contribution of tuning two modes of Ca 2+ entry-dependent exocytosis to two modes of glucose-induced electrical activity," *Channels*, vol. 3, pp. 181–193, nov 2014.

[9] F. R. Castiello, K. Heileman, and M. Tabrizian, "Microfluidic perfusion systems for secretion fingerprint analysis of pancreatic islets: applications, challenges and opportunities.," *Lab on a chip*, vol. 16, pp. 409–31, feb 2016.

[10] C. M. Kusminski, S. Shetty, L. Orci, R. H. Unger, and P. E. Scherer, "Diabetes and apoptosis: lipotoxicity.," *Apoptosis : an international journal on programmed cell death*, vol. 14, pp. 1484–95, dec 2009.

[11] T. Kadowaki, T. Yamauchi, N. Kubota, K. Hara, K. Ueki, and K. Tobe, "Adiponectin and adiponectin receptors in insulin resistance, diabetes, and the metabolic syndrome.," *The Journal of clinical investigation*, vol. 116, pp. 1784–92, jul 2006.

[12] R. Ricci and F. Bevilacqua, "The potential role of leptin and adiponectin in obesity: A comparative review," *The Veterinary Journal*, vol. 191, pp. 292–298, mar 2012.

[13] D. K. Oh, T. Ciaraldi, and R. R. Henry, "Adiponectin in health and disease.," *Diabetes, obesity & metabolism*, vol. 9, pp. 282–9, may 2007.

[14] T. Schraw, Z. V. Wang, N. Halberg, M. Hawkins, and P. E. Scherer, "Plasma adiponectin complexes have distinct biochemical characteristics.," *Endocrinology*, vol. 149, pp. 2270–82, may 2008.

[15] E. P. Plaisance, M. Lukasova, S. Offermanns, Y. Zhang, G. Cao, and R. L. Judd, "Niacin stimulates adiponectin secretion through the GPR109A receptor.," *American journal of physiology. Endocrinology and metabolism*, vol. 296, pp. E549–58, mar 2009.

[16] J. M. Friedman and J. L. Halaas, "Leptin and the regulation of body weight in mammals.," *Nature*, vol. 395, pp. 763–70, oct 1998.

[17] G. Paz-Filho, C. Mastronardi, T. Delibasi, M.-L. Wong, and J. Licinio, "Congenital leptin deficiency: diagnosis and effects of leptin replacement therapy.," *Arquivos brasileiros de endocrinologia e metabologia*, vol. 54, pp. 690–7, nov 2010.

[18] S. Margetic, C. Gazzola, G. G. Pegg, and R. A. Hill, "Leptin: a review of its peripheral actions and interactions.," *International journal of obesity and related metabolic disorders : journal of the International Association for the Study of Obesity*, vol. 26, pp. 1407–33, dec 2002.

[19] D. Langin, "Control of fatty acid and glycerol release in adipose tissue lipolysis.," *Comptes rendus biologies*, vol. 329, pp. 598–607; discussion 653–5, aug 2006.

[20] R. E. Duncan, M. Ahmadian, K. Jaworski, E. Sarkadi-Nagy, and H. S. Sul, "Regulation of lipolysis in adipocytes.," *Annual review of nutrition*, vol. 27, pp. 79–101, jan 2007.

[21] M. Lafontan, "Historical perspectives in fat cell biology: the fat cell as a model for the investigation of hormonal and metabolic pathways.," *American journal of physiology. Cell physiology*, vol. 302, pp. C327–59, jan 2012.

[22] T. S. Nielsen, N. Jessen, J. O. L. Jørgensen, N. Møller, and S. Lund, "Dissecting adipose tissue lipolysis: molecular regulation and implications for metabolic disease.," *Journal of molecular endocrinology*, vol. 52, pp. R199–222, jun 2014.

[23] G. M. Whitesides, "The origins and the future of microfluidics.," *Nature*, vol. 442, pp. 368–73, jul 2006.

[24] J. C. Brooks, K. I. Ford, D. H. Holder, M. D. Holtan, and C. J. Easley, "Macro-to-micro interfacing to microfluidic channels using 3D-printed templates: Application to time-resolved secretion sampling of endocrine tissue," *Analyst*, 2016.

[25] L. A. Godwin, M. E. Pilkerton, K. S. Deal, D. Wanders, R. L. Judd, and C. J. Easley, "Passively operated microfluidic device for stimulation and secretion sampling of single pancreatic islets.," *Analytical chemistry*, vol. 83, pp. 7166–72, sep 2011.

[26] L. A. Godwin, J. C. Brooks, L. D. Hoepfner, D. Wanders, R. L. Judd, and C. J. Easley, "A microfluidic interface for the culture and sampling of adiponectin from primary adipocytes.," *The Analyst*, vol. 140, pp. 1019–25, feb 2015.

[27] A. M. Clark, K. M. Sousa, C. Jennings, O. A. MacDougald, and R. T. Kennedy, "Continuous-flow enzyme assay on a microfluidic chip for monitoring glycerol secretion from cultured adipocytes.," *Analytical chemistry*, vol. 81, pp. 2350–6, mar 2009.

[28] A. R. Lomasney, L. Yi, and M. G. Roper, "Simultaneous monitoring of insulin and islet amyloid polypeptide secretion from islets of Langerhans on a microfluidic device.," *Analytical chemistry*, vol. 85, pp. 7919–25, aug 2013.

[29] B. A. Maynard, J. C. Brooks, E. E. Hardy, C. J. Easley, and A. E. V. Gorden, "Synthesis, structural characterization, electronic spectroscopy, and microfluidic detection of Cu +2 and UO 2 +2 [di-tert-butyl-salphenazine] complexes," *Dalton Trans.*, vol. 44, no. 10, pp. 4428–4430, 2015.

[30] K. S. Deal and C. J. Easley, "Self-Regulated, Droplet-Based Sample Chopper for Microfluidic Absorbance Detection," *Analytical Chemistry*, vol. 84, pp. 1510–1516, feb 2012.

[31] C. J. DeJournette, J. Kim, H. Medlen, X. Li, L. J. Vincent, and C. J. Easley, "Creating biocompatible oil-water interfaces without synthesis: direct interactions between primary amines and carboxylated perfluorocarbon surfactants.," *Analytical chemistry*, vol. 85, pp. 10556–64, nov 2013.

[32] J. Yakovleva, R. Davidsson, A. Lobanova, M. Bengtsson, S. Eremin, T. Laurell, and J. Emnéus, "Microfluidic Enzyme Immunoassay Using Silicon Microchip with Immobilized Antibodies and Chemiluminescence Detection," *Analytical Chemistry*, vol. 74, pp. 2994–3004, jul 2002.

[33] A. Bhattacharyya and C. M. Klapperich, "Design and testing of a disposable microfluidic chemiluminescent immunoassay for disease biomarkers in human serum samples.," *Biomedical microdevices*, vol. 9, pp. 245–51, apr 2007.

[34] X. Liang, A. Liu, C. Lim, T. Ayi, and P. Yap, "Determining refractive index of single living cell using an integrated microchip," *Sensors and Actuators A: Physical*, vol. 133, pp. 349–354, feb 2007.

[35] B. Kuswandi, Nuriman, J. Huskens, and W. Verboom, "Optical sensing systems for microfluidic devices: a review.," *Analytica chimica acta*, vol. 601, pp. 141–55, oct 2007.

[36] K. Fong Lei, *Microfluidics in Detection Science*. RSC Detection Science, Cambridge: Royal Society of Chemistry, jan 2014.

[37] M. A. Unger, H. P. Chou, T. Thorsen, A. Scherer, and S. R. Quake, "Monolithic microfabricated valves and pumps by multilayer soft lithography.," *Science (New York, N.Y.)*, vol. 288, pp. 113–6, apr 2000.

[38] S. K. Y. Tang and G. M. Whitesides, "Basic Microfluidic and Soft Lithographic Techniques," in *Optofluidics: Fundamentals, Devices, and Applications* (Y. Fainman, L. Lee, D. Psaltis, and C. Yang, eds.), ch. Chapter 2, pp. 7–32, McGraw-Hill Biophotonics, 2010.

[39] G. M. Whitesides, E. Ostuni, S. Takayama, X. Jiang, and D. E. Ingber, "Soft lithography in biology and biochemistry.," *Annual review of biomedical engineering*, vol. 3, pp. 335–73, jan 2001.

[40] J. N. Lee, C. Park, and G. M. Whitesides, "Solvent compatibility of poly(dimethylsiloxane)-based microfluidic devices.," *Analytical chemistry*, vol. 75, pp. 6544–54, dec 2003.

[41] J. Zhou, A. V. Ellis, and N. H. Voelcker, "Recent developments in PDMS surface modification for microfluidic devices," *ELECTROPHORESIS*, vol. 31, pp. 2–16, jan 2010.

[42] J. A. Vickers, M. M. Caulum, and C. S. Henry, "Generation of hydrophilic poly(dimethylsiloxane) for high-performance microchip electrophoresis.," *Analytical chemistry*, vol. 78, pp. 7446–52, nov 2006.

[43] S. Halldorsson, E. Lucumi, R. Gómez-Sjöberg, and R. M. T. Fleming, "Advantages and challenges of microfluidic cell culture in polydimethylsiloxane devices.," *Biosensors & bioelectronics*, vol. 63, pp. 218–31, jan 2015.

[44] T. M. Squires and S. R. Quake, "Microfluidics: Fluid physics at the nanoliter scale," *Reviews of Modern Physics*, vol. 77, pp. 977–1026, oct 2005.

[45] G. Hetsroni, A. Mosyak, E. Pogrebnyak, and L. Yarin, "Fluid flow in micro-channels," *International Journal of Heat and Mass Transfer*, vol. 48, no. 10, pp. 1982–1998, 2005.

[46] C.-Y. Lee, C.-L. Chang, Y.-N. Wang, and L.-M. Fu, "Microfluidic mixing: a review.," *International journal of molecular sciences*, vol. 12, pp. 3263–87, jan 2011.

[47] A. Lau, H. Yip, K. Ng, X. Cui, and R. Lam, "Dynamics of Microvalve Operations in Integrated Microfluidics," *Micromachines*, vol. 5, pp. 50–65, feb 2014.

[48] W. H. Grover, A. M. Skelley, C. N. Liu, E. T. Lagally, and R. A. Mathies, "Monolithic membrane valves and diaphragm pumps for practical large-scale integration into glass microfluidic devices," *Sensors and Actuators B: Chemical*, vol. 89, pp. 315–323, apr 2003.

[49] V. Studer, G. Hang, A. Pandolfi, M. Ortiz, W. F. Anderson, and S. R. Quake, "Scaling properties of a low-actuation pressure microfluidic valve," *Journal of Applied Physics*, vol. 95, no. 1, p. 393, 2004.

[50] P. M. Fordyce, C. a. Diaz-Botia, J. L. DeRisi, and R. Gomez-Sjoberg, "Systematic characterization of feature dimensions and closing pressures for microfluidic valves produced via photoresist reflow," *Lab on a Chip*, vol. 12, no. 21, p. 4287, 2012.

[51] R. Gómez-Sjöberg, A. A. Leyrat, D. M. Pirone, C. S. Chen, and S. R. Quake, "Versatile, fully automated, microfluidic cell culture system.," *Analytical chemistry*, vol. 79, pp. 8557–63, nov 2007.

[52] M. Mehling and S. Tay, "Microfluidic cell culture.," *Current opinion in biotechnology*, vol. 25, pp. 95–102, feb 2014.

[53] R. Gómez-Sjöberg, A. A. Leyrat, D. M. Pirone, C. S. Chen, and S. R. Quake, "Versatile, fully automated, microfluidic cell culture system," *Analytical Chemistry*, vol. 79, no. 22, pp. 8557–8563, 2007.

[54] C. J. Easley, J. M. Karlinsey, J. M. Bienvenue, L. A. Legendre, M. G. Roper, S. H. Feldman, M. A. Hughes, E. L. Hewlett, T. J. Merkel, J. P. Ferrance, and J. P. Landers, "A fully integrated microfluidic genetic analysis system with sample-in-answer-out capability.," *Proceedings of the National Academy of Sciences of the United States of America*, vol. 103, pp. 19272–7, dec 2006.

[55] E. K. Sackmann, A. L. Fulton, and D. J. Beebe, "The present and future role of microfluidics in biomedical research.," *Nature*, vol. 507, pp. 181–9, mar 2014.

[56] A. L. Paguirigan and D. J. Beebe, "Microfluidics meet cell biology: bridging the gap by validation and application of microscale techniques for cell biological assays.," *BioEssays : news and reviews in molecular, cellular and developmental biology*, vol. 30, pp. 811–21, sep 2008.

[57] J. F. Dishinger, K. R. Reid, and R. T. Kennedy, "Quantitative monitoring of insulin secretion from single islets of Langerhans in parallel on a microfluidic chip.," *Analytical chemistry*, vol. 81, pp. 3119–27, apr 2009.

[58] J. G. Shackman, K. R. Reid, C. E. Dugan, and R. T. Kennedy, "Dynamic monitoring of glucagon secretion from living cells on a microfluidic chip.," *Analytical and bioanalytical chemistry*, vol. 402, pp. 2797–803, mar 2012.

[59] J. S. Mohammed, Y. Wang, T. A. Harvat, J. Oberholzer, and D. T. Eddington, "Microfluidic device for multimodal characterization of pancreatic islets.," *Lab on a chip*, vol. 9, pp. 97–106, jan 2009.

[60] C. J. Easley, J. V. Rocheleau, W. S. Head, and D. W. Piston, "Quantitative measurement of zinc secretion from pancreatic islets with high temporal resolution using droplet-based microfluidics.," *Analytical chemistry*, vol. 81, pp. 9086–95, nov 2009.

[61] A. F. Adewola, Y. Wang, T. Harvat, D. T. Eddington, D. Lee, and J. Oberholzer, "A multi-parametric islet perifusion system within a microfluidic perifusion device.," *Journal of visualized experiments : JoVE*, jan 2010.

[62] K. Viravaidya and M. L. Shuler, "Incorporation of 3T3-L1 cells to mimic bioaccumulation in a microscale cell culture analog device for toxicity studies," *Biotechnology Progress*, vol. 20, pp. 590–597, sep 2004.

[63] X. Ni, C. Crozatier, L. Sensebé, A. Langonne, L. Wang, Y. Fan, P. He, and Y. Chen, "On-chip differentiation of human mesenchymal stem cells into adipocytes," *Microelectronic Engineering*, vol. 85, no. 5, pp. 1330–1333, 2008.

[64] P. Wang, E. Mariman, J. Renes, and J. Keijer, "The secretory function of adipocytes in the physiology of white adipose tissue.," *Journal of cellular physiology*, vol. 216, pp. 3–13, jul 2008.

[65] A. M. Clark, K. M. Sousa, C. N. Chisolm, O. A. MacDougald, and R. T. Kennedy, "Reversibly sealed multilayer microfluidic device for integrated cell perfusion and online chemical analysis of cultured adipocyte secretions.," *Analytical and bioanalytical chemistry*, vol. 397, pp. 2939–47, aug 2010.

[66] C. E. Dugan and R. T. Kennedy, "Measurement of lipolysis products secreted by 3T3-L1 adipocytes using microfluidics.," *Methods in enzymology*, vol. 538, pp. 195–209, jan 2014.

[67] A. Zambon, A. Zoso, O. Gagliano, E. Magrofuoco, G. P. Fadini, A. Avogaro, M. Foletto, S. Quake, and N. Elvassore, "High Temporal Resolution Detection of Patient-Specific Glucose Uptake from Human ex Vivo Adipose Tissue On-Chip.," *Analytical chemistry*, vol. 87, pp. 6535–43, jul 2015.

[68] K. G. Lee, K. J. Park, S. Seok, S. Shin, D. H. Kim, J. Y. Park, Y. S. Heo, S. J. Lee, and T. J. Lee, "3D printed modules for integrated microfluidic devices," *RSC Advances*, vol. 4, p. 32876, jul 2014.

[69] A. I. Shallan, P. Smejkal, M. Corban, R. M. Guijt, and M. C. Breadmore, "Cost-effective three-dimensional printing of visibly transparent microchips within minutes.," *Analytical chemistry*, vol. 86, pp. 3124–30, mar 2014.

[70] B. C. Gross, J. L. Erkal, S. Y. Lockwood, C. Chen, and D. M. Spence, "Evaluation of 3D printing and its potential impact on biotechnology and the chemical sciences.," *Analytical chemistry*, vol. 86, pp. 3240–53, apr 2014.

[71] K. C. Bhargava, B. Thompson, and N. Malmstadt, "Discrete elements for 3D microfluidics.," *Proceedings of the National Academy of Sciences of the United States of America*, vol. 111, pp. 15013–8, oct 2014.

[72] J. L. Erkal, A. Selimovic, B. C. Gross, S. Y. Lockwood, E. L. Walton, S. McNamara, R. S. Martin, and D. M. Spence, "3D printed microfluidic devices with integrated versatile and reusable electrodes.," *Lab on a chip*, vol. 14, pp. 2023–32, jun 2014.

[73] S. Begolo, D. V. Zhukov, D. A. Selck, L. Li, and R. F. Ismagilov, "The pumping lid: investigating multi-material 3D printing for equipment-free, programmable generation of positive and negative pressures for microfluidic applications.," *Lab on a chip*, vol. 14, pp. 4616–28, dec 2014.

[74] G. Comina, A. Suska, and D. Filippini, "PDMS lab-on-a-chip fabrication using 3D printed templates.," *Lab on a chip*, vol. 14, pp. 424–30, jan 2014.

[75] A. A. Yazdi, A. Popma, W. Wong, T. Nguyen, Y. Pan, and J. Xu, "3D printing: an emerging tool for novel microfluidics and lab-on-a-chip applications," *Microfluidics and Nanofluidics*, vol. 20, p. 50, feb 2016.

[76] Y. He, Y. Wu, J.-z. Fu, Q. Gao, and J.-j. Qiu, "Developments of 3D Printing Microfluidics and Applications in Chemistry and Biology: a Review," *Electroanalysis*, apr 2016.

[77] Y. Stefan, P. Meda, M. Neufeld, and L. Orci, "Stimulation of insulin secretion reveals heterogeneity of pancreatic B cells in vivo.," *The Journal of clinical investigation*, vol. 80, pp. 175–83, jul 1987.

[78] R. C. Karl, D. W. Scharp, W. F. Ballinger, and P. E. Lacy, "Transplantation of insulin-secreting tissues.," *Gut*, vol. 18, pp. 1062–72, dec 1977.

[79] J. C. Brooks, R. L. Judd, and C. J. Easley, "Culture and Sampling of Primary Adipose Tissue in Microfluidic Systems," in *Methods in Molecular Biology: Thermogenic Fat - Methods and Protocols*, New York: Humana Press/Springer, 2017.

[80] M. W. Toepke and D. J. Beebe, "PDMS absorption of small molecules and consequences in microfluidic applications.," *Lab on a chip*, vol. 6, pp. 1484–6, dec 2006.

[81] A. H. Henkin, A. M. Ortegon, S. Cho, W.-J. Shen, A. Falcon, F. B. Kraemer, S.-J. Lee, and A. Stahl, "Evidence for protein-mediated fatty acid efflux by adipocytes.," *Acta physiologica (Oxford, England)*, vol. 204, pp. 562–70, apr 2012.

[82] J. Liao, R. Sportsman, J. Harris, and A. Stahl, "Real-time quantification of fatty acid uptake using a novel fluorescence assay.," *Journal of lipid research*, vol. 46, pp. 597–602, mar 2005.

[83] M. J. McArthur, B. P. Atshaves, A. Frolov, W. D. Foxworth, A. B. Kier, and F. Schroeder, "Cellular uptake and intracellular trafficking of long chain fatty acids.," *Journal of lipid research*, vol. 40, pp. 1371–83, aug 1999.

[84] N. A. Abumrad, R. C. Perkins, J. H. Park, and C. R. Park, "Mechanism of long chain fatty acid permeation in the isolated adipocyte.," *The Journal of biological chemistry*, vol. 256, pp. 9183–91, sep 1981.

[85] J. A. Hamilton and F. Kamp, "How are free fatty acids transported in membranes? Is it by proteins or by free diffusion through the lipids?," *Diabetes*, vol. 48, pp. 2255–69, dec 1999.

[86] O. Varlamov, R. Somwar, A. Cornea, P. Kievit, K. L. Grove, and C. T. Roberts, "Single-cell analysis of insulin-regulated fatty acid uptake in adipocytes.," *American journal of physiology. Endocrinology and metabolism*, vol. 299, pp. E486–96, sep 2010.

[87] A. A. Spector, K. John, and J. E. Fletcher, "Binding of long-chain fatty acids to bovine serum albumin.," *Journal of lipid research*, vol. 10, pp. 56–67, jan 1969.

[88] A. A. Spector, "Fatty acid binding to plasma albumin.," *Journal of lipid research*, vol. 16, pp. 165–79, may 1975.

[89] C. M. Harmon, P. Luce, A. H. Beth, and N. A. Abumrad, "Labeling of adipocyte membranes by sulfo-N-succinimidyl derivatives of long-chain fatty acids: inhibition of fatty acid transport.," *The Journal of membrane biology*, vol. 121, pp. 261–8, may 1991.

[90] J. Kim, J. Hu, A. B. Bezerra, M. D. Holtan, J. C. Brooks, and C. J. Easley, "Protein Quantification Using Controlled DNA Melting Transitions in Bivalent Probe Assemblies," *Analytical Chemistry*, vol. 87, pp. 9576–9579, oct 2015.

[91] J. Hu, J. Kim, and C. J. Easley, "Quantifying Aptamer-Protein Binding via Thermofluorimetric Analysis," *Anal Methods*, vol. 7, no. 17, pp. 7358–7362, 2015.

[92] J. Hu, Y. Yu, J. C. Brooks, L. A. Godwin, S. Somasundaram, F. Torabinejad, J. Kim, C. Shannon, and C. J. Easley, "A reusable electrochemical proximity assay for highly selective, real-time protein quantitation in biological matrices.," *Journal of the American Chemical Society*, vol. 136, pp. 8467–74, jun 2014.

[93] J. Hu, T. Wang, J. Kim, C. Shannon, and C. J. Easley, "Quantitation of femtomolar protein levels via direct readout with the electrochemical proximity assay.," *Journal of the American Chemical Society*, vol. 134, pp. 7066–72, apr 2012.

[94] C. A. Rowe, L. M. Tender, M. J. Feldstein, J. P. Golden, S. B. Scruggs, B. D. MacCraith, J. J. Cras, and F. S. Ligler, "Array Biosensor for Simultaneous Identification of Bacterial, Viral, and Protein Analytes," *Analytical Chemistry*, vol. 71, pp. 3846–3852, sep 1999.

[95] E. Heyduk, B. Dummit, Y.-H. Chang, and T. Heyduk, "Molecular pincers: antibody-based homogeneous protein sensors.," *Analytical chemistry*, vol. 80, pp. 5152–9, jul 2008.

[96] L. Tian and T. Heyduk, "Bivalent ligands with long nanometer-scale flexible linkers.," *Biochemistry*, vol. 48, pp. 264–75, jan 2009.

[97] X. Zhang, A. Daou, T. M. Truong, R. Bertram, and M. G. Roper, "Synchronization of mouse islets of Langerhans by glucose waveforms.," *American journal of physiology. Endocrinology and metabolism*, vol. 301, pp. E742–7, oct 2011.

[98] J. K. Gimzewski, J. Reed, M. A. Teitell, and P. G. Malan, *The Immunoassay Handbook*. Gulf Professional Publishing, 2005.

[99] R. S. YALOW and S. A. BERSON, "Assay of Plasma Insulin in Human Subjects by Immunological Methods," *Nature*, vol. 184, pp. 1648–1649, nov 1959.

[100] A. H. B. Wu, "A selected history and future of immunoassay development and applications in clinical chemistry.," *Clinica chimica acta; international journal of clinical chemistry*, vol. 369, pp. 119–24, jul 2006.

[101] G. KÖHLER and C. MILSTEIN, "Continuous cultures of fused cells secreting antibody of predefined specificity," *Nature*, vol. 256, pp. 495–497, aug 1975.

[102] R. D. Grange, J. P. Thompson, and D. G. Lambert, "Radioimmunoassay, enzyme and non-enzyme-based immunoassays.," *British journal of anaesthesia*, vol. 112, pp. 213–6, feb 2014.

[103] K. L. Cox, V. Devanarayan, A. Kriauciunas, J. Manetta, C. Montrose, and S. Sittampalam, *Immunoassay Methods*. Eli Lilly & Company and the National Center for Advancing Translational Sciences, 2004.

[104] A. Voller, A. Bartlett, and D. E. Bidwell, "Enzyme immunoassays with special reference to ELISA techniques.," *Journal of clinical pathology*, vol. 31, pp. 507–20, jun 1978.

[105] G. A. Bonwick and C. J. Smith, "Immunoassays: their history, development and current place in food science and technology," *International Journal of Food Science and Technology*, vol. 39, pp. 817–827, oct 2004.

[106] B. Giri, B. Pandey, B. Neupane, and F. S. Ligler, "Signal amplification strategies for microfluidic immunoassays," *TrAC Trends in Analytical Chemistry*, vol. 79, pp. 326–334, 2016.

[107] I. A. Darwish, "Immunoassay Methods and their Applications in Pharmaceutical Analysis: Basic Methodology and Recent Advances.," *International journal of biomedical science : IJBS*, vol. 2, pp. 217–35, sep 2006.

[108] T. Portsmann and S. Kiessig, "Enzyme immunoassay techniques. An overview.," *J Immunol Methods*, no. 150, pp. 5–21, 1992.

[109] D. B. Morton, "Removal of blood from laboratory mammals and birds. First report of the BVA/FRAME/RSPCA/UFAW Joint Working Group on Refinement.," *Laboratory animals*, vol. 27, pp. 1–22, jan 1993.

[110] S. Fredriksson, M. Gullberg, J. Jarvius, C. Olsson, K. Pietras, S. M. Gústafsdóttir, A. Ostman, and U. Landegren, "Protein detection using proximity-dependent DNA ligation assays.," *Nature biotechnology*, vol. 20, pp. 473–7, may 2002.

[111] H. Zhang, F. Li, B. Dever, C. Wang, X.-F. Li, and X. C. Le, "Assembling DNA through affinity binding to achieve ultrasensitive protein detection.," *Angewandte Chemie (International ed. in English)*, vol. 52, pp. 10698–705, oct 2013.

[112] M. Gullberg, S. M. Gústafsdóttir, E. Schallmeiner, J. Jarvius, M. Bjarnegård, C. Betsholtz, U. Landegren, and S. Fredriksson, "Cytokine detection by antibody-based proximity ligation.," *Proceedings of the National Academy of Sciences of the United States of America*, vol. 101, pp. 8420–4, jun 2004.

[113] S. Schreiber-Gosche and R. A. Edwards, "Thermodynamics of Oligonucleotide Duplex Melting," *Journal of Chemical Education*, vol. 86, p. 644, may 2009.

[114] S. M. Gustafsdottir, E. Schallmeiner, S. Fredriksson, M. Gullberg, O. Söderberg, M. Jarvius, J. Jarvius, M. Howell, and U. Landegren, "Proximity ligation assays for sensitive and specific protein analyses.," *Analytical biochemistry*, vol. 345, pp. 2–9, oct 2005.

[115] M. Gullberg, S. Fredriksson, M. Taussig, J. Jarvius, S. Gustafsdottir, and U. Landegren, "A sense of closeness: protein detection by proximity ligation," *Current Opinion in Biotechnology*, vol. 14, pp. 82–86, feb 2003.

[116] J. N. Zadeh, C. D. Steenberg, J. S. Bois, B. R. Wolfe, M. B. Pierce, A. R. Khan, R. M. Dirks, and N. A. Pierce, "NUPACK: Analysis and design of nucleic acid systems," *Journal of Computational Chemistry*, vol. 32, pp. 170–173, jan 2011.

[117] H. A. Erlich, "Principles and applications of the polymerase chain reaction.," *Reviews in immunogenetics*, vol. 1, no. 2, pp. 127–34, 1999.

[118] A. Fairchild, M. D. Lee, and J. J. Maurer, "PCR Basics," in *PCR Methods in Foods*, pp. 1–25, Springer US, 2006.

[119] M. Arya, I. S. Shergill, M. Williamson, L. Gommersall, N. Arya, and H. R. Patel, "Basic principles of real-time quantitative PCR," *Expert Review of Molecular Diagnostics*, vol. 5, pp. 209–219, mar 2005.

[120] F. Ponchel, C. Toomes, K. Bransfield, F. T. Leong, S. H. Douglas, S. L. Field, S. M. Bell, V. Combaret, A. Puisieux, A. J. Mighell, P. A. Robinson, C. F. Inglehearn, J. D. Isaacs, and A. F. Markham, "Real-time PCR based on SYBR-Green I fluorescence: an alternative to the TaqMan assay for a relative quantification of gene rearrangements, gene amplifications and micro gene deletions.," *BMC biotechnology*, vol. 3, no. 1, p. 18, 2003.

[121] C. A. Heid, J. Stevens, K. J. Livak, and P. M. Williams, "Real time quantitative PCR.," *Genome Res*, vol. 6, pp. 986–994, oct 1996.

[122] C. G. B. Caraguel, H. Stryhn, N. Gagné, I. R. Dohoo, and K. L. Hammell, "Selection of a cutoff value for real-time polymerase chain reaction results to fit a diagnostic purpose: analytical and epidemiologic approaches.," *Journal of veterinary diagnostic investigation : official publication of the American Association of Veterinary Laboratory Diagnosticians, Inc*, vol. 23, pp. 2–15, jan 2011.

[123] J. Kim, J. Hu, R. S. Sollie, and C. J. Easley, "Improvement of Sensitivity and Dynamic Range in Proximity Ligation Assays by Asymmetric Connector Hybridization," *Analytical Chemistry*, vol. 82, pp. 6976–6982, aug 2010.

[124] R. S. Surwit, C. M. Kuhn, C. Cochrane, J. A. McCubbin, and M. N. Feinglos, "Diet-induced type II diabetes in C57BL/6J mice.," *Diabetes*, vol. 37, pp. 1163–7, sep 1988.

[125] K. P. Nichols, R. R. Pompano, L. Li, A. V. Gelis, and R. F. Ismagilov, "Toward Mechanistic Understanding of Nuclear Reprocessing Chemistries by Quantifying Lanthanide

Solvent Extraction Kinetics via Microfluidics with Constant Interfacial Area and Rapid Mixing," *Journal of American Chemical Society*, 2011.

[126] C. T. Riche, C. Zhang, M. Gupta, and N. Malmstadt, "Fluoropolymer surface coatings to control droplets in microfluidic devices," *Lab Chip*, vol. 14, no. 11, pp. 1834–1841, 2014.

[127] R. Seemann, M. Brinkmann, T. Pfohl, and S. Herminghaus, "Droplet based microfluidics.," *Reports on progress in physics. Physical Society (Great Britain)*, vol. 75, p. 016601, jan 2012.

[128] S.-Y. Teh, R. Lin, L.-H. Hung, and A. P. Lee, "Droplet microfluidics," *Lab on a Chip*, vol. 8, no. 2, p. 198, 2008.

[129] Y. Zhu and Q. Fang, "Analytical detection techniques for droplet microfluidics-A review," jul 2013.

[130] J. H. Lee, Z. Wang, J. Liu, and Y. Lu, "Highly sensitive and selective colorimetric sensors for uranyl (UO2(2+)): development and comparison of labeled and label-free DNAzyme-gold nanoparticle systems.," *Journal of the American Chemical Society*, vol. 130, pp. 14217–26, oct 2008.

[131] S. Cheng, F. Shi, X. Jiang, L. Wang, W. Chen, and C. Zhu, "Sensitive detection of small molecules by competitive immunomagnetic-proximity ligation assay.," *Analytical chemistry*, vol. 84, pp. 2129–32, mar 2012.